NONLINEAR OPTICAL SWITCHING PROPERTIES OF DYE-DOPED INORGANIC/ORGANIC COMPOSITE FILMS

by

NATHAN STEVENS

A dissertation submitted to the Graduate Faculty in Chemistry in partial fulfillment of the requirements for the degree of Doctor of Philosophy, The City University of New York

2006

This manuscript has been read and accepted for the Graduate Faculty in Chemistry in satisfaction of the dissertation requirements for the degree of Doctor of Philosophy.

_____ Dr. Daniel L. Akins
Date   Chair of Examining Committee

_____ Dr. Gerald Koeppl
Date   Executive Officer

Dr. Lynn C. Francesconi

Dr. Mary Potasek

Dr. John R. Lombardi
Supervisory Committee

THE CITY UNIVERSITY OF NEW YORK

Abstract

THE NONLINEAR OPTICAL SWITCHING PROPERTIES OF DYE-DOPED

INORGANIC/ORGANIC COMPOSITE FILMS

by

Nathan Stevens

Advisor: Dr. Daniel L. Akins

The sol-gel method has been employed in the fabrication of easily processable, high quality composite films consisting of a non-ionic surfactant, Pluronic P123, as the organic component, and silica as the inorganic component. These films served as the host matrix for various organic dyes and quenchers. Ultrafast time-resolved spectroscopic studies revealed that the excited state lifetimes of the intercalated dyes varied from hundreds of picoseconds, to a few nanoseconds in the absence of any energy acceptors or aggregate formation. For cyanine-type dyes, preparative procedures that induced H- and J-type aggregates, led to significant reductions in the excited state lifetimes. In the case of squarylium-, xanthene-, and rhodamine-type dyes, addition of various electron and energy acceptors, resulted in lifetime values in the low picosecond and femtosecond domain. The efficient energy transfer processes observed was indicative of the formation of tightly coupled dye/acceptor complexes. The excellent optical properties, along with the ultrafast optical responses of the intercalated dye/acceptor complexes, made these composite films ideally suited for use as the photonic layer in an all-optical ultrafast switching device.

Preface

The saying that history repeats itself does certainly apply in the utilization of many apparently mature technologies in modern applications. In regards to the modern telecommunication network, that saying certainly has some truth. The very first telegraphs were not based on the transmission of electrical signals, but on the transmission of optical signals to disseminate information over long distances. Such a telegraphic network, known as a semaphore was invented by Claude Chappe and was operated in France from 1792 to 1846. However, with the advent of the electrical telegraph in 1837 by Samuel Morse, such optical networks were rapidly abandoned, and for the next 150 years, telecommunication was dominated by use of electrical signals to transmit information. Not until the late 1980s, when the first transatlantic fiber optic cable became operational, did communication networks start to make the return to optical signals for the long range transmission of information. Indeed, history has once again repeated itself.

In this dissertation, photonic materials are explored for their use as the active components in optical switching devices that will be the foundation for next generation, ultrahigh bandwidth optical networks. The first chapter discusses the principles of optical switching, switching devices, photonic materials, and excited state deactivation. The second chapter deals with the experimental methods and procedures used in the evaluation of the photonic materials. The remaining chapters, with the exception of chapter seven, are devoted to the characterization of the various photonic materials explored. Chapter seven summarizes the key findings and makes suggestions for the future direction of this work.

Acknowledgments

First and foremost, I would like to extend thanks and appreciation to my mentor, Professor Daniel L. Akins. Without him providing the financial support and intellectual freedom to pursue the topics that were of interest to me, this work would have never come to be. I would also like to thank my family, especially my parents, Rosemarie and Allwyn, whose hard work, determination, and encouragement have been central in getting me to this point. Special thanks also needs to be extended to my loving fiancée, Diana Samaroo, who has been an instrumental part of my life in so many ways, and without whose input and suggestions, this dissertation would not have been completed. The administrative staff of CASI, along with the former and current members of the Akins' group also need to be thanked. Specifically, I would like to thank Dr. Metin Aydin for his work on the quantum chemical calculations, and Fleumingue Jean-Mary for his help with the AFM measurements. For help with pore structure determination on the composite materials, I would like to thank Professor Terresa J. Bandosz. Also, I would like to thank Professor Charles M. Drain for the use of the Fluorolog τ3 emission spectrometer.

I also thank my committee members, Professors Lynn C. Francesconi, John R. Lombardi, and Mary Potasek for their input over the years. My undergraduate mentor, Professor Harry D. Gafney, also deserves thanks for encouraging me to pursue a graduate degree. Lastly, special thanks needs to be extended to Dr. Charles Hicks, with whom I conducted research with as an undergraduate, for his guidance and thoughtful discussions over the years.

In memory of my uncle,

Jose Mitchell

Table of Contents

List of Tables

List of Figures

1. Introduction

1.1 Ultrafast Optical Switching

The recent growth in network connected devices has lead to an ever increasing demand on the telecommunications network to interconnect these devices with the lowest data transfer latency possible. Whereas, five years ago, personal computers and servers accounted for the majority of microprocessor containing devices on the network, today, more and more consumer electronics devices are being network enabled. The current trend in the CE industry is to embed microprocessors and assign IP address to virtually all the electronic devices we use on a daily basis. Cell phones are a prime example of this trend. Essentially every cell phone sold today has an embedded microprocessor that allows the sending of emails, browsing of websites, and in some cases the viewing of streaming multimedia content. This type of functionality has, or is also being added to other devices, such as personal digital assistants, games consoles, televisions, and even household refrigerators and appliances. As the number of these devices and their processing capabilities increase, the data transmission throughput of the fiber optic network backbone will need to be significantly increased to keep pace with the demand for digital content. Current predictions are that the data throughput, or bit rate, of the fiber optic backbone will have to be increased one hundred fold from the current 10 Gb/s, to over 1Tb/s by the year 2010 [1].

The 10 Gb/s bit rate is achieved using a technique called wavelength-division multiplexing (WDM) in which data is simultaneously transmitted using different, closely spaced (spectrally) wavelength channels. This is illustrated in Figure 1-1a. The multiplexer encodes and combines separate wavelengths of light and transmits them

(a)

Multi-Wavelength
Lasers

λ_1

λ_2

Wavelength
Multiplexer

Fiber Optic
Link

Wavelength
Demultiplexer

Wavelength
Detectors

λ_1

λ_2

(b)

Laser Pulses

$|\,0_A|\,1_A\,|$

$|\,0_B|\,1_B\,|$

time

High Speed
Multiplexing
Switch

Fiber Optic
Link

multiplexed
pulses

$|\,0_A|\,0_B|\,1_A|\,1_B\,|$

High Speed
Demultiplexing
Switch

Pulse
Detectors

$|\,0_A|\,1_A\,|$

$|\,0_B|\,1_B\,|$

space
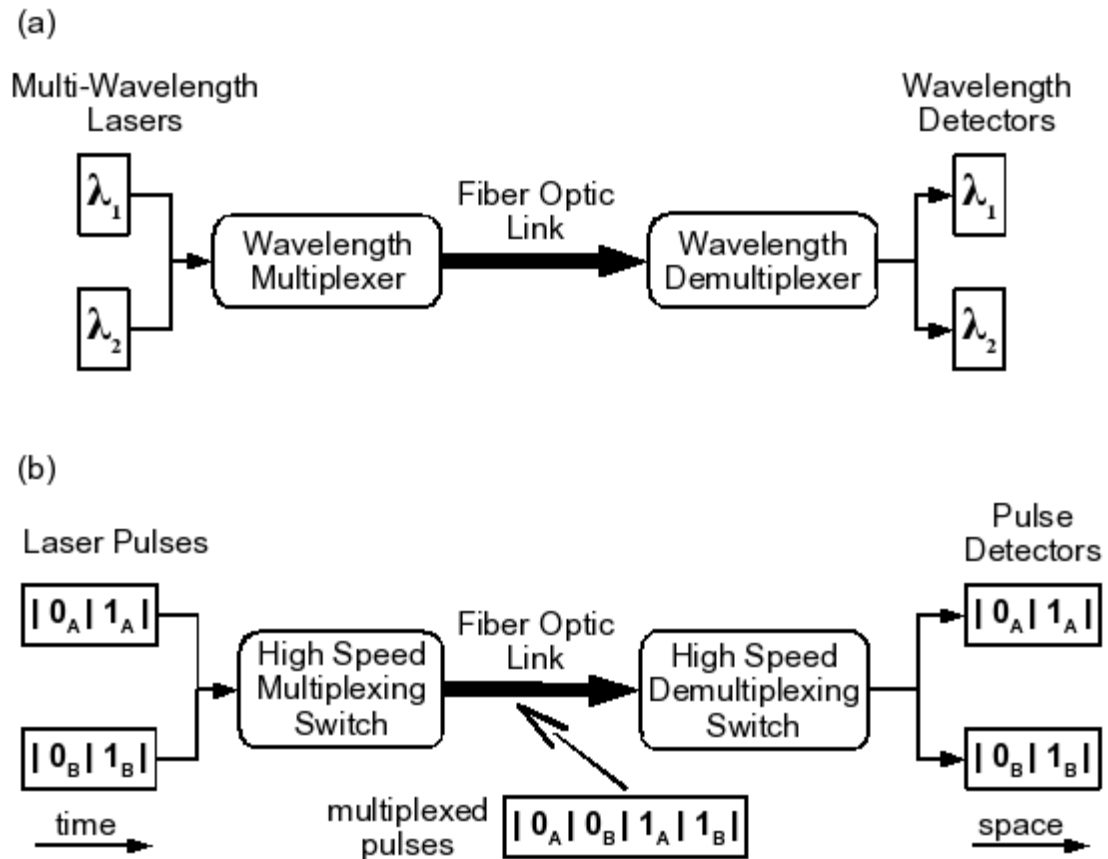
Figure 1-1. Block diagram of (a) wavelength-division multiplexing (WDM) and (b) time-division multiplexing (TDM) systems.

down the fiber optic link, while the demultiplexer receives the encoded light waves and

disperses them onto their respective detectors. The advantage of this method is that the

bit rate can easily be increased by using a greater number of wavelength channels. Since

the available wavelength range from the laser source is finite, and the ability to manage

large number of wavelength channels becomes impractical above a 100 channels or so,

the upper data throughput limit on a realistic system is about 100 Gb/s [1]. A second

approach being employed to increase the data throughput is time-division multiplexing

(TDM). As shown in Figure 1-1b, data is transmitted as a series of pulses over a single

wavelength with the throughput being determined by how closely packed the pulses are in time. The advantage of this system is that it avoids the wavelength management issues of the WDM method, however, due to the limitations of the electronics components involved, the maximum throughput is limited to a few tens of Gb/s over a single wavelength channel [2]. Multiple wavelength channels can be used to form a hybrid WDM/TDM system, but the wavelength management and electronic limitations would still limit the maximum throughput below 1 Tb/s. The practical data throughput limitations of WDM and TDM systems, as well as the optical time-division multiplexing (OTDM) systems being developed to surpass those limits are presented in Figure 1-2.
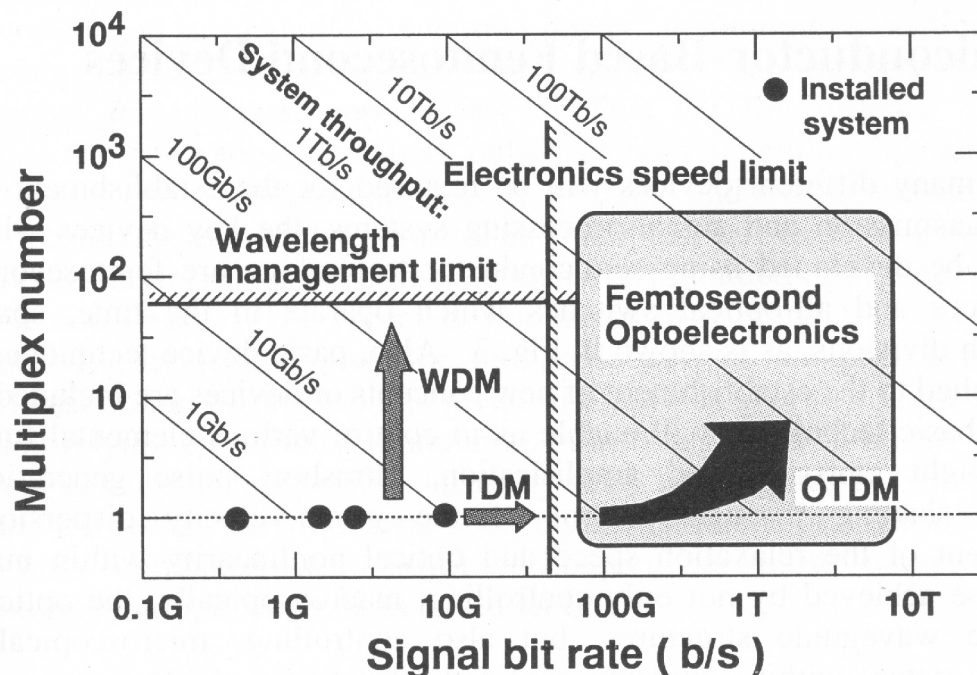
Figure 1-2. The practical data throughput limits of WDM and TDM systems. The expected throughput of femtosecond optical time-division systems (OTDM) is also presented. (adapted from reference 1)

1.2 Optical Switching Devices

Central to the operation of an OTDM system are optical switching devices, whose on and off cycles are controlled by pulses of light (the gating or control pulse) [1]. A multiplexing switching device is used to create and encode the data pulse stream, while a second switching device is used to carry out the demultiplexing operation. Since all switching operations are optically controlled, the limitations of the electronic components is no longer the determining factor in the data throughput rate. This rate is now determined by the gating pulse temporal width, and more importantly, the nonlinear optical response of the photonic switching material. Given the advances over the past ten years or so, in the development of high power femtosecond laser sources, the gating pulse should be a non-factor, if it is not already.

When a light wave propagates through a transparent material, its electromagnetic field exerts a force on the valence electron cloud causing it to be polarized in the direction of the electric field vector. At low field strength the degree of polarization is directly proportional to the field strength, and overall polarizability is given by,

$$P = \epsilon_0 \chi E,$$ (1.1)

where χ is the electric susceptability and E is the electric-field amplitude [3]. As the field strength is increased, the response of the electron cloud becomes nonlinear and consequently, additional terms need to added to the above equation to properly describe its polarization. The polarizability is now written as,

$$P = \epsilon_0 (\chi E + \chi_2 E^2 + \chi_3 E^3 + \cdots).$$ (1.2)

Since the linear susceptability, χ, is much greater than the coefficients of the nonlinear terms χ_2, χ_3, etc., the latter only contribute at very high field strengths, such as those

produced by a laser. The second order term, χ_2, is responsible for second harmonic generation (SHG) in non-centrosymmetric materials i.e., material with no center of inversion. The third order term gives rise to a nonlinear refractive index and saturation absorption. It is these two phenomena that have been exploited in the development of ultrafast all-optical switching devices.
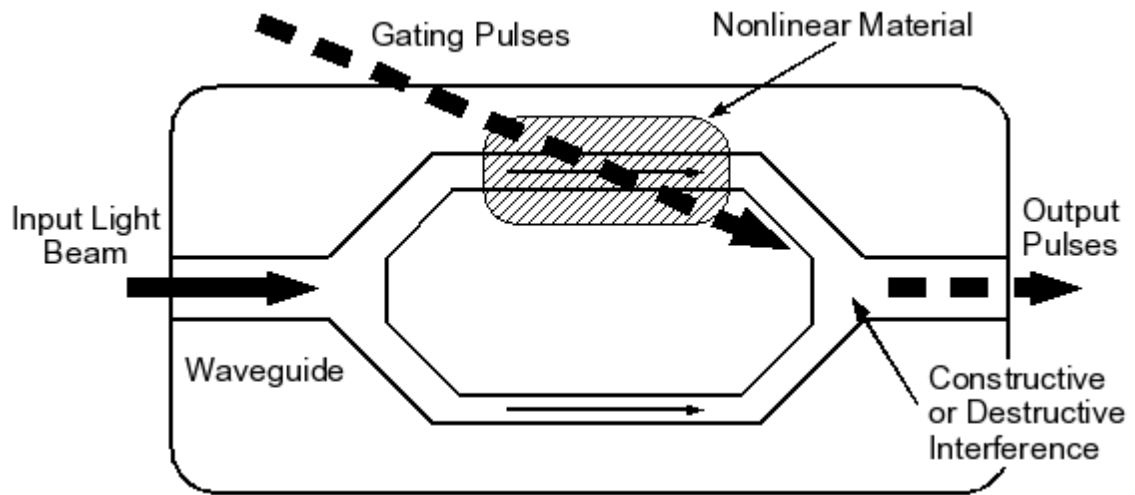
Figure 1-3. Optically gated Mach-Zehnder interferometer acting as ultrafast optical modulator.

An example of an optical switching device that uses nonlinear refractive index change as a means to perform ultrafast data multiplexing on a beam of light is the Mach-Zhehnder (MZ) interferometer [2]. A diagram of such a device is shown in Figure 1-3. When an intense light pulse passes through materials that possess a large third order susceptability term, its refractive index is no longer constant, but is now given by,

$$n = n_0 + \frac{1}{2}n_2|E|^2.$$ (1.3)

Where n_0 and n_2 are the linear and nonlinear refractive index terms, respectively. Since the nonlinear contribution to the refractive index incerases as one-half the square of the electrical field strength, it can contribute significantly to the overall refractive index as

the field strength is increased. As a result of the dependences on the refractive index change on the applied field, the speed at which light propagates through this material can be readily controlled by tuning the field strength. In a MZ interferometer, a waveguide is divided into two separate arms and then recombined some distance later. Inserted into one of these arms, is a nonlinear photonic material whose refractive index value is modulated by a laser gating pulse. Provided the distance in the two arms are equal, the recombined light beams from the two arms will undergo constructive interference, and a signal will be detected at the exit port. If, however, the intensity of the gating pulse is sufficient to generate a refractive index change that will delay one of the beams by half a wavelength, destructive interference will occur at the exit port, and no signal will be detected. By using femtosecond gating pulses and combining several of these devices, pulse streams consisting of pulses spaced by a few 100 femtoseconds can be realized. This translates into delivering about 10 trillion pulses per second, or a bit rate of 10 Tb/s.

The demultiplexing of such a high frequency pulse stream has been shown possible by employing an all-optical serial-to-parallel pulse converter [4] that operates on the nonlinear principle of saturation absorption. A sketch of such a device is provided in Figure 1-4. Essentially, this device is an optical shutter that takes a series of femtosecond signal pulses, closely spaced in time (a picosecond or less) and spatially disperses them so the distance between them corresponds to their temporal separation. In order to accomplish this, a femtosecond gate pulse which is angled relative to the plane of the thin-film photonic layer, is used to excite specific regions in sequence as it propagates. Upon excitation, the transparency of a particular region increases according to the following equation [5],
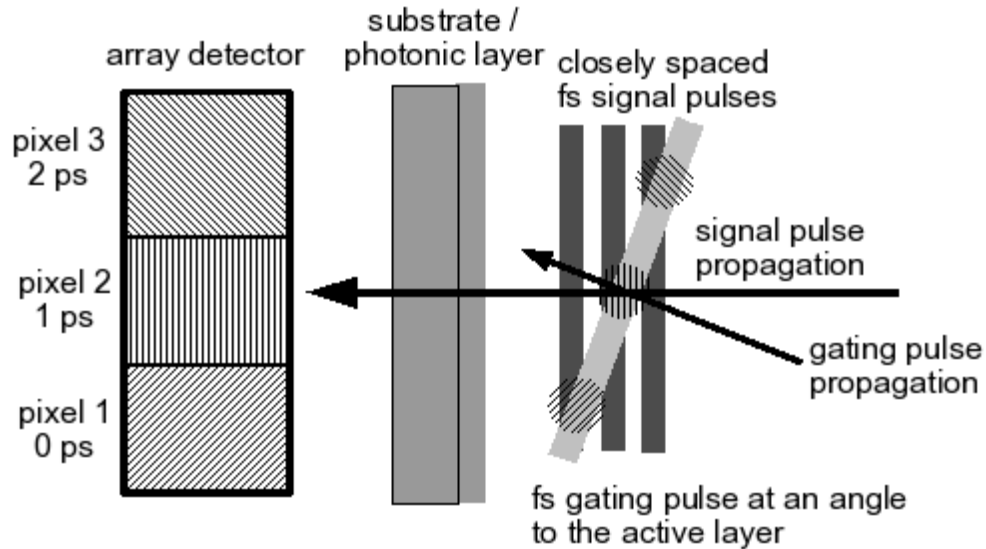
Figure 1-4. Simplified sketch of an all-optical time-to-space pulse converter. For clarity the signal and gating pulses are shown to overlap before the photonic layer, but in actuality they would overlap within this layer.

$$T(I_i) = \exp\left[\frac{-\alpha_0 L}{1+I_i/I_{sat}}\right]. \tag{1.4}$$

I_i is the intensity of the gating pulse incident on active layer of length L, and I_{sat} is the

saturation intensity. The linear absorption coefficient is given by α_0. This allows the

area of the signal pulse that spatially overlaps this region to undergo an exponential

increase in its transmission as it passes through. As subsequent signal pulses arrive,

different regions of those pulses undergo this process. The signal pulses can now be

detected as distinct signals in adjacent regions of an array detector, with this separation

them corresponding to their separation in time. In theory such a device has the ability to

separate signal pulses that are spaced in time on the order of their duration; however, the

rate of ground state recovery, which is related to the optical response, of the photonic

layer would be the limiting factor. The faster this response, the better the overall

performance of the device.

1.3 Photonic Materials

Thus far, the materials that have shown the most promise to be used as the thin-film photonic layer are molecular beam epitaxy (MBE) grown semiconductors and neat organic dyes films [1,4]. Initially, high temperature grown (500 ^{0}C) semiconductors were attractive candidates due to their extremely high photostability, however, their relatively slow (2 ns) optical response precluded their use. Application of a strong electrical field can reduce the optical response down to 5 ps, but this is still not sufficient to be used for ultrafast optical switches. Further improvements in the optical response has been achieved by growing semiconductor structures at low temperatures (200 ^{0}C) and doping with beryllium atoms. With optical responses in the sub-picosecond time domain optical, these materials proved suitable for use as the photonic layer in ultrafast optical switching devices. Nonetheless, because of the stringent growth conditions required and the associated cost, combined with the fact that they have to be used in a reflective geometry, these semiconductors may not be the most suitable photonic layer materials.

Organic films are certainly a more cost effective photonic material since they can be readily fabricated at room temperature and atmospheric pressure, using various spin- and dip-coating techniques. Such films have been shown to have excellent transmission characteristics and optical responses well into the sub-picosecond domain. But, unlike their semiconductor counterparts, these films tend to suffer from poor photostability, which greatly limits their use as the photonic layer. The ideal active layer material would be one that combines high photostability of the semiconductors and the ease of fabrication as well as transmission characteristics of organic films.

A proven method to fabricate such hybrid materials, is by incorporating low molecular weight organic dyes into optically inert inorganic matrices. This can be accomplished using several different methods, but the sol-gel method has probably been the most extensively employed over the years [6-10]. In this method, the fabrication of glass-like materials is accomplished through the hydrolysis and condensation of the desired metal alkoxide [11]. By far, the most widely fabricated inorganic matrices are silicate based, due to the excellent physical and optical properties of the resultant materials. The typical preparation uses an alkoxide such as tetra-ethylorthosilicate (TEOS) combined with water, and a suitable alcohol in specific ratios with either acid or base being used to catalyze the reaction. This process is outlined in Figure 1-5. In the initial step, the hydrolysis of the TEOS takes place, resulting in the formation of silica nanoparticles in the range from 1 to 100 nm (the sol). These nanoparticles then become linked during the polycondensation process forming a rigid porous network (the gel). If

Hydrolysis :

$$Si(OCH_2CH_3)_4 + nH_2O \rightarrow Si(OCH_2CH_3)_{4-n}(OH)_n + nHOCH_2CH_3$$
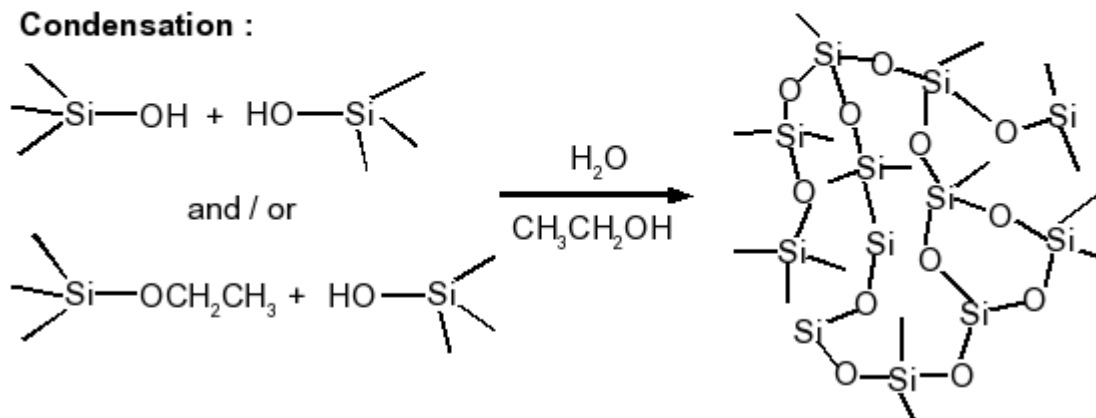
Condensation :

Figure 1-5. The hydrolysis and condensation processes involved in formation of a rigid, porous silica network using the sol-gel method.

dye addition is done at the initial stages of the polycondensation process, then the free space within the porous network will be occupied by dye as well as solvent molecules. Once evaporation of the solvent molecule takes place, a porous silica framework, xerogel, containing intercalated dye molecules remains.

The isolation of the organic dye molecules within silica framework often leads to enhancements in the photophysical properties, as well as overall photostability of the dye [12], which coupled with the ability to cast the dye containing sol into various forms such as thin films, monoliths and powders have made it possible to utilize the resulting composite materials in a wide range of applications. Due to the porous nature and short diffusion pathlength of the thin film structures, small molecules and ions can readily interact with the sequestered dyes within. As a result, a considerable number of studies have focused on the applicability of these materials as sensors [13-15]. Monoliths and thin film structures containing organic laser dyes have shown great potential for use as the gain material in optically pumped, solid state tunable dye lasers [16-18]. Thin films have also been used as decorative, as well as functional coatings for glassware and cathode ray tubes (CRTs) [19]. By intercalating dye molecules which exhibit strong two-photon absorption and emission, Canva et al. have also demonstrated the usefulness of these films towards true 3D displays [20]. Indeed, the use of these sol-gel composites have been quite extensive, but to the author's knowledge, they have never been employed as the photonic layer in ultrafast optical switching devices.

The requirement that the material used to form the photonic layer must possess an ultrafast optical response is the most likely reason why dye containing silica films have yet to be employed in this role. As stated above, intercalation of dyes within a silica

matrix tends to enhance their photophysical properties as a result of isolation within the photochemically stable inorganic micro-environment. In such an environment, the number of deactivation pathways that are available for return to the ground state after photoexcitation is substantially reduced for the majority of dyes. This inherently leads to a longer lived excited state, and hence a reduction in the optical response. For example, upon light absorption, many dyes containing unsaturated linkages often undergo cis-trans isomerization as the initial step in the deactivation process [21]. However, within the confines of the silica matrix, this process is significantly inhibited, or eliminated all together, leading to significant increases in the lifetimes. Moreover, excited state deactivation through bimolecular quenching interactions between the dyes and other molecules is also greatly reduced because diffusion no longer takes place to any significant degree. However, this process is not completely eliminated, because small molecular quenchers, such as oxygen, can still interact with the dyes due to the porous nature of the silica matrix [22]. In short, most deactivation mechanism that rely on conformational changes, or molecular collisions taking place will, in all likelihood, be reduced or eliminated within the silica matrix.

1.4 Excited State Deactivation

One approach for decreasing the excited state lifetimes into the sub-picosecond domain of the intercalated dyes, is to induce molecular aggregate formation between individual dye molecules. In such aggregates, strong van der Waals-like attractive forces causes to the transition dipoles of the individual molecules (monomers) to become coupled, and therefore coherently respond to optical excitation [30,31]. In other words, the optical excitation will be delocalized over several monomers within the aggregate

rather than remaining isolated on a single molecule. This coherent response has been explained in terms of exciton theory. In this context, an exciton can be thought of as neutral excitation "particle" consisting an electron and a positive hole which travels along the aggregate structure [32]. Also, the motion of the exciton along the coherently coupled monomer units is referred to as exciton dynamics. Without going into detail, exciton theory models these aggregate structures as a collection of N (number of monomers which are coherently coupled) two-level systems with oriented transition dipoles which give rise to new electronic transition bands, i.e. exciton bands [32,33]. If the transition dipoles are oriented in a head-to-tail fashion, the exciton band is red-shifted relative to the monomer's absorption band. Aggregates with such exciton bands are referred to as J-aggregates (J for Jelly, one of the first persons to carry out studies on this type of aggregates) and the correspond exciton band is called a J-band for an obvious reason. When the dipole moments are oriented parallel to each another, the exciton band is blue-shifted relative to monomer's absorption band. H-aggregates (H for hypsochromic) is the term used to describe such aggregates and likewise the exciton band is called a H-band. The degree to which the J- or H- bands are shifted relative to the monomer's band is proportional to the number of monomers which are coherently coupled. The greater the number of coupled monomers, the larger the exciton's band shift, and vice versa.

Within these coherent aggregates, the rate of ground state recovery is no longer dependent on the intrinsic properties of individual dye molecule, but rather, that of the aggregate. As a result of the exciton dynamics throughout the coherently coupled monomers, the ground state recovery rate is significantly enhanced. The ultrafast optical

response of H- and J-type aggregates has been well documented, through work in this lab as well as others [23-26], and further details as to the nature of this ultrafast optical response will be provided in latter chapters. Moreover, Zhou et al. have already shown that it is possible to incorporate H- and J-aggregates of cyanine dyes within spin-coated silica films using the sol-gel method [27,28]. Several attempts to duplicate this work, however, were met with limited success. Although films containing J-aggregates were fabricated, they were of poor optical quality. Rather than forming smooth amorphous films, significant cracks and other defects developed during the spin-coating process. Also, because of the low pH of the precursor sol, and consequently the acidic nature of the resulting films, cyanine dyes that readily formed H- and J-aggregates were found to be inadequate for the purpose. The main difficulty being the acid-base interactions between the dyes and the free silanol groups of the silica matrix, rapidly caused protonation of the dyes, resulting in an almost complete loss of the visible absorption band [29].

Another, more interesting approach for attaining the desired sub-picosecond optical response of the dyes within the silica matrix is to co-intercalate a suitable excited state quencher. Depending on the energy transfer mechanism taking place between the dye molecule (donor) and quencher (acceptor), ground state recovery can occur into the sub-picosecond time domain [21]. There are three different mechanisms that govern the energy transfer process. In the "trivial" mechanism, energy transfer occurs through emission of a photon from one molecule and then absorption of this photon by another molecule in the ground state. This is two step process and is shown below.

$$D^* \rightarrow D + h\nu \tag{1.5}$$

$$A + h\nu \rightarrow A^* \tag{1.6}$$

The excited donor molecule is designated as D^* while the acceptor is A. The rate of this transfer mechanism is dependent on the quantum yield of emission of the D^*, the number of molecules of A capable of intercepting the emitting photon, the absorption coefficient of A, and the overlap between the emission spectrum of D^* and the absorption spectrum of A. An interesting note is that the energy transfer rate does not depend on the distance between D^* and A, only that there are sufficient A available to intercept the emitted photons from D^*.

The second mechanism to consider is the transmitter-antenna, or the Coulombic mechanism. In this mechanism, a molecule in the excited state is viewed as an oscillating dipole (transmitter) which can transfer its oscillation to a molecule in the ground state (antenna). For this to occur, a spectral overlap must exist between the emission of D^* and absorption of A, and unlike the "trivial" mechanism, the D^* and A must be in close proximity to each other. The energy transfer rate for this mechanism was shown by Förster to be [21],

$$k_{ET}(Coulombic) = k\frac{\kappa^2 k_D^o}{R_{DA}^6}J(\varepsilon_A). \tag{1.7}$$

The term k is a constant that depends on experimental conditions, while κ^2 is a constant that takes into account the orientation of the D^* and A in space. The spectral overlap of the donor's emission and acceptor's absorption is given by $J(\varepsilon_A)$ term. The term k^o is the pure radiative rate constant and R_{DA} is the distance between the donor and acceptor. Because the rate depends on R^{-6}, energy transfer can still occur to a significant degree, even at a separation of several molecular diameters (30 - 50 Å). An illustration of processes in this mechanism is shown in Figure 1-6.
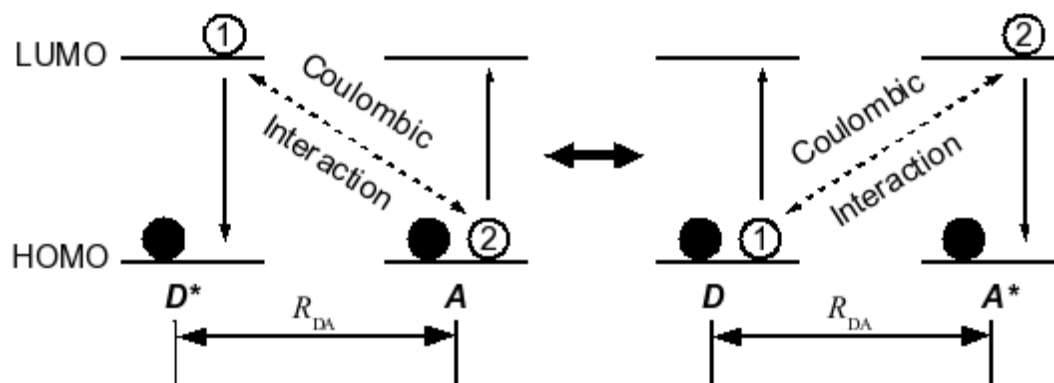
Figure 1-6. Donor (D^*) and acceptor (A) orbital and electron interactions involved in the Coulombic energy transfer process. No electron transfer occurs between the donor and acceptor, only the energy is transfered.

The last energy transfer mechanism to examine is the electron exchange or overlap mechanism. In this mechanism, energy transfer occurs via electron transfer between D^* and A. The electron transfer can occur in one or several steps. In the single step concerted exchange of electrons, an electron from the donor's LUMO is exchanged simultaneous for an electron in the acceptor's HOMO. In the two-step charge transfer (CT) exchange, an electron in the donor's LUMO is first transferred to the LUMO of the acceptor forming a radical ion pair. An electron from the acceptor radical's HOMO is then transferred to the donor radical's HOMO in the second step, completing the exchange process. Another two-step electron exchange mechanism involves the formation of a transient chemical bond by an electron transfer from the HOMO of the acceptor to the HOMO of the donor. The resulting di-radical is undone by the electron transfer from the donor's LUMO to the acceptor's LUMO. Whether electron transfer occurs through a one or two step process, the result is always the same: donor returns to the ground state while the acceptor goes to the excited state. Figure 1-7 shows these electron exchange processes. The energy transfer rate for this mechanism is given by the
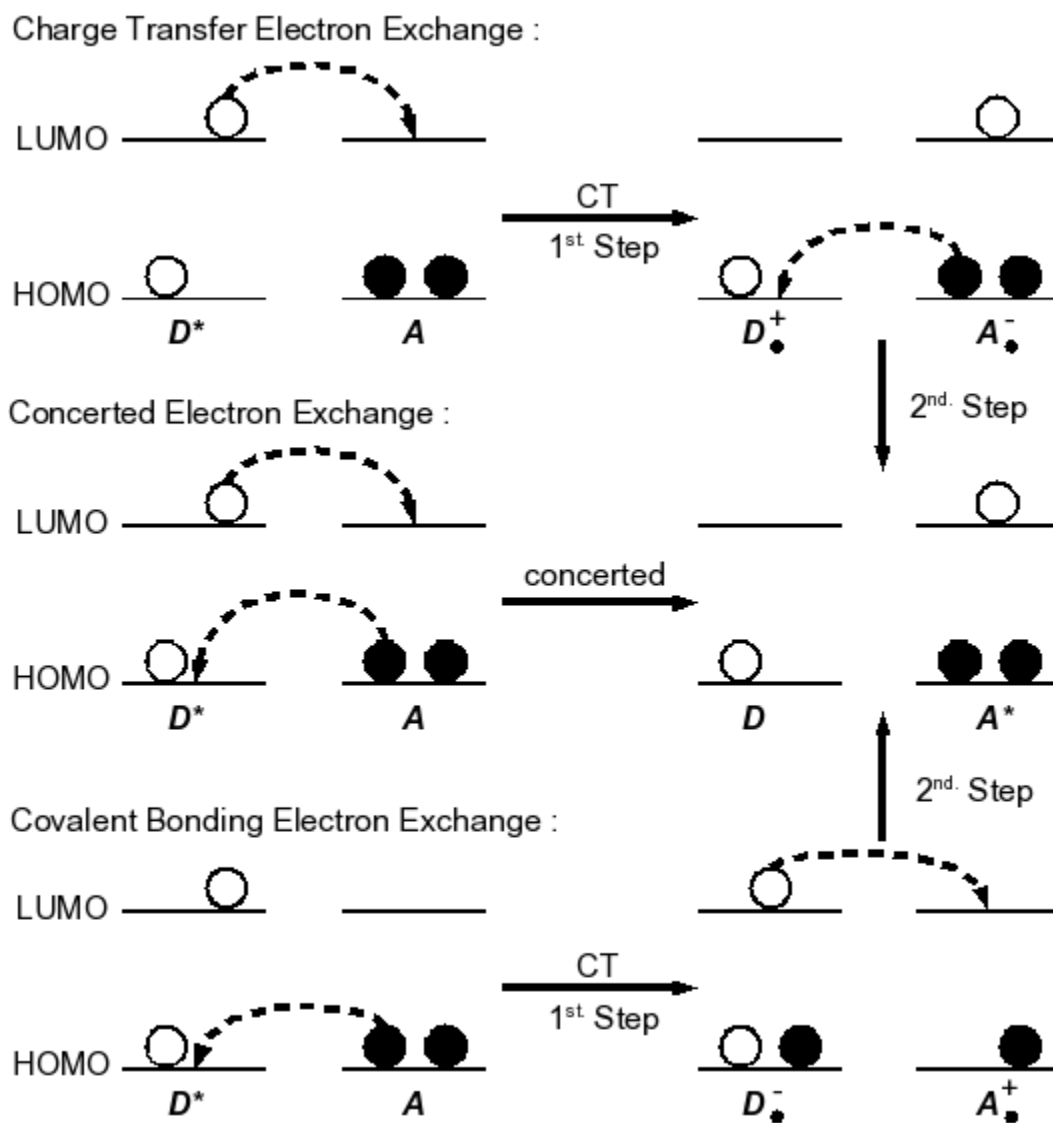
Figure 1-7. The orbital interactions and electron exchange processes that occur during energy transfer by the electron exchange mechanism. In concerted electron exchange, electrons from the donor and the acceptor are simultaneously exchanged. In the two-step, charge transfer and covalent bonding mechanisms, a transient radical ion is first formed.

Dexter equation,

$$k_{ET}(exchange) = KJexp(-2R_{DA}/L) \tag{1.8}$$

The term K is related to orbital interactions, J is the normalized spectral overlap integral, and R_{DA} is the donor-acceptor spacing relative to their van der Waals radii, L. Since J is normalized for the extinction coefficient of the acceptor, it is not necessary that the acceptor absorb in the spectral region of the donor's emission. As a result of the exponential factor in Eq. 1.8, the distance between D^* and A must be within a few molecular diameters (5 - 10 Å) for the energy transfer rate to be competitive with the excited state deactivation rate of D^*.

Though these energy transfer mechanisms were developed with solution systems in mind, they are still valid within the confines of a solid matrix of a thin film, with a few exceptions. Due to the relatively short path length of most films, energy transfer by the "trivial" mechanism is not likely to be observed when the excitation and collection are done in a front-face configuration. In a waveguide configuration it can be observed because of the much extended path length in this configuration. As such, this mechanism will no longer be considered here, because the photonic thin films for optical switching devices are exclusively employed in the front-face configuration. Also, the absence of diffusion means that the donor and acceptor distance remain constant during the donor's excited state lifetime, so a new concept needs to be introduced to account for this fact. This concept is the Perrin formulation [21]. According to this formulation, when an electronically excited donor (D^*) and an acceptor (A) are held fixed in space, there exists a quenching sphere that governs whether or not energy transfer occurs. When an acceptor is within this sphere, the quenching efficiency is unity, but when it is outside, no quenching takes place. These situations are illustrated in Figure 1-8. The radius of

$\phi_{ET} = 1$
$R \leq R_D + R_A$

$\phi_{ET} = 0$
$R \geq R_D + R_A$

quenching
sphere

electronically
excited donor molecule
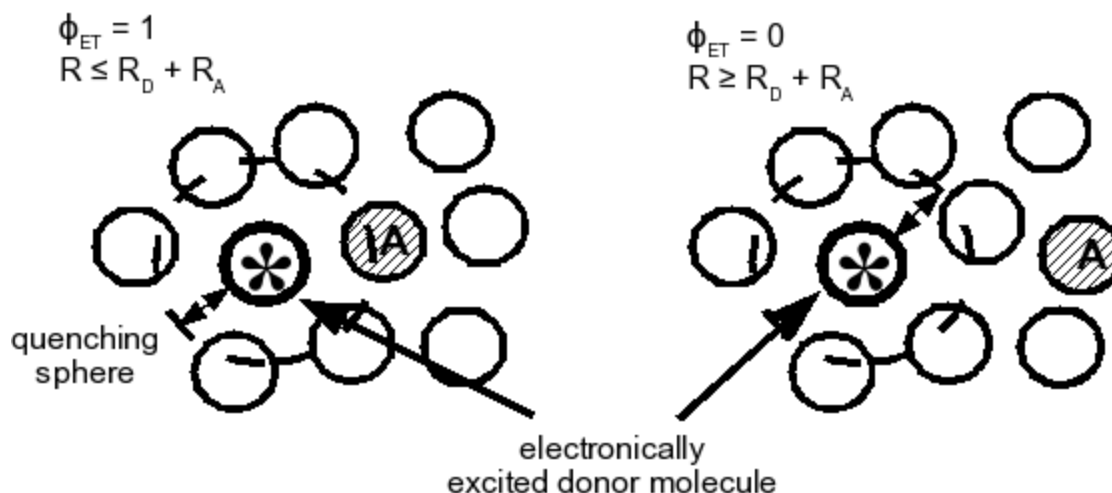
Figure 1-8. Sketch showing the proximity requirement between the donor and acceptor that govern quantum yield of energy transfer according to the Perrin formulation.

the quenching sphere is related to the acceptor concentration by the following,

$$R = 6.5[A]^{1/3}, \tag{1.9}$$

where R is the radius (in Å) of the sphere and $[A]$ is the concentration of the acceptor (in moles/liter, M). A visual representation of average donor/acceptor distance, R_{DA}, as a function of $[A]^{1/3}$ is presented in Figure 1-9. Clearly implicit by this figure is that unless the concentration of the acceptor is above a certain value (ca. 10^{-2} M), the average distance to a donor will probably be too great for energy transfer to occur to a notable extent, even through the Coulombic exchange mechanism defined above. Energy transfer by the electron exchange mechanism requires an even higher acceptor concentration (~1 M), due to the short-range nature of this mechanism.

The use of energy acceptors to increase the optical response of dyes intercalated into silica films provides several advantages. For one, because the Perrin formulation does not require any specific molecular interactions between the donor and acceptor molecules for energy transfer to occur, the excited state deactivation rate of the donor can
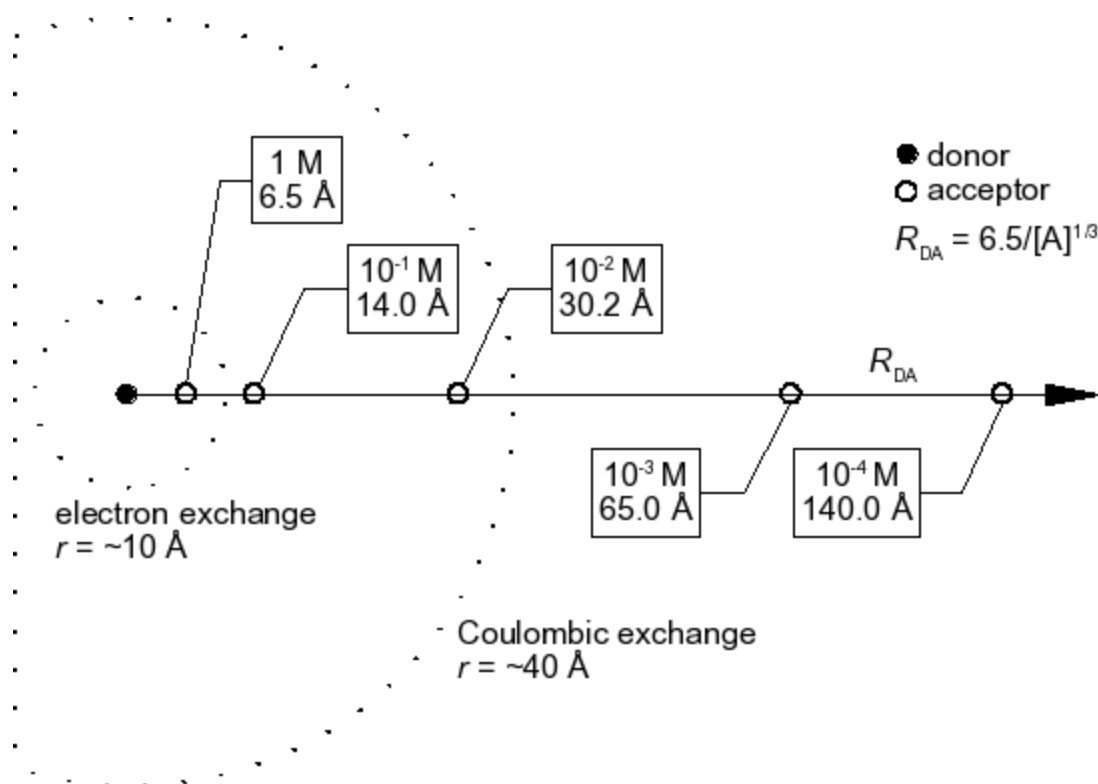
Figure 1-9. The relationship between acceptor concentration, and the average donor-acceptor spacing, R_{DA}. The distances at which energy transfer through the electron and Coulombic exchange mechanisms occur are also indicated.

readily approach the diffusion limit of 10^{13} sec^{-1}, provided an acceptor is in close enough

proximity. Also, because a donor can undergo energy transfer with multiply acceptors,

as long as they are within the quenching sphere, the time between consecutive photon

absorption by the donor, can become limited only by the energy transfer rate. For

example, if a 1 : 1 donor/acceptor ratio exists, following the initial photon absorption and

energy transfer processes, the rate of ground state recovery will be determined by the

energy transfer rate. However, the rate of ground state recovery following absorption of

an additional photon prior to the acceptor returning to the ground state, will now depend

on the natural rate of ground state recovery of the donor. This situation can easily be

avoided if a donor/acceptor ratio greater than 1 : 2 is used instead. In this situation, even if one of the acceptors is in the excited state, others are available to accept the excitation energy from the donor. In this situation, the rate of ground state recovery of the donor will still be determined by the energy transfer process. Another advantage of this approach, is that readily available dyes and energy acceptors which have good photostability and well known photophysical properties, can be mixed and matched to tune the properties of the resulting composite film. For example, laser dyes possessing good photostability and a high absorption coefficient at the wavelength of the gating pulse can be combined with one of the many known excited state quenchers to produce energy transfer complexes possessing ultrafast optical responses. The synthesis of dyes which possess all these properties would most likely prove to be a difficult and time consuming undertaken. As the proverbial saying goes: "why reinvent the wheel?"

1.5 Project Outline

In this work, the development of a simple sol-gel based method for producing high quality inorganic/organic composite films using TEOS as the silica source, and a non-ionic surfactant, Pluronic P123, as the organic component is reported. The hybrid nature of the precursor sol allowed films to be casted using a variety of methods, namely drop-casting, dip-, or spin-coating. These films serve as the host environment for H- and J-type aggregates of cyanine dyes, as well as for various donor/acceptor complexes. Films containing squarylium cyanine dyes, as energy donors, and either methyl viologen, *p*-nitroaniline, or rhodamine 800 as acceptors were fabricated. Energy transfer complexes formed between the xanthene dyes, rose bengal and fluorescein, with either cyanine-type squarylium dyes or crystal violet serving as energy acceptors, have also been

incorporated into these films. Lastly, films containing the laser dye, rhodamine 6G, without, and without the energy acceptor bromophenol blue, were casted. In the rhodamine 6G films containing no energy acceptor, aggregation was induced by using relatively high concentrations of the dye. Film quality and properties, such as thickness and pore structure were ascertained using atomic force microscopy (AFM) topography, reflectometry, and nitrogen absorption isotherms. Photophysical properties were evaluated using a variety of steady-state and time-resolved techniques. Absorption and emission spectroscopy were used to characterize the absorption and fluorescence properties of the films. Picosecond time-resolved fluorescence and femtosecond transient absorption studies were conducted to elucidate the excited state dynamics of the energy transfer complexes within the films. Quantum chemical calculations were also performed in order to provide greater insight into the charge transfer complexes involving squarylium cyanine dyes. From the experimental data obtained, the efficiency and rates of the energy transfer processes were computed. From this, the viability for these composite films to be used as the photonic layer in an all-optical time-to-space converter was assessed.

2. Experimental Methods and Procedures

2.1 Photonic Film Fabrication

The synthesis of the silica/organic sol follows a formulation used in an earlier study to prepare a pure silica sol [1]. For this study, 40.0 ml of tetraethylorthosilicate (TEOS, Fisher Scientific), 106.6 ml ethanol, 11.4 ml distilled water, and 0.2 ml of HCl (2.6 M) were placed into a 250 ml Erlenmeyer flask and vigorously stirred for 1 hour. Ten grams of Pluronic P123 (BASF) poly(ethylene oxide)-poly(propylene oxide)-poly(ethylene oxide) (PEO-PPO-PEO) triblock copolymer paste was then added to the now partially hydrolyzed sol, and stirred for an additional 4 hours, until the sol was visually clear. This sol, was placed into a sealed glass bottle where it remained stable for at least six months or more. From this point forward this sol will be referred to as solP123. After solvent evaporation, the silica to Pluronic P123 weight ratio in the resulting xerogel material was approximately 1 : 1.

The dyes and quenchers used were either obtained from commercial suppliers or in the case of cyanine-type squarylium dyes synthesized. The xanthene dyes, rose bengal (RB) and fluorescein (FR) were obtained from Fisher and Aldrich respectively. The laser dyes, rhodamine 6G (R6G) and rhodamine 800 (LD800), were obtained from Exciton, Inc. The cyanine dyes 3,3'-diethyloxadicarbocyanine (DODC), was obtained from Aldrich, while 5,5',6,6'-tetrachloro-1,1'-diethyl-3,3'-bis(4-sulfobutyl)-benzimidazolocarbocyanine (TDBC) was purchased from Few Chemicals. The energy acceptors, *p*-nitroaniline (*p*NA), methyl viologen (MV), bromophenol blue (BPB), and crystal violet (CRV) were obtained from Sigma-Aldrich. All chemicals were used without further purification. Their chemical structures are provided in Figure 2-1.
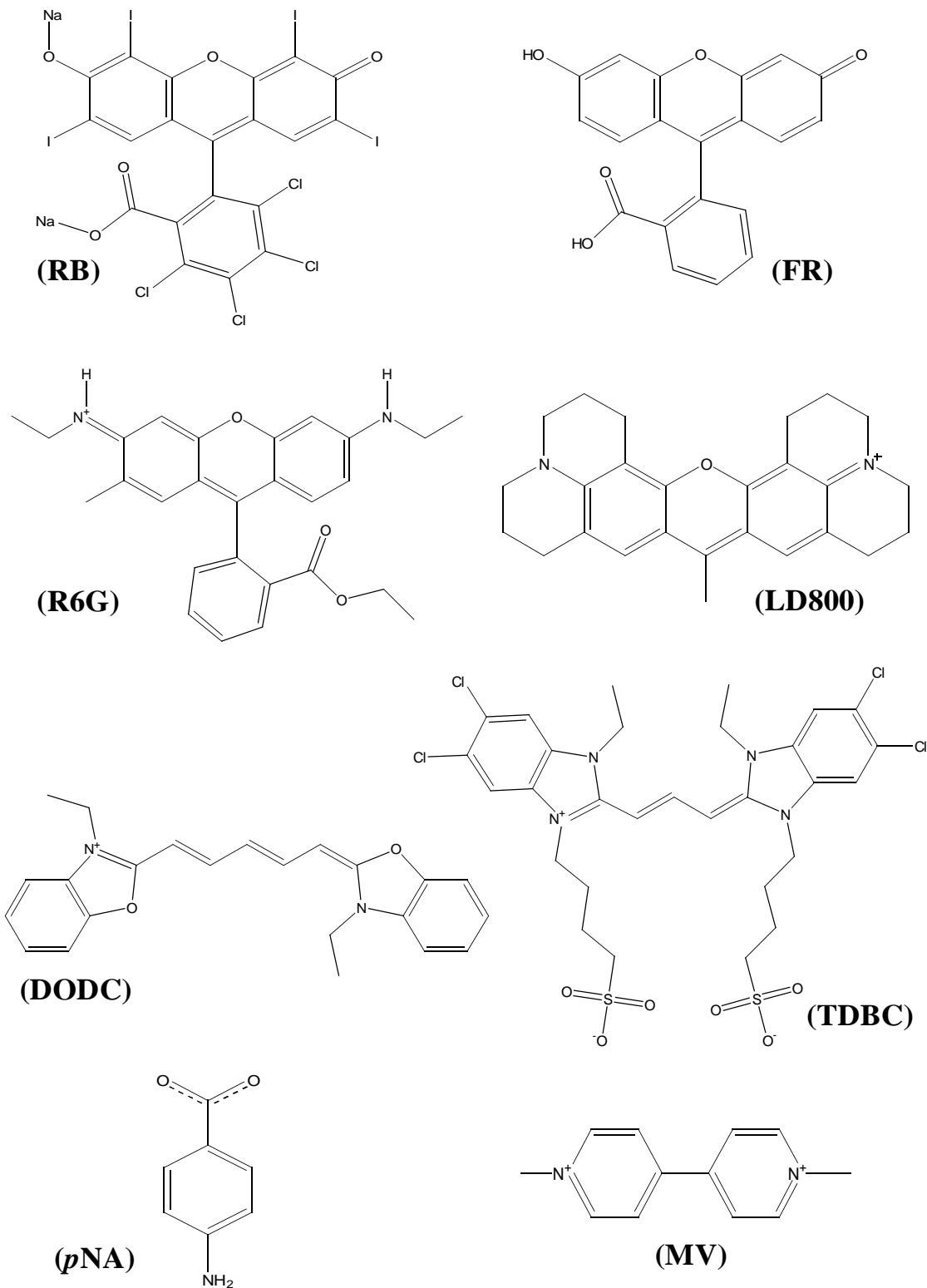
Figure 2-1. Molecular structures of the dyes and energy acceptors used in the fabrication of the composite films.

(BPB)

(CRV)

(SQ-Cy1)

(SQ-OH3)

(SQ-Cy2)
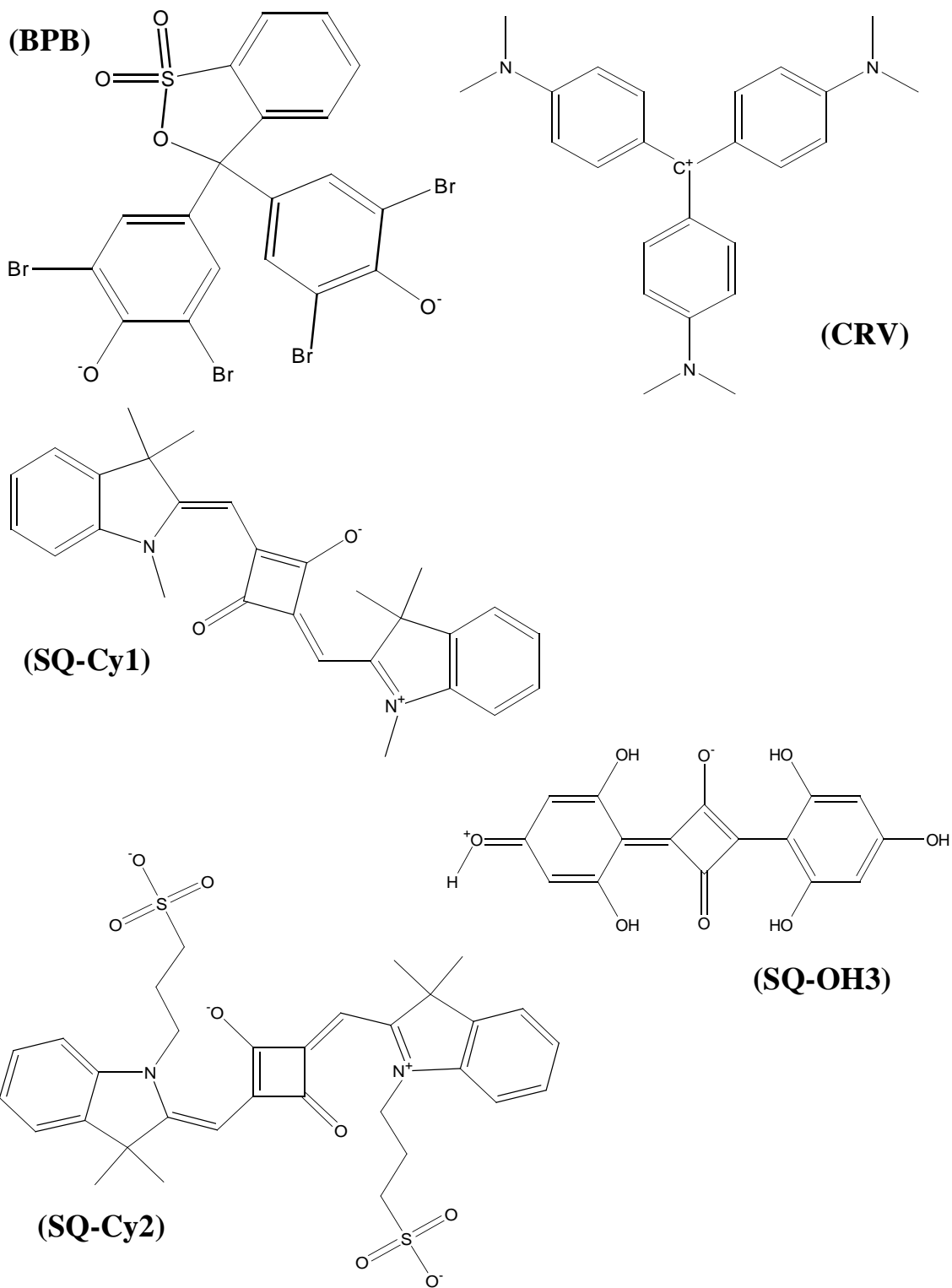
Continuation of Figure 2-1.

The dye containing precursor sol was prepared by adding various quantities of donor dye molecules and energy acceptors to aliquots of solP123. In all cases, sonication was used to aid in the dissolution process. Once the added molecules were dissolved, films were prepared by either drop-casting, dip-, or spin-coating onto glass coverslips or slides.

Drop-casting was done simple by taking a small volume (ca. 50 μl) of the solP123 and spreading across the surface of the glass substrate, and allowing it to air dry overnight. Dip-coating was done using a Nima Technologies D1L using a dipping and withdrawal speed of 68 mm/min. In one instance, when a drop-casted film was too optically dense, a vertical spin-coating [2] technique was used for film preparation. This method was used, rather than the customary approach where the substrate is mounted in such a way that the centrifugal force disperses material radially within the plane of the substrate, because the air flow across the substrate aids in the rapid formation of defect free films from the starting solP123. A diagram of the vertical spin-coating apparatus can be seen in Figure 2-2. The exact concentration of dyes and quenchers used was dependent on the particular molecules employed, however, the optical absorption of the obtained films was maintained between one and two absorbance units, whenever possible.
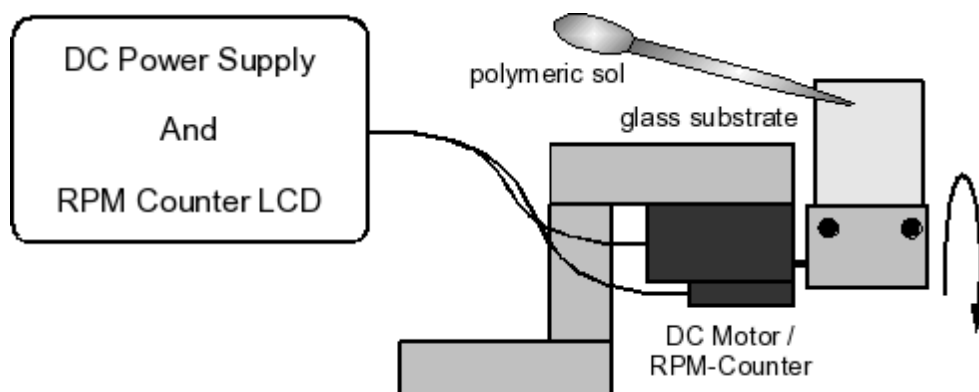
Figure 2-2. Diagram showing the components of the custom-built vertical spin-coating apparatus.

2.2 Squarylium Dye Synthesis

The squarylium dyes, 1,3-bis(3,3-dimethyl-2-methyleneindolenine)squarylium cyanine (SQ-Cy1), 1,3-bis[N-(3-sulfonylpropyl)-3,3-dimethyl-2-methyleneindolenine] squarylium cyanine (SQ-Cy2), and bis-(2,4,6-trihydroxyphenyl)squaraine (SQ-OH3) were synthesized according to the procedures outlined in the literature [3-5]. In a typical preparation of SQ-Cy1, 0.114 g of squaric acid (Fisher Scientific) and 0.606 g of 1,2,3,3-tetramethyl-3H-indolium iodide (Fisher Scientific) were place in a 50 ml round-bottom flask containing a 4 : 1 mixture of 1-butanol : toluene. This mixture was refluxed azeotropically for 3 hours, during which the color changed from yellow to dark green. Following refluxing, the solution was cooled to room temperature, and crystallization of the product was induced by scraping the walls of the flask with a glass rod. After cooling in an ice bath for an additional 2 hours, dark green crystals were recovered using vacuum filtration. The obtained crystals were subjected to several washes using diethyl ether to remove any impurities and then vacuumed dried. The crystalline product was placed in a glass vial and stored in the dark until needed. The preparation of SQ-Cy2 was carried out in a similar manner, except for the additional sulfonation step. To prepare the 2,3,3-trimethyl-1-(3-sulfopropyl)-3H-indolium starting material, 1.2 ml of 2,3,3-trimethylindolenine and 1.382 g of 1,3-propene sultone were placed in a 100 ml round-bottom flask containing 50 ml of toluene, and the mixture was refluxed for 18 hours. At the end of refluxing, crude, reddish-pink crystals were obtained. This crude product was purified, first by washing with 3 x 10 ml of acetone, followed by re-crystallizing using a 50 : 50 mixture of methanol : diethyl ether. The final product (SQ-Cy2) was obtained by refluxing 0.564 g of the now pure sulfonated indolium, and 0.114

g squaric acid in a 50 ml round-bottom flask containing 48.0 ml 1-butanol, 12.0 ml toluene, and 3.0 ml pyridine. Pyridine serves to catalyze the reaction, as well as being a counter ion in the final product. After refluxing, purified dark green crystals were obtained using the same washing and drying procedures used to obtain SQ-Cy1. The synthesis of SQ-OH3 follows the same procedure as that for SQ-Cy1, except that 0.253 g of phloroglucinol was substituted for the indolinium salt, and a 1 : 1 1-butanol : toluene mixture was used for refluxing. The purity of these dyes were ascertained by verifying that their resulting absorption spectra matched those of the literature [3-5]. The chemical structure for these dyes are also provided in Figure 2-1.

2.3 Quantum Chemical Calculations

As a result of the structural similarities between SQ-Cy1 and SQ-Cy2, computational studies were focused solely on SQ-Cy1. Time-dependent density functional theory (TD-DFT) was used to calculate conformational dependent ground- and excited-state energies, dipole moments, and the oscillator strengths for the $S_0 \rightarrow S_1$ and $S_0 \rightarrow S_2$ transitions. Ground- and excited-state geometries were optimized using density functional theory (DFT) with functionals [6], specifically, B3LYP, in which the exchange functional is of Becke's three parameter type, including gradient correction [7], and the correlation correction involves the gradient-corrected functional of Lee, Yang and Parr [8]. The basis set of split valence type 6-31G(d,p) [9], as contained in the Gaussian 98 software package, was used.

2.4 Instrumentation

UV-Vis absorption measurements of the coated films, and solution samples were performed using a Perkin-Elmer Lambda 18 spectrometer. Detector spectral response,

and lamp profile corrected fluorescence spectra were obtained using a Spex Fluorolog τ3 spectrometer. Film thickness was measured using a Mikropack NanoCalc-2000 spectroscopic reflectometer. Surface topology and roughness were measured using a Thermomicroscope Explorer^{TM} atomic force microscope (AFM). The pore structure of the obtained xerogel composites were determined from adsorption of nitrogen at its boiling point: a SAP 2010 (Micromeritics) was used for the measurements of adsorption isotherms. The pore structure determination of three xerogel samples was conducted. One sample was the control and was formed from the pure solP123 with nothing else added. The other contained ~ 0.2 wt% antimony doped tin oxide nanoparticles, Nanophase Technologies (NanoTek®), with an average particle size quoted as 30 nm. The final sample contained ~ 0.2 wt% of the squarylium dye, SQ-OH3.

2.5 Streak Camera System

For time dependent fluorescence measurements, a streak camera system, for which a simplified optical layout is depicted in Figure 2-3, was utilized. At the heart of this system is a Hamamatsu streak camera (Model C4334) and an optically coupled charge-coupled-device (CCD) array detector combination, positioned at the exit plane of a Chromex 250i imaging spectrometer. The limiting time resolution for the system, as indicated by the instrument response to the incident laser pulse of 100 fs, is ca. 30 ps. Fluorescence from the solution or film samples is coupled into the spectrometer through one of the outputs of fiber optic probe which can be positioned for either front-face (FF) or right-angle (RA) collection geometry. The remaining output of the fiber optic probe is coupled to an Ocean Optics miniature CCD spectrometer (Model HR4000). This setup allows the simultaneous acquisition of both the time-resolved and steady-state
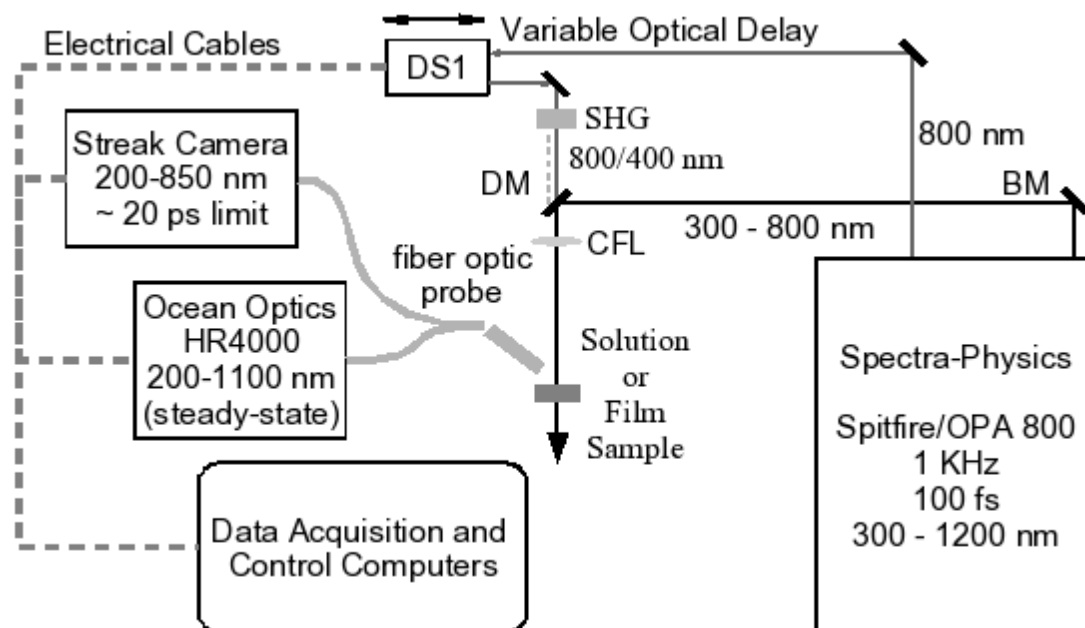
Figure 2-3. Simplified layout diagram of the streak camera system used to acquire simultaneous time-resolved, and steady-state fluorescence spectra. Delay stage 1 (DS1), broad band mirror (BM), dichroic mirror (DM), second harmonic generator (SHG), cylinder focusing lens (CFL).

fluorescence spectra. The excitation radiation was supplied by a femtosecond laser (Spectra Physics Spitfire), which was coupled to an optical parametric amplifier (OPA; Spectra Physics OPA800). The tunable output (300 - 800 nm) output from OPA, is directed to the sample using a series of mirrors and is horizontally focused using a cylinder lens. The residual 800 nm pump pulse from the OPA can also be employed as a secondary excitation source for conducting two-photon fluorescence studies, or its second harmonic (400 nm) can be used when high power excitation is needed. Temporal peak intensities for specific emission features were converted to lifetime coefficients using Hamamatsu TA-Fit or the InstruView program. The lifetime results from either program always agreed within one percent. Further details about the InstruView program are provided in section 2.6.

2.6 Femtosecond Pump-Probe System

The femtosecond pump-probe experimental setup for transient absorption

measurements was based, in part, on previously reported pump-probe setups [10,11].

The optical components and mechanical mounts were purchased from a variety of

commercial sources, or designed and fabricated in house. A simplified view of the

system is presented in Figure 2-3.

The pump and probe beams are supplied by the same laser source used for the streak

camera system above. In Figure 3, it can be seen that the two pump beams are possible.

The OPA provides pump beams in the spectral region from 300 - 800 nm whose energy

per pulse varies from 1 μJ to 18 μJ. For a higher energy pump beam the second

harmonic (400 nm) of the residual OPA pump is used. Prior to generating the 400 nm

beam, the residual beam goes through a 90/10 beam splitter, then a computer controlled

Figure 2-4. Femtosecond pump-probe system. Beam splitter (BS), white continuum generator (WCG).

optical delay stage (DS1). The energy of this beam is ca. 100 μJ. Either of these pump

beams first passes through a half-wave plate, which rotates the plane of polarization

accordingly, then to a long focal length lens, before being steered towards the sample.

The spot size of the pump beam at the sample ca. 1.5 mm in diameter. The white

continuum probe beam is generated by focusing the 10 % split of the residual OPA pump

into a 2 mm thick sapphire window. The white continuum is directed towards the second

optical delay stage (DS2) that allows for variability in the time at which it and the pump

beam arrive at the sample. Once the desired delay is imposed on the probe, it goes

through a 50/50 beam splitter, then the resulting beams are focused onto the sample with

a spot size less than 0.5 mm. The spectral profiles, shown in Figure 2-4 of the signal and

reference probe beams are detected by a dual channel Ocean Optics miniature

spectrometer (Model SD2000). The temporal resolution of this setup is ca. 200 fs, as
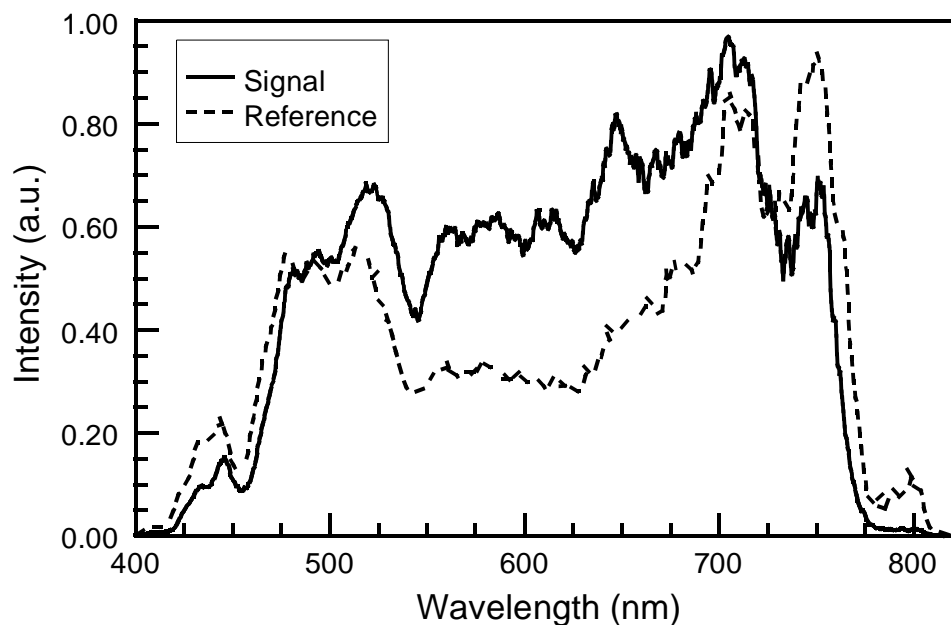
Figure 2-5. The spectra of the signal and reference probe beams. The differences in the spectra are due to the reflectance and transmission characteristics of the 50/50 beam splitter.

determined by sum frequency mixing of the pump and probe beams in a 1 mm thick BBO nonlinear crystal (Inrad). Sum frequency mixing is also used to determine time zero, the time at which the pump and probe beams have the maximum temporal overlap in the sample.

As a result of the high peak powers of the pump and probe beams used, steps must be taken to reduce the photo-degradation of the sample over the course of an experiment. For solution samples, a low volume flow-cell system, consisting of a miniature electric pump (Cole-Parmer) and a 0.5 mm pathlength quartz flow-cell (NSG Precision Cells) was used. For film samples, a custom designed computer controlled rotation stage was used. The rotation stage uses a two inch polarizer mount (Thorlabs) which holds the sample, and a high torque stepper motor (Lin Engineering) to drive the rotation. A picture of these systems are shown in Figure 2-6.

Synchronization of data collection, rotation stage motion, and translation of optical delay stages, was accomplished using a custom written Java based program called TimeStep. In Figure 2-7, a diagram showing the key functions of this program can be seen. The primary function of this program is the translation of the delay stages (DS1 and DS2) in a predetermined sequence, through a serial port connection to motorize stage controller A. Concurrent with the translation of the stages, is the renaming of data files from the spectrometer control software. If a film sample is being studied, the program also controls the rotation cell through a second serial port connection to the motorize stage controller B. Moreover, this program is also responsible for the acquisition and processing of the photodiode data from the oscilloscope through a GPIB connection.

Figure 2-6. Optical images of the custom designed low volume flow-cell (solution samples) and computer controlled rotation stage (film samples).
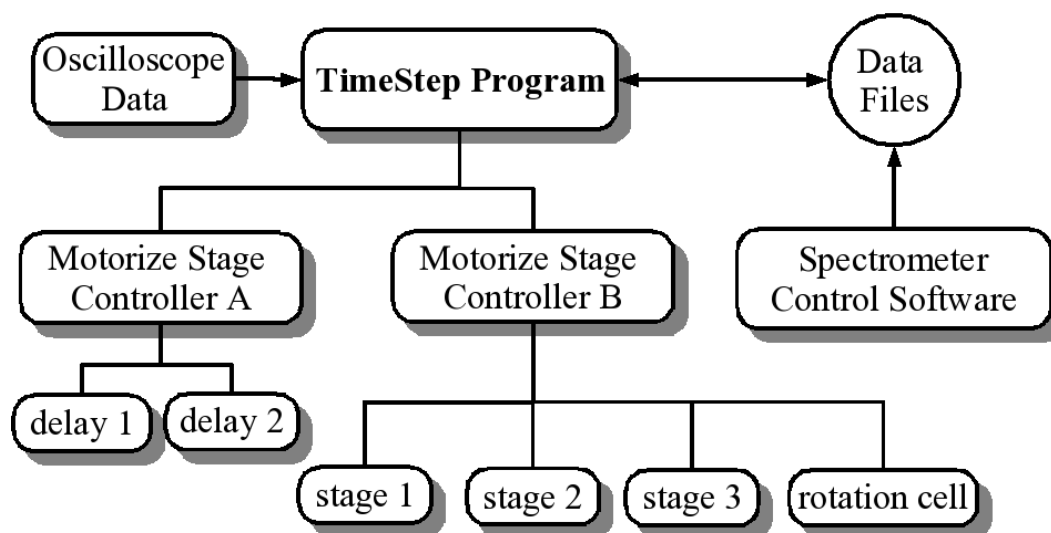
Figure 2-7. Diagram presenting the key functions of the custom Java based control and data acquisition program, TimeStep, for the pump-probe systems.

2.7 Data Analysis and Management

Experimental data collected from the various experiments was acquired with the specific goal of elucidating the nature of the ultrafast nonlinear optical responses of the composite films. From the corrected fluorescence and normalized absorption spectra, one can readily obtain the the quantum yield for radiative decay using the following equation [13],

$$Q = Q_R \frac{I}{I_R} \frac{OD_R}{OD} \frac{n^2}{n_R^2}. \tag{2.1}$$

Here, Q is the quantum yield of the unknown, Q_R is the quantum yield of the standard sample, I and I_R are the integrated intensity for the unknown and standard, respectively, OD is the optical density and n is the refractive index. The standard used for the quantum yield determination was cresyl violet in methanol, which has a quantum yield of 0.54 in the spectral range 600 - 650 nm [14]. From measured quantum yields, the rate constants for radiative, and non-radiative decay are obtained using the equations,

$$k_r = \frac{Q}{\tau}, \tag{2.2}$$

$$k_{nr} = \frac{(1 - Q)}{\tau}, \tag{2.3}$$

where k_r and k_{nr} are the radiative and nonradiative rate constants, and τ is the measured lifetime. The quantum yield, lifetime, and rate values allow the excite-state dynamics of the intercalated dyes to be ascertained to a high degree of certainty.

For films containing energy transfer complexes, the excited state dynamics and energy transfer parameters can be understood by employing an additional set of equations. The relevant energy transfer parameters that need to be obtained are the efficiency, transfer rate, and the spatial relationship between the donor and acceptor.

The efficiency of the energy transfer process is given by,

$$E = 1 - \frac{I}{I_0}.$$ (2.4)

The terms I_0 and I are the integrated fluorescence intensity of the donor in the absence and presence of an acceptor respectively [13]. When energy transfer occurs through an electron exchange mechanism, the well known Stern-Volmer equation, modified to account for a quenching sphere of action,

$$\frac{I_0}{I} = 1 + k_q \tau_0 [A] \exp([A] VN / 1000),$$ (2.5)

can be used to obtain the electron transfer rate. In this expression, k_q is the bimolecular quenching constant, τ_0, is the measured lifetime of the donor, and [A] is the concentration of the acceptor. For energy exchange by the Coulombic mechanism, the rate is given by the following equation,

$$k_{ET} = \frac{1}{\tau_0} \left[\frac{R_0}{r} \right]^6,$$ (2.6)

where R_0 is the Förster distance and r is the donor-acceptor distance. The Förster distance specifies the donor-acceptor distance at which half the excited donor molecules will undergo energy transfer. This equation is the same as equation 1.7, except the experimental parameters have been folded into R_0, and R_{DA} is now stated as r. Since the wavelength of the collected data is expressed in nanometers, and the donor and acceptor can be assumed to be randomly oriented within the film, the Förster distance, in angstroms, can be conveniently given by,

$$R_0 = 0.211 \left[(2/3)^2 n^{-4} Q_D J(\lambda) \right]^{1/6},$$ (2.7)

where the term $J(\lambda)$ is the normalized spectral overlap integral. The spectral overlap defines the area where the fluorescence curve of the donor, and the absorption curve of the acceptor overlap with each other. The greater this overlap, the bigger R_0 and vice

versa. Having obtained both E and R_0 from the experimental data, one can now use the following equation,

$$r = R_0 \left[\frac{(1 - E)}{E} \right]^{1/6},$$ (2.8)

to derive the average donor-acceptor distance, r, in angstroms.

Evident by the above set of equations, is that extraction of the relevant information from the experimental data requires a substantial number of mathematical operations to be performed. In order to expedite the analysis process, a custom Java based program, InstruView [15], was developed. The diagram illustrating the various functions of this program is presented in Figure 2-8. Central to this program, is the ability to store and organize the data from various instruments in a common data format, and to apply the required mathematical operations to this data, in order to obtain the desired results. Whereas, several tedious operations would have to be done to obtain the energy transfer parameters using a typical scientific analysis program, now, only a few mouse clicks is all that is needed. Another advantage of having a common data format, is that it makes it possible to rapidly search and visualize large data sets in much the same way one can do with a collection of MP3 music files.
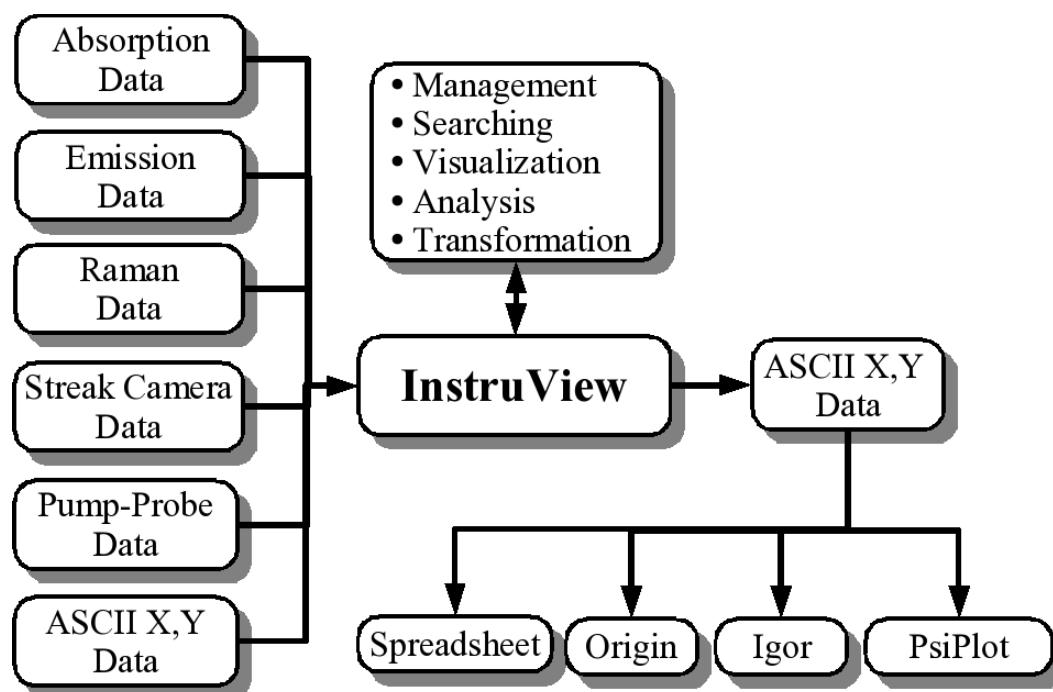
Figure 2-8. Diagram showing the key functions of the custom Java based data management, visualization, and analysis program, InstruView, used to streamline the data analysis process.

3. Composite Film and Dye Aggregation

3.1 Introduction

In deciding the material for the thin-film photonic layer, a number of factors need to be taken into account. First and foremost, is the ability of the film's matrix to effectively solubilize relatively high concentrations (10^{-3} to 10^{-2} M) of the various dye and quencher molecules being used. Such high concentrations is necessitated by the need for the films to exhibit appreciable absorbance (0.5 to 1.5 absorbance units), even when their thickness is as little as 200 nm. If the molecules are not effectively dispersed within the host matrix, the optical as well as the physical properties of the films tend to be negatively influenced. For example, broadening of the dye's absorption band along with loss in its intensity, and decrease light transmission through the film, are some of the adverse effects that might result. The processability and overall quality of the resultant films are the next factors to be considered when deciding upon the film's composition. Film fabrication needs to be conducted with relative ease, using the proven deposition techniques of drop-casting, dip-, or spin-coating. This would allow a large number of films, containing a variety of dyes with, or without additional molecular quenchers, to be evaluated on an expeditious basis. The greater the number of film/dye combinations studied, the better the chances of finding one or more that possesses the desired properties. Irrespective of the fabrication procedure used, the films must be of the highest optical quality in order to minimize signal looses due to light scattering from internal defects within the matrix, such as pits and cracks. As a result, the materials that are most suited for use as the thin-film photonic layer are polymers, sol-gel derived inorganic xerogels, or organic/inorganic composites.

When it comes to polymer films, a significant volume of work exist on the intercalation of low molecular weight organic dyes, and the resulting photophysical properties of the obtained films [1-5]. As a matter of fact, the use of dye containing, conductive polymer films, is widely employed in OLED industry to tune the emitted color of the display material [6,7]. Given the extensive use of dye doped polymer films, it seems only natural to employ them as the photonic layer. However, use of polymer films present a significant drawback, that, in this author's opinion, would forestall their use as the photonic layer. Due to the high peak power lasers involved in the operation of a time-to-space converter, it is likely that irreversible photo-bleaching of the dyes within the polymer matrix would result. Upon photo excitation, the dyes may undergo inter-system crossing (ISC) to the long lived triplet state, then chemically react with the surrounding polymer environment. This would lead to the formation of radical species which would no longer absorb at the wavelength of the gating pulse, causing the optical switching device to become inoperative. This kind of photochemical reaction, between the intercalated dyes and the polymer network, has been shown to be a primary dye degradation pathway [8-10].

Dyes incorporated into sol-gel derived inorganic films, specifically silica based, would not undergo such photochemical degradation to the same extent as in the presence of a polymer environment. This is due to the photochemically inert nature of silica matrices, as discussed in chapter 1. Dye degradation still occurs through the formation of a triplet state, but now the reactive species is either molecular oxygen, or another dye molecule, but not the host matrix [11]. The silica matrix does suffer from some disadvantages though. For one, the polar nature of the matrix makes it difficult to

effectively solubilize some of the hydrophobic dyes used in the study. Secondly, and more problematic are the chemical reactions that occur between the silica matrix as it forms, and a few of the dyes. In the case of cyanine-type squarylium dyes, such a reaction leads to a significant loss in the dye's absorption band over a period of several days. The loss in the absorption intensity is most likely attributable to the reaction of one of the oxygens on the central four member ring of the squarylium dye with a silicon atom to form the colorless *leuco* form of the dye [12]. Limited film fabrication options is another disadvantage that results from using of sol-gel derived silica films. Detailed studies looking at the experimental parameters that leads to the highest quality silica films, show that for spin-coated films, the spinning speed and the viscosity of the precursor sol must be judiciously controlled [13]. Such requirements would serve to limit the number of dye systems that can be evaluated. Furthermore, fabrication using the other, more facile methods mentioned above results in films that are laden with defects.

The ease of fabrication of the polymer films, and the photochemical stability of the silica films, can be attained in a single film by combining elements of these two systems. Such composite films, containing inorganic and organic domains, can be obtained using two different approaches. The most straight forward of these is the addition of low molecular weight organic molecules into the precursor sol. The presence of the organic molecules would serve to both improve the processability of the sol, and to protect the dye molecules from the reactive silanol groups of the silica network [14]. Improved processabilty arises because the organic molecules act as a drying controlling agent (DCA), controlling the rate of solvent evaporation, thereby, minimizing the formation of

defects in the resulting material. This effect, however, is limited to concentration range in which the organic additive and the silica sol remain as a homogeneous mixture. If phase separation takes place, high quality films can no longer be obtained, no matter the fabrication process used. The second, more involved approach, requires the use of organically modified silicates (ORMOSiL) with specific functional groups. The composite materials obtained using these modified silicates have already been shown to be well suited for the incorporation of a range of dye molecules, with excellent retention of their optical properties [15-17]. These ORMOSiL also have the advantage, that the weight percent of the organic component can be much higher since no phase separation can occur. This higher organic content, translates into a greater ability to solubilize the added dye molecules, but this turns out be disadvantageous when the goal is the incorporation of dye aggregates, or energy transfer complexes, as is the case in this work.

3.2 Silica/Pluronic P123 Composite

Whether it is the formation of dye aggregates, or energy transfer complexes within the films, both require a microenvironment that favors intramolecular interactions taking place. In solution, the surface of nanoparticles, or core of self-assembled mesostructures, i.e. micelles, formed by surfactant molecules, provides such an environment [18,19]. Unfortunately, the microenvironment within a silica, or hybrid silica/organic film is one that favors the isolation of the individual dye molecules at the concentrations necessary to obtain the desired optical and physical properties of the film. At higher concentrations, aggregation or formation of energy transfer complexes would in fact occur, but now the films would be too optically dense, and significant defects would most likely be present, due to phase separation taking place. An elegant solution to this

problem, and the one that is employed, is to incorporate self-assembled mesostructures within silica matrix. These mesostructures would provided a favorable microenvironment for the dyes and/or quenchers to reside in, while at the same time, reducing the effective volume of the film. The volume is effectively reduced because the hydrophobic nature of the dyes makes it energetically favorable for them to reside predominantly within the mesostructures, and not within the more polar silica framework.

Incorporation of such micelles at relatively high weight content (ca. 50 %) into the silica framework presented a bit of a challenge though. Since the ethanol content of the precursor sol is so high, few surfactants would form stable micelles at the required concentration. Also, because of the surface charges on the silica nanoparticles present in the sol, only nonionic surfactants can be used. Surfactants which are charged, either negative or positive, tend to destabilize the sol mixture by causing the silica nanoparticles to aggregate together. Though several nonionic surfactants are tried, the one that results in the highest quality films is Pluronic P123. The chemical structure as well as the cartoon representation for this molecule is presented in Figure 3-1. One of the most remarkable properties of the composite films derived from using this surfactant, is the shear ease of fabricating high quality films using the different casting methods.

$$\text{HO[-CH}_2\text{-CH}_2\text{-O]}_{20}\text{[-CH-CH}_2\text{-O-]}_{70}\text{[-CH}_2\text{-CH}_2\text{-O-]}_{20}\text{H}$$
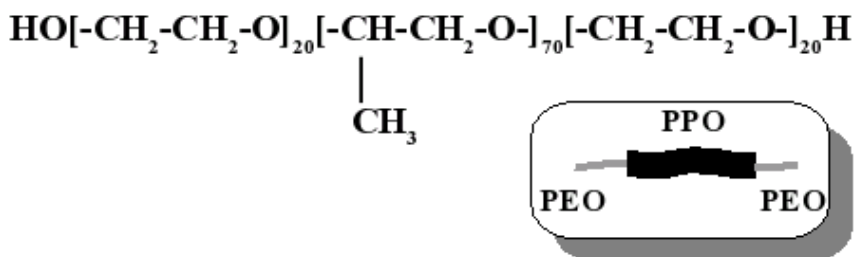
Figure 3-1. The molecular structure of the non-ionic surfactant Pluronic P123. The insert show the cartoon representation for this molecule. PEO and PPO are abbreviations for poly(ethylene oxide) and poly(propylene oxide), respectively.

Figure 3-2a and 3-2b show the AFM topographic scans of a drop-casted and dip-coated

films respectively. The diagonal features seen in the drop-casted image are small surface

ripples that occurred during the solvent evaporation process, and their consistency point

to a surface with very little defects. The average thickness for dip-coated films are 200 ±

4 nm, whereas drop-casted films have an average thickness of approximately 6 ± 0.5 μm.

Film thicknesses for the drop-casted films are less exact because little attention is given

to the exact quantity of sol used in making them. The more sol used, the thicker the film,

and vice versa. A remarkable property of these two films, is that even though there is a

substantial difference in their thickness, there is little variation in their surface roughness.

Dip-coated films had a RMS surface roughness of 1.2 nm, while films prepared by the

drop-casting method have an average roughness only slightly greater at 2.4 nm. This

indicates that the structural integrity of the films is maintained over a wide thickness

range, which is generally not the case for pure silica films [13]. Aside from exhibiting

good physical properties, these films also have excellent transparency throughout the

visible and near-IR region, with the average percent transmission of the films being

drop-casted   dip-coated
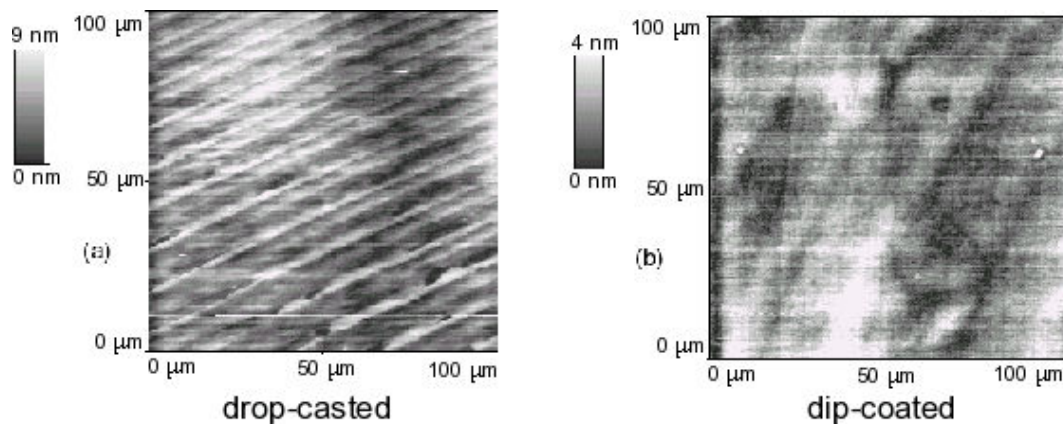
Figure 3-2. AFM topographic images of a 100 x 100 μm area of a drop-casted (a) and a
dip-coated (b) film. The ripples seen in image for the drop-casted film are due to the
solvent evaporation process.

greater than that of the bare substrates. This increase results from the well known anti-reflective properties inherent to silica or silica/organic hybrid films [20-22].

The outstanding processability and optical properties of these composite films are no doubt due to their inorganic/organic hybrid nature, more specifically, the interaction between the silicate framework and the non-ionic surfactant Pluronic P123. Given the concentration and the temperature used to prepare the sol, individual Pluronic P123 molecules are expected to self-assemble into micelle structures, of various shapes and sizes, that serve as a template around which the silica framework forms, once the condensation process has been initiated [23-25]. Within the resulting films or monoliths, these supramolecular assemblies occupy a significant portion of the overall volume, leading to distinct hydrophobic domains, at the core of Pluronic P123 assemblies, and hydrophilic domains at the interfacial regions between the hydrophilic poly(ethylene oxide) blocks of Pluronic P123 molecules and silanol groups of the silica framework. It is those hydrophobic regions that can serve as favorable microenvironments in which dye aggregation can take place and dye/quencher complexes can form. Support for the existence of these mesostructures derives from the fact that when no dye is added to the sol, the resulting xerogel material is nonporous. However, upon addition of the squarylium dye, SQ-OH3, the xerogel becomes mesoporous, with an average pore size distribution of 2.7 ± 0.1 nm. As a control, antimony doped tin oxide nanoparticles (Nanophase Technologies), with an average particle size distribution of 20 nm is added to the sol at the same weight percent as the dye. In this case, the resulting xerogel is only slightly porous. The porosity difference between the dye and nanoparticle containing xerogels can be seen in Figure 3-3. This difference can be understood by looking at what

type (rod or spherically shaped) of mesostructures that is energetically favored upon dye or nanoparticle addition.

In the absence of the hydrophobic dye molecules, or when nanoparticles are present, the Pluronic P123 are most likely assembled as spherically shaped mesostructures, or micelles, causing the matrix to have little porosity. Micelles are energetically favored because they allowed the hydrophobic PPO blocks of the Pluronic P123 to remain separated from either the hydrophilic silica framework, or the nanoparticle's surface. However, when dye molecules are present, rod shape mesostructures are now the energetically favorable structure. The hydrophobic interactions between the dyes and PPO block of Pluronic P123 molecules would drive the formation of rod-shaped mesostructures, because given the concentration of both species in the sol, that would be
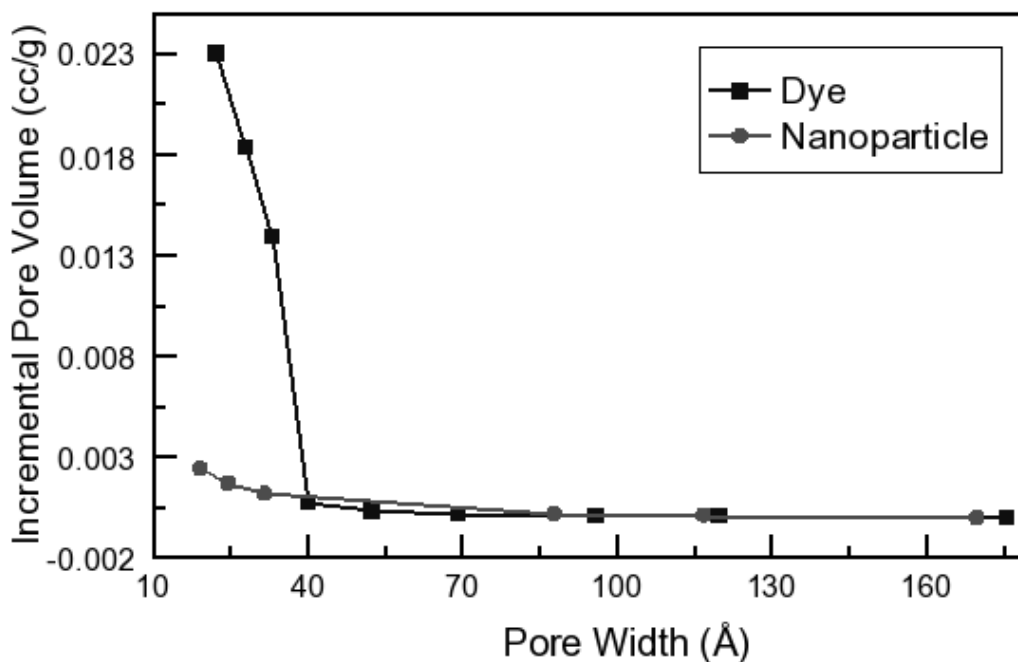
Figure 3-3. Plot of pore volume versus pore diameter of the composite xerogel materials containing a squarylium dye, or nanoparticles at equivalent weight percent.

the structure best able to segregate the hydrophilic and hydrophobic elements within the film. Since these rods, unlike micelles, are open ended, the matrix they reside in attains a certain level of porosity. Mesoporous silica and tinania films containing highly ordered pore structure have already been fabricated using these rods [26] as templates, so it is not unreasonable to believe the current films possess a similar pore structure. A cartoon suggesting how the dye and/or quencher, Pluronic P123, and framework silica likely interact to form the composite film is shown in Figure 3-4.
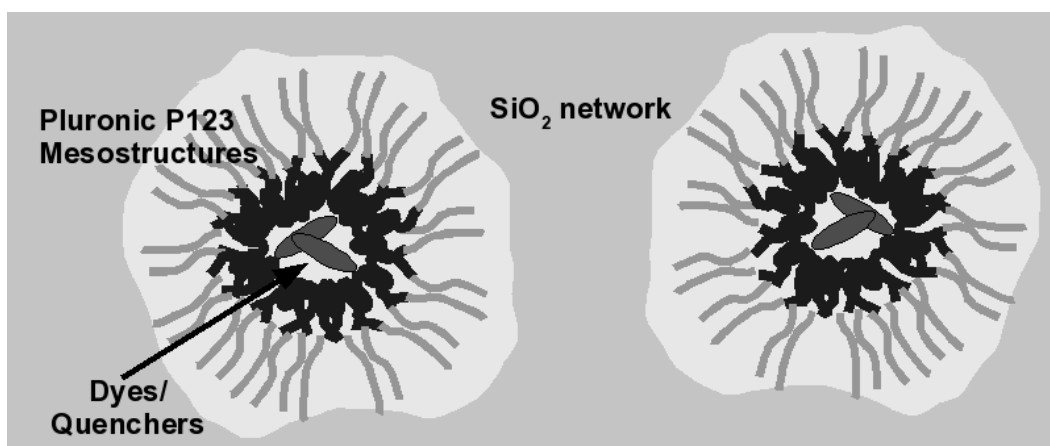
Figure 3-4. Illustration showing internal structure silica/Pluronic P123 films. The hydrophobic organic dyes and quenchers selectively reside within the pores of these self-assembled mesostructures.

3.3 TDBC J-type Aggregates

The formation of J- or H-aggregates in dye systems, have long been known to lead to significant, ultrafast nonlinear optical responses as a result of exciton dynamics [27-31]. Whereas, free or monomer dye molecules exhibit excited state lifetimes in the tens of picoseconds to the several nanoseconds, as part of a molecular aggregate, those lifetimes were reduced down to a few picoseconds. Such is the optical response of these aggregates, that a neat film of J-aggregated squarylium dye has already been employed

as the photonic layer in an all-optical time-to-space converter [32]. The exciton

dynamics leading to ultrafast excited state deactivation can be understood by using a

model system consisting of a homogeneous one-dimensional Frenkel exciton delocalized

over several molecules within the coherent aggregate [33]. When the incident excitation

energy is above a certain threshold, as would be the case in an optical switching device, a

two-exciton state can be created through the absorption of a second photon by the one-

exciton aggregate. The occupancy of the coherent aggregate by multiple excitons leads

to the process of exciton-exciton annihilation. This process can be represented as

follows:

$$|1e\rangle + |1e\rangle \xrightarrow{\text{Auger process}} |2e\rangle + |0e\rangle \xrightarrow[\text{photon emission}]{\text{phonon or}} |1e\rangle + |0e\rangle. \tag{3.1}$$
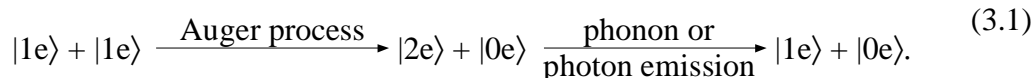
As a result of long-range interaction between the excitons, one of them relaxes to the

ground state, 0e, through non-radiative recombination by the Auger process [34], while

the other gets promoted to the two-exciton state, 2e, and immediately relaxes back down

to the one-exciton state, 1e. Relaxation from the two-exciton to one-exciton state can

occur by the nonradiative phonon vibrations within the aggregate structure, or radiative

decay. The latter is what gives rise to the superradiance phenomena observed for the J-

aggregates of certain cyanine dyes by Akins et al. [35]. Regardless of the deactivation

mechanism, the transition from the two-exciton to the one-exciton state has been shown

to occur in the femtosecond domain, while the transition from the one-exciton to the

ground state occurs in less than 2 picoseconds [33].

Along with a greatly reduced excited state lifetime, superradiance (viz. coherent

spontaneous emission (CSE)) also results in the J-aggregate having a substantially higher

quantum yield of fluorescence compared to the monomer [33]. This is of importance

because such rapid deactivation through a radiative pathway is desirable over deactivation through a thermal relaxation pathway. The latter will inherently result in thermal decomposition of the dye units in the aggregate. As such, it helps to have a better understanding of this phenomena. Superradiance is comparable to a stimulated emission process in which a photon emitted from the 2e to the 1e state causes an identical photon to be emitted from the 1e state simultaneously. This can occur because the energy spacing between the ground and 1e state is close to the spacing between the 1e and 2e state. The spacing is not identical, however, and this causes the stimulated photon to be slighter higher in energy than an unstimulated photon from the 1e state. In any case, it is this simultaneous emission of photons that causes the significant reduction in aggregates excited state lifetime, as well as enhanced fluorescence.

The primary factors governing the ultrafast exciton dynamics, are the aggregate's structure, solvent interactions, and static and dynamic disordering. Since the aggregate structures that will be discussed here were intercalated into a solid matrix, solvent interactions are not expected to affect to the overall ultrafast exciton dynamics. However, the other factors will, and among those, probable the most deterministic will be the overall aggregate structure. One-dimensional J-aggregates have been shown to possess a hierarchical structure consisting of small-sized coherent aggregates, and large-scaled, rod-shaped aggregates whose subunits are composed of the coherent aggregates. The coherent aggregates, in which exciton de-localization occurs, have been termed mesoaggregates, while the rod-shaped aggregates are called macroaggregates [36]. In solution, the size of these aggregates will be dictated by the solute-solvent interactions and temperature, but within a solid matrix, their size will depend on the free space within

the matrix. Moreover, since the aggregate's optical properties are intrinsically linked to its structural properties, there will certainly be spectral differences between the aggregates in solution and those confined within a matrix. As a result of a higher degree of static disordering [37] within the aggregates, the aggregate's absorption band will exhibit smaller Stoke shifts than in solution. The H-aggregate band will be less shifted to the blue, while the J-aggregate band will be less shifted to the red, relative to the monomer band. Also, significant spectrally broadening would likely occur, due to the coexistence of aggregates with slightly different coherence length. Such spectral changes in the J-band of a cyanine dye, have already been observed upon encapsulation into mesoporous silicates [38,39].

In order to study aggregate formation within the composite films, the cyanine dye TDBC is used. The chemical structure, as well as a cartoon representation of the head-to-tail stacking involved in J-aggregate formation of this dye is shown in Figure 3-5. Three other cyanine dyes were tried, but none resulted in films exhibiting a well defined J-aggregate band, or J-band for short. In Figure 3-6, the absorption spectra of the TDBC J-aggregate in an aqueous solution containing silica nanoparticles, monomer within the film, and mixed monomer/J-aggregate within the film are presented. The respective TDBC concentration for the samples are 2.4×10^{-5} M, 1.75 mg/ml, and 3.63 mg/ml (mg/ml refers to mg of TDBC to ml of precursor sol). The J-band in solution is centered at 589 nm. In the film, the monomer band occurrs at 526 nm when no aggregate is present, but shifted to 531 nm when it is. The blue shoulder is also enhanced when aggregates are present, possible due to the formation of dimers, or vibronic coupling to the aggregates phonon modes. The J-band within the film is much less red-shifted, now
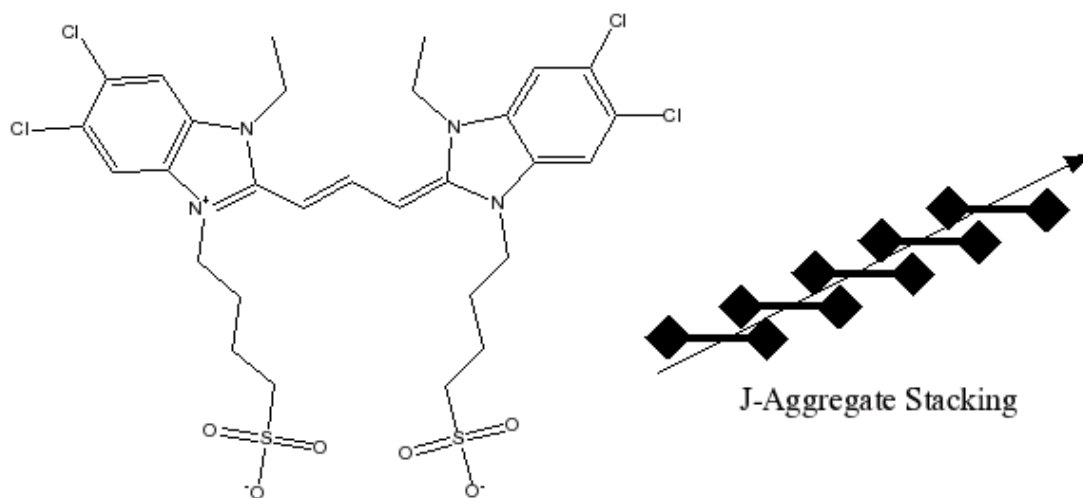
Figure 3-5. The chemical structure of TDBC with a cartoon representation of the head-to-tail stacking involved in the formation of J-aggregates. The arrow indicates the slip angle between the individual dye molecules.
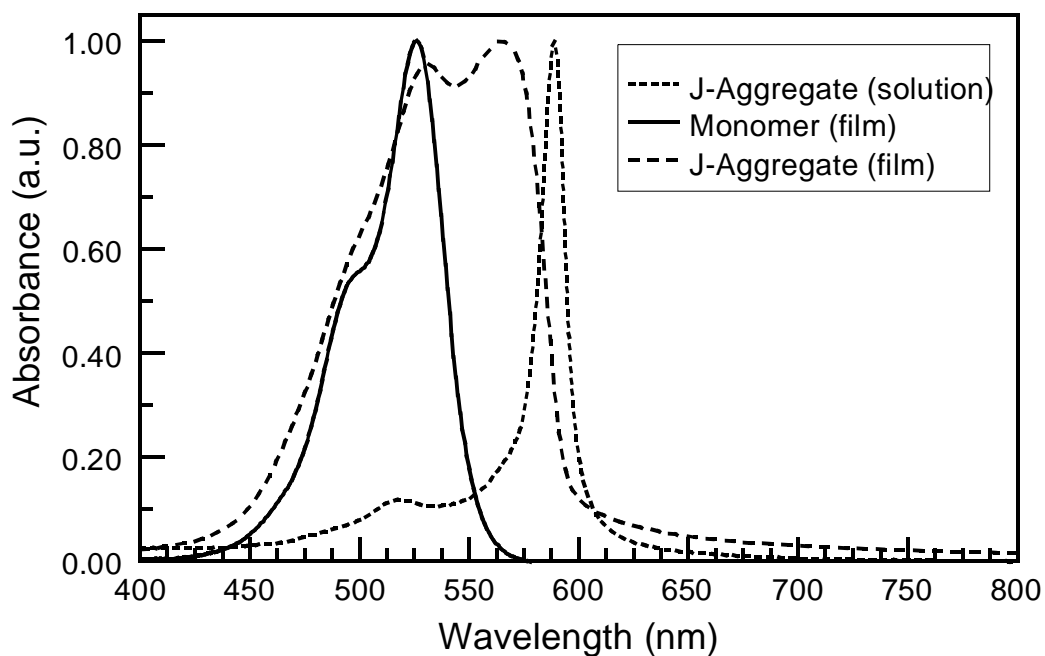
Figure 3-6. The normalized absorption spectra of TDBC aqueous solution based J-aggregate (short dash line), along with the composite film based monomer (solid line) and mixed monomer/J-aggregate (long dash line).

occurring at 565 nm. The significant spectral overlap between the monomer and the aggregate band, in the film, might be due to shorter coherence length for the J-aggregate than in the solution. The decreased steepness of the wing of the J-band past 600 nm is also another unique feature seen in the film's absorption spectrum. This might be indicative of the coexistence of various, as defined by differences in their coherence length, J-type aggregates within the composite film.

The steady-state fluorescence spectrum of the J-type aggregate within the film is also a point of interest. The normalized fluorescence spectra for the solution based J-aggregate, the film based monomer, and aggregate systems are shown in Figure 3-7. The fluorescence spectrum for the solution based J-aggregate is characterized by a relatively narrow band, with the maximum occurring at 594 nm, while the film based monomer's
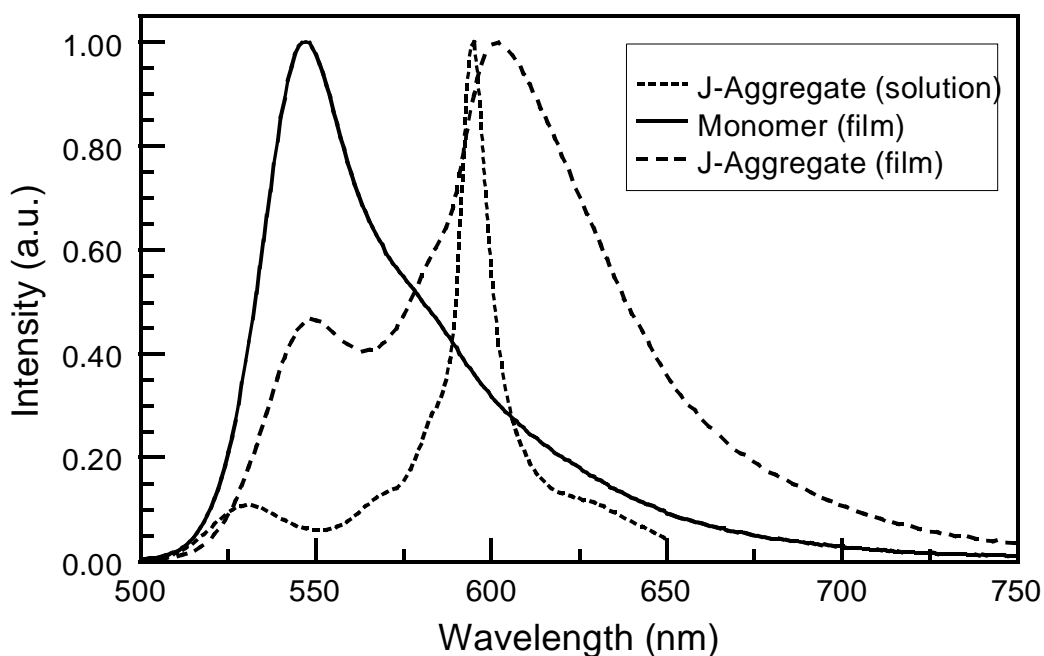
Figure 3-7. The normalized fluorescence spectra of TDBC solution based J-aggregate (short dash line) (λ_{ex} 480 nm), along with the composite film based monomer (solid line) (λ_{ex} 475 nm) and J-aggregate (long dash line) (λ_{ex} 475 nm).

fluorescence maximum occurs at 547 nm. The film based aggregate spectrum consists of two bands, whose maxima occurred at 547 nm and 601 nm. The lower intensity peak at 547 nm is undoubtedly that of the monomer, and the one at 601 nm, undoubtedly that of the aggregate. The broad nature of the aggregate's fluorescence band further supports the above contention about the existence of an ensemble of J-type aggregates within the composite film.

Although the reduced red-shift for the TDBC J-band is indicative of a smaller number of molecules coherently coupled to form the mesoaggregate, it does not indicate the number of mesoaggregates that compromise the macroaggregate. To get an idea of this, an AFM topographic scan was acquired, and the resulting image can be seen in Figure 3-8. Unlike the pristine composite film, the film containing TDBC aggregates contained micron-sized (in width) surface features, which are most likely macroaggregates. Formation of these macroaggregates conceivable occurs as follows. When TDBC is added to the precursor sol at a certain weight percent, aggregate formation takes place, as is indicated by the opaque nature of the resulting mixture. The formation of the Pluronic P123 rod-shaped mesostructures around these aggregates limited their size in one direction. This would explain the reduced coherence length. However, many of these aggregates would be stacked within this rod. Such stacking would have little effect on the observed J-band, since only weak electronic coupling would be expected to exists between the individual coherent aggregates. If strong electronic coupling did in fact occur, then the J-band would be expected to under go a greater red-shift and it would be substantially broadened due to increased exciton-exciton interactions. None of these effects are observed in the absorption or the fluorescence
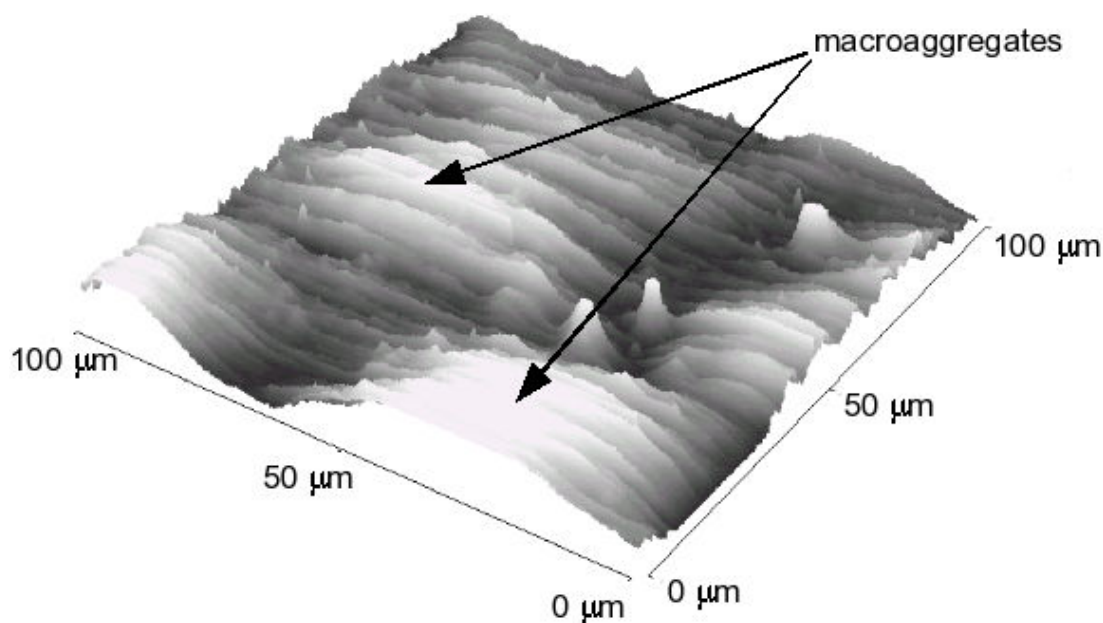
Figure 3-8. A 3D AFM topographic image of a 100 x 100 μm area of a drop-casted film containing TDBC J-aggregates. The arrows points to the micron size, in width, macroaggregates which are dispersed throughout the surface.

spectra. Upon solvent evaporation, many of these rod-like mesostructures containing the

aggregates, would cluster together to form the structures seen in the AFM image.

Formation of the J-type aggregates, as indicated by the absorption and fluorescence

spectra, is not enough to determine the applicability of these films as the photonic layer,

though. These J-type aggregates have to also exhibit rapid excited state deactivation.

The simplest way to ascertain this is by studying their fluorescence decay dynamics.

Due to stimulated emission from a two-exciton photon causing a one-exciton photon to

be emitted (i.e. superradiance), ultrafast excited state deactivation would take place. This

would show up as a rapid, instrument limited, intensity decrease in the time-resolved

fluorescence decay profile. In Figure 3-9, the decay profiles for the monomer and

aggregate within the film are presented, and for comparison, their solution based counter parts are also provided. In solution, the mean lifetime for the monomer is 151 ps, and the J-aggregate is 150 ps. The monomers and J-aggregate have similar lifetime because it has been shown that for cyanine dyes, a rapid, barrierless *cis-trans* isomerization process is the dominant deactivation pathway [40].

The decay dynamics for TDBC within the composite is vastly different. For one, the monomer's mean lifetime increases to 547 ps, which is attributable to inhibition of the isomerization process; it should be noted that the monomer's decay profile can only be fitted using a three component model whose lifetime values are 1074 ps (15%), 670 (45%), and 211 ps (40%). Secondly, and more importantly, the decay profile of the J-type aggregates exhibites a dominant instrument limited component, 27 ps (63%), along
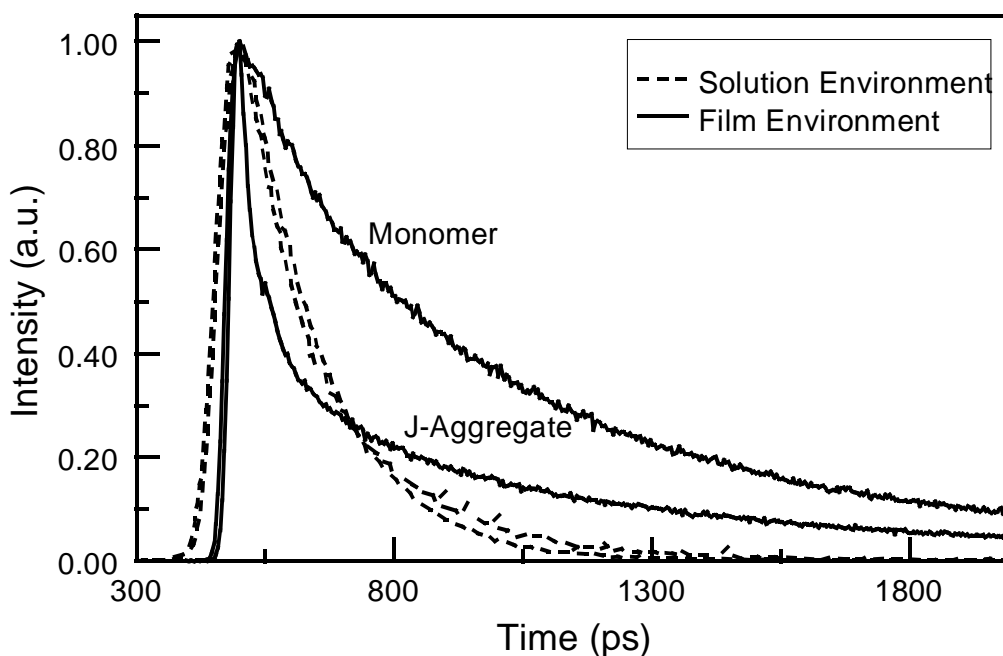
Figure 3-9. The fluorescence decay profiles of TDBC monomer and J-aggregate in solution (dash lines), and their counterparts within the composite film.

with two less significant, longer lived components, with lifetime values of 155 ps (20%) and 863 ps (17%). Since the excitation (475 nm) is resonant with the monomer's absorption band, the J-aggregate fluorescence occurs through an energy transfer process from the monomer to the aggregate. This energy transfer process, in conjunction with the shorter coherence length of the film based aggregate, increased the likelihood that a two-exciton state would form, causing the decay dynamics to be dominated by stimulated emission i.e. superradiance, and exciton-exciton annihilation. Additional evidence for this can be seen in Figure 3-10, which shows the time-resolved spectral evolution of the aggregate's fluorescence acquired using the streak camera system. Within the initial 200 ps following excitation with the 100 fs laser pulses, the aggregate's fluorescence band had a maximum at 594 nm, but as time progressed, this band
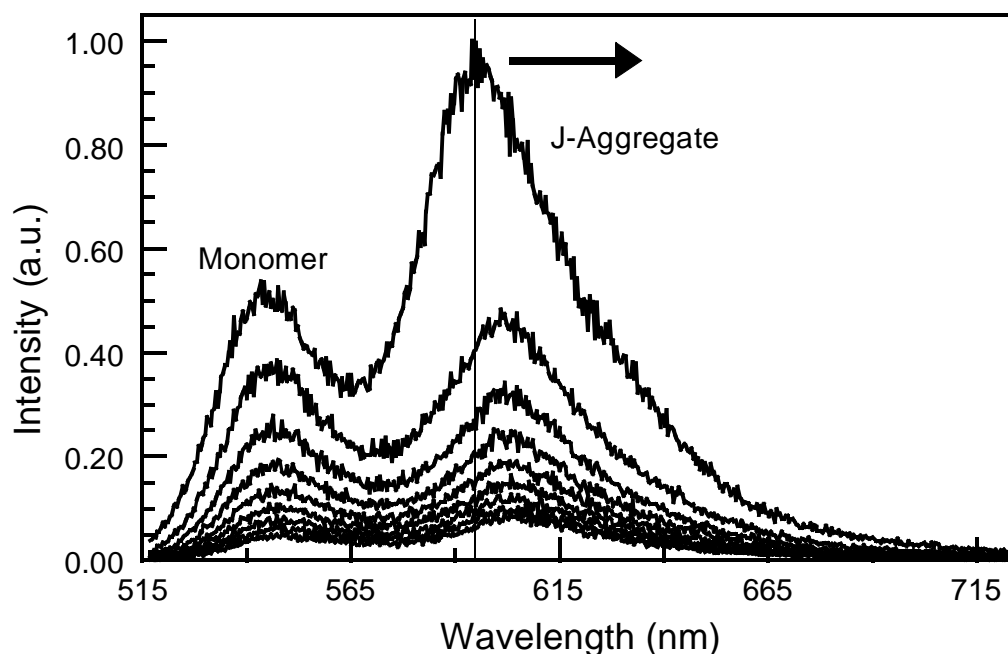
Figure 3-10. The time-resolved fluorescence spectra of the composite film based TDBC J-aggregate. Each spectra represents a 200 ps time window and as can be seen, the J-aggregate's fluorescence maximum undergoes a shift to the red as time progresses.

progressively shifted to the red. This initial blue-shift in the fluorescence maximum is indicative of a stimulated emission process [41].

3.4 DODC H-type Aggregates

In contrast to TDBC, incorporation of the cyanine dye DODC within the composite film, results in the formation of H-type aggregates. The chemical structure, as well as a cartoon representation of the parallel stacking involved in H-aggregate formation of this dye is shown in Figure 3-11. Like the aggregates of TDBC, aggregates of DODC exhibited distinct spectroscopic features from those formed in solution. In Figure 3-12 it can be seen that the absorption spectrum of DODC in an aqueous solution containing silica nanoparticles is dominated by a band at 497 nm, corresponding to the H-aggregate, and a lower intensity band at 577 nm, corresponding to the monomer. In the same figure, the spectra of the monomer and aggregate within the film are also presented. The respective DODC concentration for these samples are 4.8 x 10^{-5} M, 0.46 mg/ml, and 4.15 mg/ml. The monomer band is red-shifted to 590 nm, as a result of the less polar environment within the composite film, while the aggregate band is now centered at 542 nm. There is also a smaller Stokes shift between the aggregate and the monomer band
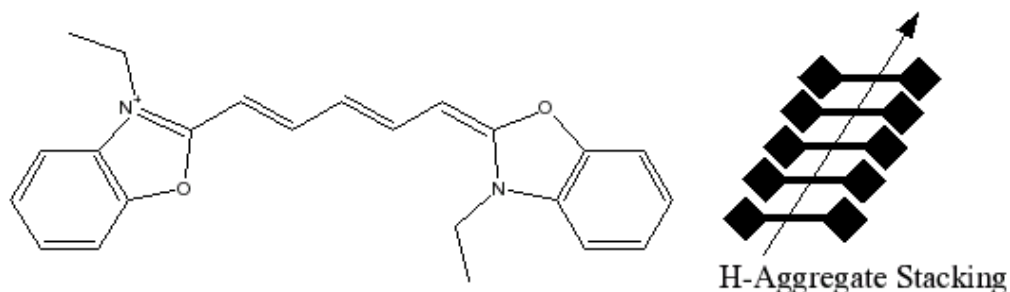
Figure 3-11. The chemical structure of DODC with a cartoon representation of the parallel stacking involved in the formation of H-aggregates. The arrow represents the slip angle between the individual dye molecules.
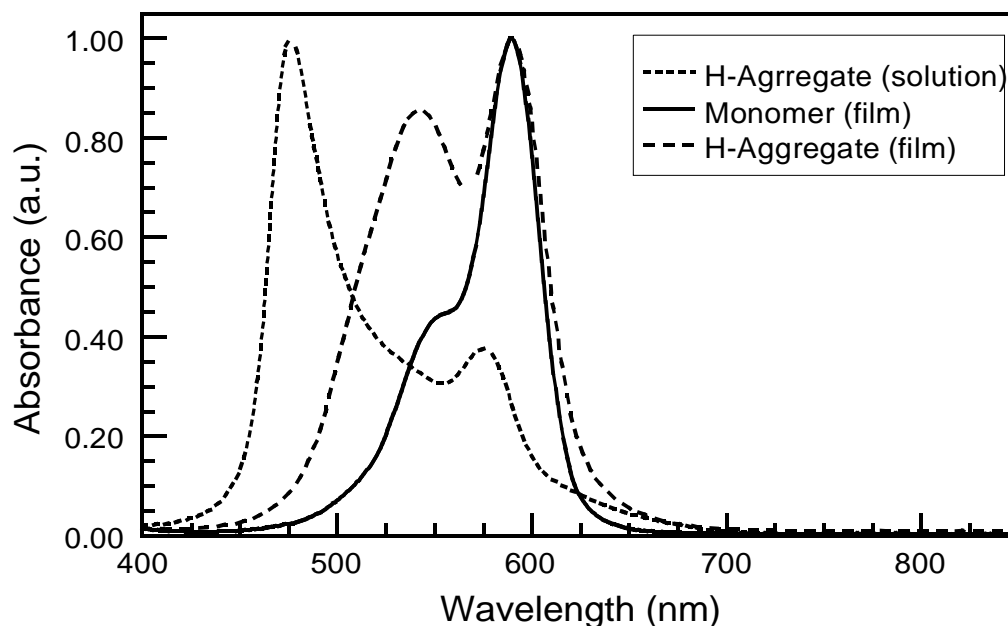
Figure 3-12. The normalized absorption spectra of DODC solution based H-aggregate (short dash line), along with the composite film based monomer (solid line) and a mixture of monomer/H-aggregate (long dash line).

within the film, compared to that in solution, i.e., 48 nm versus 79 nm, respectively. This suggest that the exciton length of the film based aggregate is less than the solution based counterpart. As in the case of TDBC, the coherence length of the DODC aggregate appears to be governed by internal dimensions within the Pluronic 123 rod-shaped mesostructures.

As expected, little fluorescence is observed for aggregates both in solution or within the film, due to the non-emissive nature of H-aggregates [42]. The fluorescence spectrum of the film based aggregates is characterized by a broad, low intensity band that appears to be a combination of the monomer fluorescence and possible emission from an electronically forbidden H-aggregate state or more likely, a vibronic band of the monomer. A plot of this spectrum, and for comparison, that of the monomer in the film

and H-Aggregate in solution, are presented in Figure 3-13. An interesting note is that even though the absorption spectrum indicates that a substantial amount of monomers remained in the film, little fluorescence from them is observed when exciting on the aggregate band. This indicates a rapid excited state deactivation from the exciton band to the ground state before any energy transfer to the monomer can take place. Even if energy transfer does take place, deactivation of the monomer can still occur through a back energy transfer process to the lower-level of the H-aggregates exciton band. An energy level structure and population dynamics scheme for these processes are shown in Figure 3-14. A qualitative measure for the rate of this deactivation process can be ascertained by looking at the fluorescence decay dynamics. The decay profile for films containing predominantly monomer, and a mixture of monomer and aggregates can be
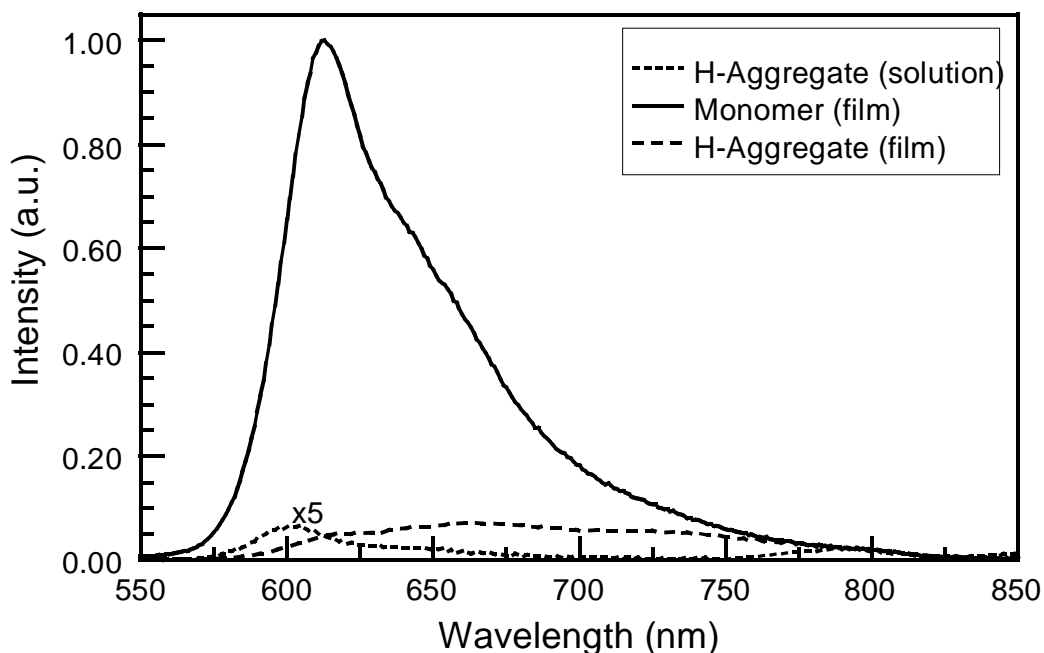
Figure 3-13. The normalized fluorescence spectra of DODC solution based J-aggregate (short dash line) (λ_{ex} 500 nm), along with the composite film based monomer (solid line) (λ_{ex} 540 nm) and J-aggregate (long dash line) (λ_{ex} 540 nm).
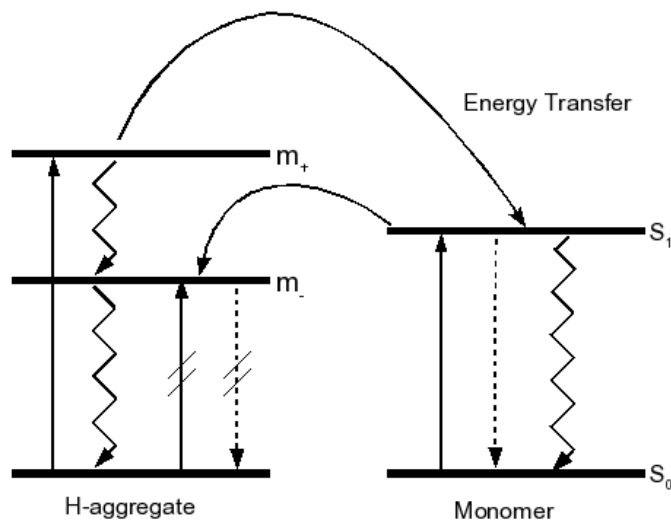
Figure 3-14. Photodynamic scheme to explain the fluorescence decrease that accompany the formation of H-aggregates. Solid arrows indicate absorption, broken arrows fluorescence and wavy arrows internal conversion, and crossed lines represent forbidden transitions. Energy transfer is indicated by the curved arrows.

seen in Figure 3-15, along with the decay profile for DODC in ethanol. The decay profile of films containing aggregates, is fitted using a three component model in which the dominant component decayed with a time constant of 56 ps (78%), with the two slower components decaying with time constants of 268 ps (17%) and 1288 ps (5%) respectively. The monomer containing film exhibits a two component decay, but now the time constants are 452 ps (13%) and 64 ps (87%). This relatively short lifetimes is most likely due to a self quenching process, because in ethanol, the mean lifetime of DODC is 1997 ps.
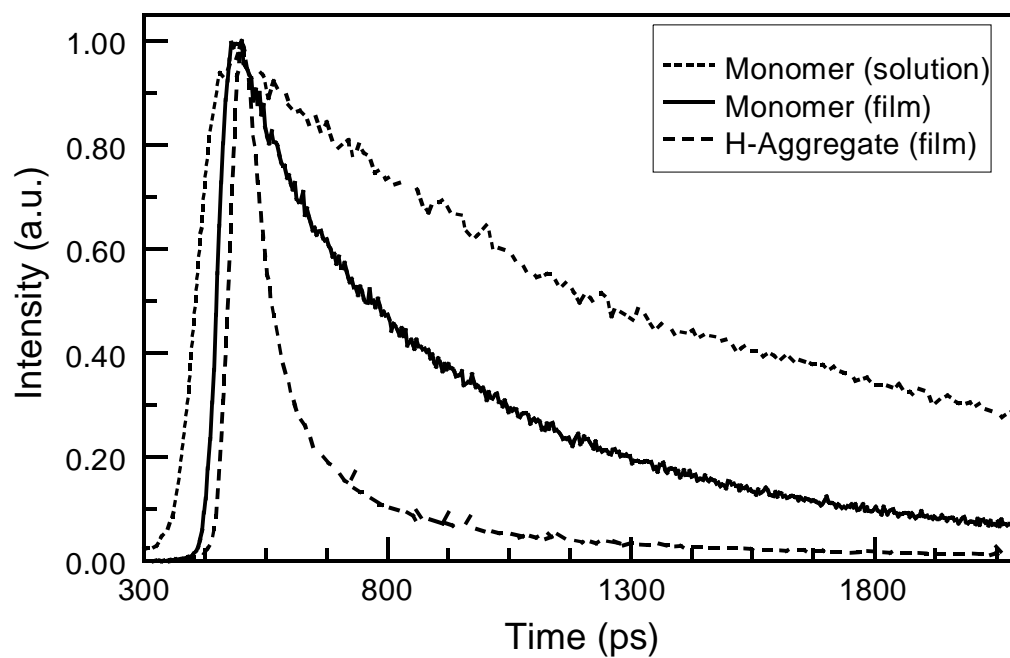
Figure 3-15. The fluorescence decay profiles of DODC solution based monomer (short dash line), along with the composite film based monomer (solid line) and a mixture of monomer/H-aggregate (long dash line).

4. Cyanine-type Squarylium Dyes

4.1 Introduction

For squarylium dyes (such as shown in Figure 4-1), intense absorptions and, in some cases, strong fluorescences in the long-wavelength and near-IR regions of the visible spectrum have been exploited for a range of applications, including uses as active agents in photovoltaics, xerography, chemical sensors, and nonlinear photonic systems [1-4]. In such applications in which squarylium molecules play key roles, the photophysical properties that are utilized, generally, owe their character to energetics and kinetics properties of donor-acceptor-donor (D-A-D) entities within the dyes [5]. Both semiempirical [6], and more recently *ab initio* [7] calculations show that in the ground state, significant intramolecular charge transfer (ICT) from the two donor moieties, D, to the central C_4O_2 electron-withdrawing group (A) causes these dyes to adopt an essentially planar structure. The high molar extinction coefficient for absorption to the lowest lying singlet state, was also shown to be due to a combination of the ground state ICT and an excited state CT process that is confined within the central C_4O_2 group. In the excited state CT, electron density from an oxygen is transferred to the central four-membered cyclobutane ring. As a result of the coupling between these CT processes, the observed photophysical properties are strongly dependent on the nature of donor side groups.

In the two cyanine-type squarylium dyes investigated in this study, two indolenine groups serve as the donors, which leads to the parent dyes having significant nonpolar character as well as a slight deviation from planar structure as found for most other squarylium dyes [8,9]. As shown in Figure 4-1, these dyes differ only by the substitution

SQ-Cy1   R = CH$_3$

SQ-Cy2   R = C$_3$H$_6$SO$_3^-$ HN$^+$
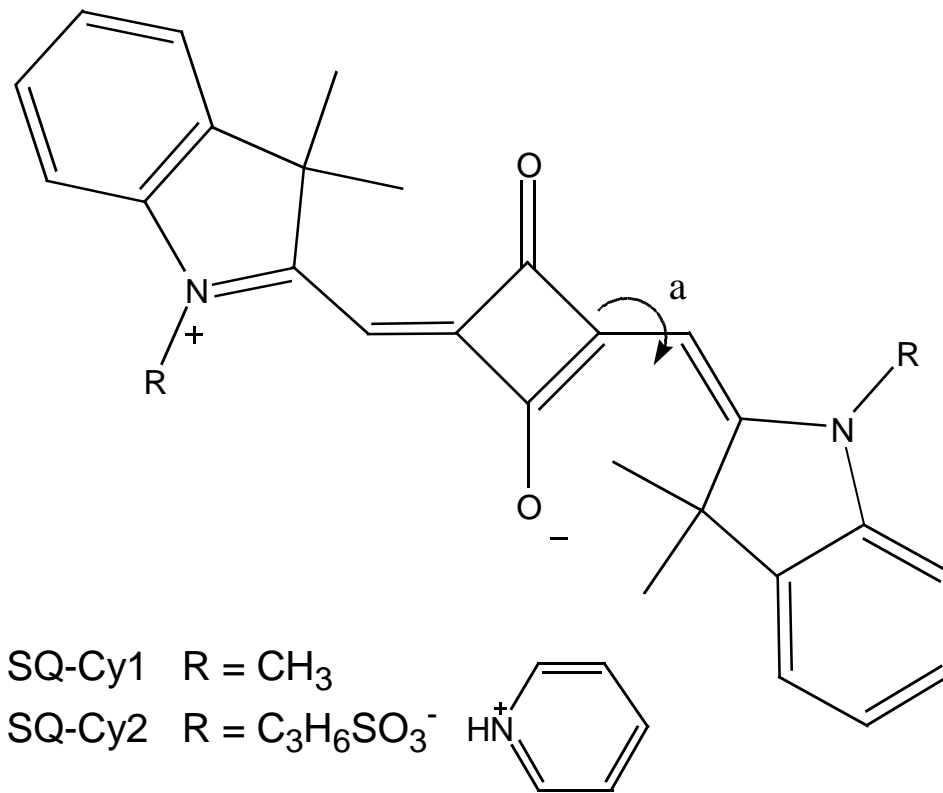
Figure 4-1. Chemical structure of SQ-Cy1 and SQ-Cy2 cyanine-type squarylium dyes.

of the methyl groups on the nitrogens in the case of SQ-Cy1, with alkyl sulfate groups in

the case of SQ-Cy2. This nonpolar character makes these dyes well suited for

incorporation into polymer matrices [10], but not for incorporation in polar, inorganic

matrices, as was done with other, more polar, squarylium dyes [11]. However, the

hybrid nature of the silica/Pluronic composite developed here, made it an ideal host

matrix for these dyes, because they can be readily occluded within the nonpolar region of

the Pluronic P123 mesostructures.

Intercalation of these cyanine-type squarylium dyes within the composite films to

form the photonic layer in an all-optical switching device, described in chapter 1, would

be advantageous on several fronts. First and foremost, is that the photostability of

squarylium dyes match, or even surpass, the photostabilities of most laser dyes, which are among the most photostable organic dyes known. This enhanced stability is partly due to the low intersystem crossing (ISC) efficiency from the singlet to the triplet state [12,13] (Reactive triplet state intermediates have been shown to play be a significant role in the photochemical degradation of organic dyes [14]). Secondly, and more importantly, is the significant third-order nonlinear susceptibility that squarylium dyes possess [15]: third-order nonlinear susceptibility is central to the ultrafast optical response necessary for the functioning of an all-optical switch.

Although the properties discussed above make composite films containing squarylium dyes well suited towards the desired application (i.e. optical switching), there is one drawback that is inherent to the intercalation of these dyes into a solid matrix. As discussed in chapter 1, the optical response of any material is primarily governed by the rate of excited state deactivation. The greater this rate, the faster the optical response, and vice versa. Prior studies have shown that an excited state isomerization, related to twisting about the bond connecting the central squaraine moiety to an indolenine group (rotation "a" in Figure 4-1), is the major deactivation pathway for squarylium dyes [16]. Consequently, the steric restriction imposed by the composite film, would severely hinder this isomerization process, leading to a significantly lengthened excited state lifetime.

In this work, the excited state quenchers *p*-nitroaniline (*p*NA) and methyl viologen (MV) are employed to rapidly deactivate the squarylium dyes within the composite films by an electron exchange mechanism. Formation of the dye/quencher complexes is studied by steady-state absorption and fluorescence spectroscopy. From this data, and

use of the well-known Stern-Volmer equation, estimates for the forward electron transfer rate and quenching efficiency are found. Time-resolved fluorescence studies are used to ascertain the dynamics of the electron transfer process. Back electron transfer dynamics, from the quencher to the dye, is studied using femtosecond pump-probe spectroscopy. The laser dye, rhodamine 800 (LD800), is also used for excited state deactivation, however, a long range energy transfer mechanism is found to play a dominant role. As such, Förster equations are used to derive the energy transfer rates and other relevant experimental parameters, such as the spatial relationship between the squarylium dyes and LD800.

4.2 Nonlinear Theory

As mentioned above, the third-order susceptibility is central to the operation of an all-optical switch. However, theoretical models that accurately describe the mechanisms that contribute to the third-order polarizability (γ for the molecular property and χ_3 for the bulk) have not been developed, as a result of the complexities inherent in such models. In the case of squarylium dyes, Dirk et al. proposed a simplified model that takes a qualitative, and semiqualitative approach for elucidating the source of their nonlinear properties, and this will be presented here [7]. This model involves the simplification of a relatively complex one-dimensional, nine-term, three-level model to a more manageable three-term expression,

$$\gamma \approx \gamma_c + \gamma_n + \gamma_{tp} \tag{4.1}$$

where $\gamma_c = -K\mu_{01}^4 D_{11}$ contributes only in centrosymmetric molecular system,

$\gamma_n = K\mu_{01}^2 (\Delta\mu_{01})^2 D_{111}$ contributes in noncentrosymmetric systems, and

$\gamma_{tp} = K\mu_{01}^2 \mu_{12}^2 D_{121}$ is the contribution arising from two-photon processes. The

transition moment terms μ_{01} and μ_{12} are for transitions to the significant one-photon state and transitions between the one-photon and two-photon state, respectively. The term $\Delta\mu_{01}$, is defined as $\mu_{00} - \mu_{11}$, D_{lm} and D_{lmn} are dispersion terms, and K is a positive constant defined by the optical process.

Since the squarylium dyes used here exist predominantly in the *trans* configuration, resulting in them being centrosymmetric, the term γ_n is effectively zero. In this situation, equation 4.1 can be further simplified to

$$\gamma \approx \gamma_c + \gamma_{tp}. \tag{4.2}$$

As can be seen above, the terms γ_c and γ_{tp} are opposite in sign making their contribution to the overall third-order polarizability competitive. If the magnitude of μ_{01} is greater than μ_{12}, then γ will be negative; whereas if it is less, then γ will be positive. In general, μ_{12}, the two-photon term, is the dominant transition moment, so most molecules only display positive third-order nonlinearities. However, squarylium dyes are an exception since the optical nonlinearities they display are strongly negative; even though there is significant contribution from the two-photon transition moment, μ_{01}. This indicates that the magnitude of μ_{01} is quite substantial, and has been attributed to the π-electron delocalization nature over the D-A-D moieties of these dyes.

4.3 Photophysics

Direct evidence for the inclusion of the squarylium dyes within the Pluronic P123 mesostructures of the film can be ascertained from a comparison of the absorption and emission spectra in solution and in the film. Due to the charge transfer (CT) nature of the electronic transitions that take place in squarylium dyes, the intensities and positions

of absorption and emission bands are very sensitive to the solvent environment [17]. In the case of cyanine-type squarylium dyes, going from a more polar to a less polar environment causes both the fluorescence and absorption maxima to undergo bathochromic shifts. Figure 4-2 provides normalized absorption spectra for SQ-Cy1 in solution and in film. The absorption spectra for SQ-Cy2 is essentially identical, except for a 5 nm red-shift due to the sulfate groups. As can be seen, the absorption maximum in the film is red-shifted by 9 nm and the blue shoulder is slightly enhanced when compared to the spectrum in ethanol. Such little variation between solution and film spectra are to be expected since the CT transition is localized on the central C_4O_2 moiety. As a result, only minor deviations from the initial ground state structure occurs following photoexcitation [16] so the fluorescence spectra in these two environments should differ only slightly.

The fluorescence spectra in ethanol and in the film for SQ-Cy1, is presented in Figure 4-3. Note that, the spectra for SQ-Cy2 is virtually identical to that of SQ-Cy1, aside from a minor blue shift. Unlike the absorption spectra, the fluorescence spectra of SQ-Cy1 and SQ-Cy2 in the film exhibited two noticeable differences compared to that in ethanol. Firstly, the maximum in the film is red-shifted by only 2 nm versus the 9 nm red shift observed for the absorption maximum. This corresponds to Stokes shifts of 18 nm and 14 nm for solution and film, respectively. Secondly, the red shoulder for dyes in solution are enhanced compared to that in the film. This is opposite to what would be expected based on the intensity of the corresponding blue shoulders in the absorption spectra. The absorbance of the shoulders in the film and solution are more, or less identical, so this relationship might be expected to be maintained in the fluorescence
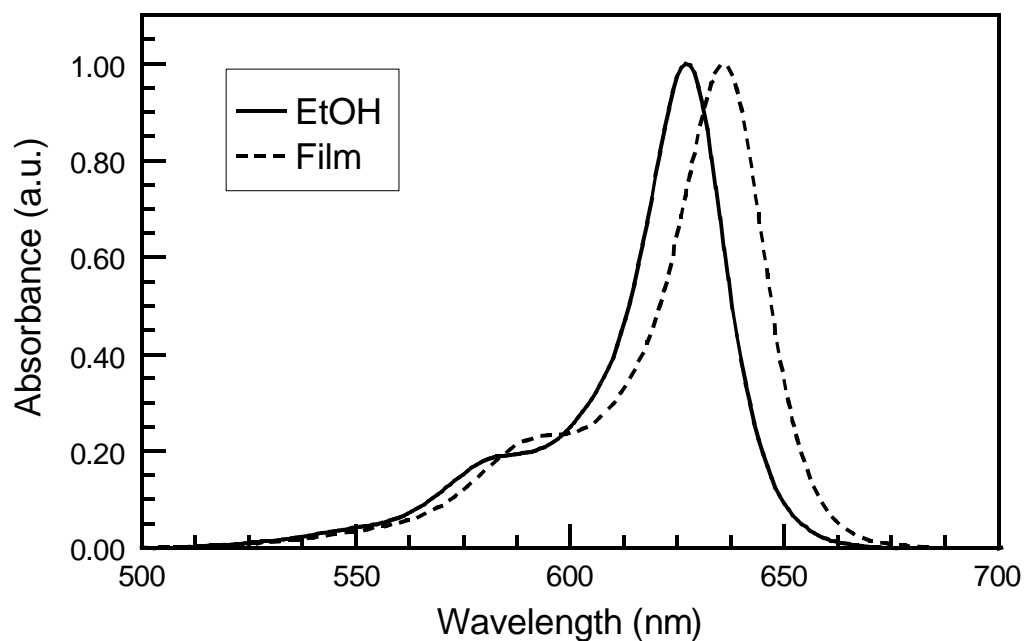
Figure 4-2. The normalized absorption spectra of SQ-Cy1in ethanol and intercalated into a silica/Pluronic P123 drop-casted film.
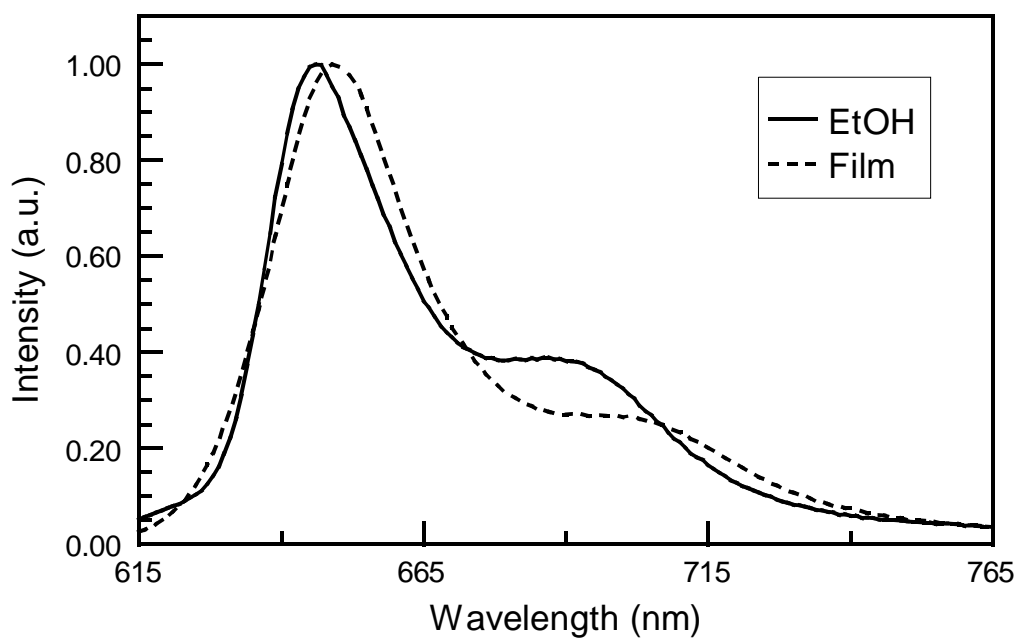
Figure 4-3. The normalized fluorescence spectra of SQ-Cy1in ethanol and intercalated into a silica/Pluronic P123 drop-casted film. λ_{ex} 600 nm.

spectra if these shoulders are derived from purely vertical Frank-Condon transitions. An obvious explanation is that the radiative states that contributed the red shoulder's intensity in solution and within the films are different. As stated above, the initial excited state structure of squarlium dyes, for the most part, retains the nuclear geometry of the ground state structure, so this would suggest that a structural change occurs within the film preceding the initial excitation. Indeed, prior studies have shown that a relaxed excited state, related to twisting about the bond connecting the central squaraine moiety to an indolenine group, contributes to the red shoulder's intensity in solution [16]. Therefore, the steric restriction imposed by the film would severely hinder the formation of this and other twisted relaxed excited states causing a decrease in the red shoulder's intensity.

The existence of these relaxed excited state conformers is strongly suggested by the measured radiative lifetimes and quantum yields which are provided in Table 4-1. One notes that in solution, SQ-Cy1 exhibits a two-component fluorescence decay with the dominant component corresponding to a lifetime of 371 ps (83%) and the minor component of 175 ps (17%). While, in the case of SQ-Cy2, the dominant component exhibits a somewhat longer lifetime of 690 ps (90%) and the minor component had a substantially longer lifetime of 2257 ps (10%). These differences are consistent with the hindered isomerization concept, in which the sulfate groups of SQ-Cy2 are expected to hinder the excited-state isomerization to a greater extent than the methyl groups of SQ-Cy1. Also, as expected with this concept, the differences in lifetime of the two dyes decrease when the dyes were intercalated into the films: the lifetimes of the dominant components for SQ-Cy1 and SQ-Cy2, at a concentration of 0.5 mg/ml, are found to be

Table 4-1: Lifetime and quantum yield values for SQ-Cy1 and SQ-Cy2 in various environments.

Dye	Solvent	Concentration[a]	Lifetime (ps)	Quantum Yield[b]
SQ-Cy1	EtOH	2.43×10^{-5}	371 (83%)	0.087
			175 (17%)	
	film	1.2	1770 (92%)	0.220
			338 (8%)	
	film	0.5	2730 (84%)	0.237
			140 (16%)	
	film	0.2	3105 (91%)	0.670
			338 (9%)	
	film	0.1	3092 (90%)	1.000
			1309 (10%)	
SQ-Cy2	EtOH	2.43×10^{-5}	690 (90%)	0.153
			2257 (10%)	
	film	1.0	1422 (90%)	0.100
			381 (10%)	
	film	0.5	2874 (100%)	0.230
	film	0.2	3205 (91%)	0.720
			241 (9%)	
	film	0.1	3312 (94%)	0.885
			742 (6%)	

[a] Concentration in mole/L in EtOH and mg per 1 ml of sol in films. [b] Quantum yields calculated from Eq. (2.1), using a refractive index of 1.476 for the films.

2730 and 2874 ps, respectively, and the lifetime of the second component for SQ-Cy1 is reduced, while no second component is observed for SQ-Cy2. This latter observation suggests that the minor components probably derive from twisted conformations, i.e. relaxed excited states, whose populations are either reduced or eliminated in the film environment. Also, lowering the dye concentration leads to increases in the lifetime for both the major and minor components.

The quantum yields are observed to increase in concert with diminution of conformational freedom, but not as expected. If as suggested above, the primary nonradiative deactivation pathway in squarylium dyes is an excited state isomerization, then within the confines of the films this process should be significantly reduced or

eliminated, and the quantum yield for the emission should approach unity. However, this is not what is observed for either SQ-Cy1 or SQ-Cy2 when their concentrations are 0.2 mg/ml and above. At these concentrations the quantum yields remains below 72 %, and only when the concentration is reduced to 0.1 mg/ml did the quantum yield become unity, but only for SQ-Cy1 not SQ-Cy2. This indicates the presence of at least a second nonradiative deactivation pathway. As can be seen in Table 4-1, with an increase in dye concentration the lifetimes and quantum yields decrease for both dyes. This behavior is interpreted as indicating that an intermolecular quenching process occurs when two or more dye molecules occupy the same mesostructural cavity and are in close enough proximity for electron or energy transfer to take place. The effect is found to be more pronounced for SQ-Cy2 than for SQ-Cy1 which is attributed to the involvement, along with ground-state SQ-Cy2 molecules, of the pyridinium counter ions in the quenching process.

A quantum chemical approach is, additionally, utilized to aid in shedding light on the conformation question. Time dependent density functional theory (TD-DFT) was performed at the B3LYP level with a 6-31G(d,p) basis set to calculate conformational dependent electronic coupling of the SQ-Cy1 dye. Ground- and excited-state energies for several conformations of SQ-Cy1, in which the bond connecting the central squaraine moiety with an indolenine group is rotated, were calculated. Although the transitions energies are overestimated with this approach, the relative differences are found to be correct. The results are displayed in Figure 4-4. Two trends are evident: first, as the twist angle is increased, the energy gap between the ground state, $S_0(^1A_{1g})$, and the first excited state, $S_1(^1B_{1u})$, decreases; second, the excited-state dipole moment is found to
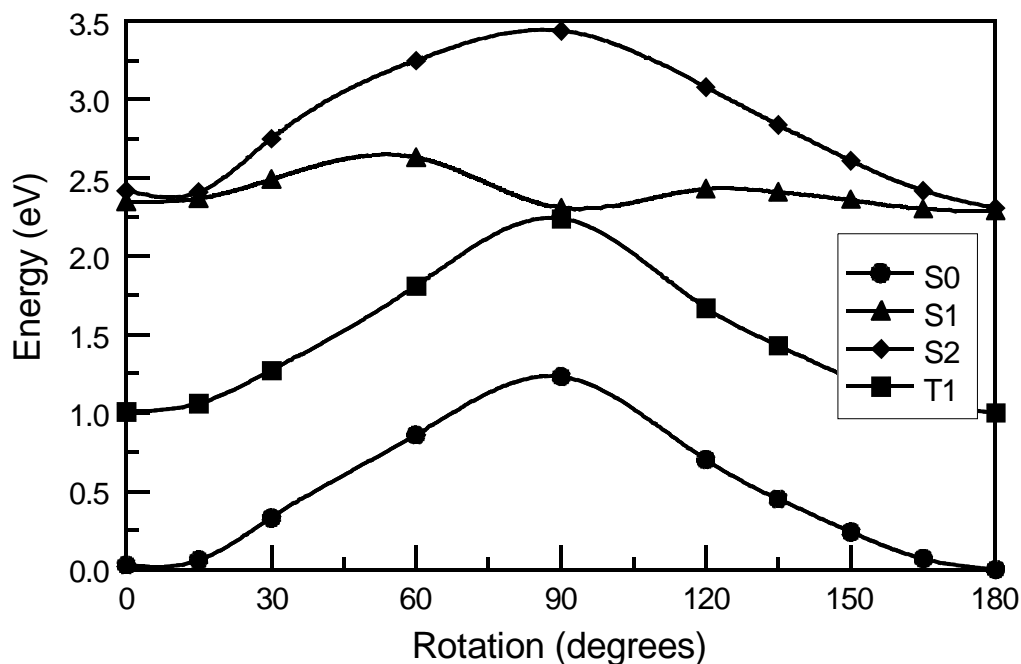
Figure 4-4. Ground- and excited-state energies for planar and several rotational conformers of SQ-Cy1. Rotation occurs along the bond that connects the central squaraine moiety and the indolenine groups.

increase by several orders of magnitude. For the S_0, S_1, and S_2 states at 0/90 degrees, the calculated dipole moments are 1.4/6.0, 0.5/14.2 and 2.1/13.4 Debye, respectively. This result agrees well with the findings by Rettig et al. [17] obtained using a structural analog of SQ-Cy1 and supports the assertion of the existence of a range of radiative conformational states. At a twist angle of 0 degrees, the relative energy gap between the S_1 and ground state is at its maximum. But as the twist angle increases from 0 to 90 degrees, the energy gap decreases to the minimum value. Examination of the S_1 potential energy surface (PES) also reveals that it is nearly isoenergetic with the T_1 state at its minimum, potentially leading to a twisted intersystem crossing (TISC) process taking place. Previous studies, however, have indicated that squarylium dyes exhibit very low intersystem crossing efficiencies, unless a triplet sensitizer is employed [12,13].

It is more likely that the squarylium molecule will undergo a rapid nonradiative decay process at this point. From this, it is clear that a range of radiative states can occur as a result of transitions taking place along different points on the S_1 potential energy surface (PES) to the ground state. Thus, in ethanol, a radiative state that has a larger twist angle, and hence greater polarity would be energetically favored, while within the mesopores of the composite film, a radiative state with a lower, or no twist angle would be favored. Such changes in the fluorescence spectra of squarylium dyes, as a result of matrix confinement, have previously been observed [16].

4.4 Excited State Deactivation By Electron Exchange

The co-intercalation of electron acceptors, often referred to as quenchers, with squarylium dyes into the composite films provides an appealing solution for drastically reducing the excited state lifetime, and thereby, increasing the film's optical response. In recent years, numerous femtosecond transient absorption studies have shown that the forward electron transfer from the donor to the acceptor occurs on a sub-picosecond time scale [18-21]. Furthermore, quantum chemical calculations by Paterson et al., have helped elucidate the mechanistic steps involved in the photoexcited electron transfer from a squarylium dye to an electron acceptor (a semiconductor nanoparticle) [7]. An illustration of the steps involved in this process is provided in Figure 4-5. The first step in this process is the electron transfer from an oxygen into the central cyclobutane ring upon excitation. At this point, the excited dye can either undergo deactivation through normal radiative or nonradiative pathways or go on to form an excited state charge transfer complex with a nearby ground state acceptor. If such a charge transfer complex is formed then electron transfer can take place from the squarylium dye to the acceptor
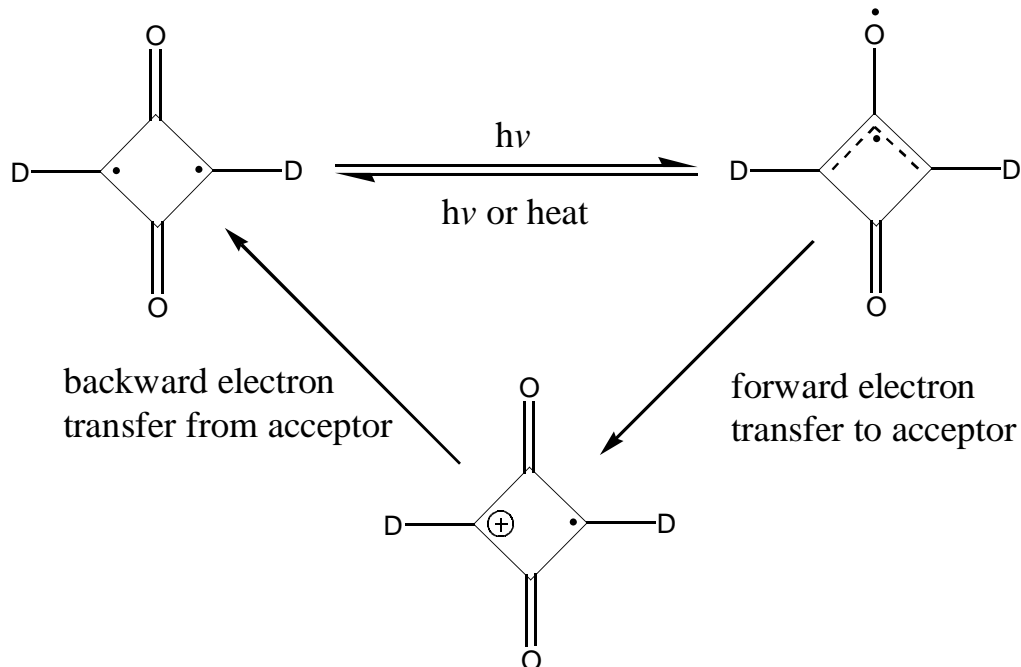
Figure 4-5. The forward and backward steps involved in the electron transfer processes that takes place between a photoexcited squarylium dye, to a nearby electron acceptor.

leading to the formation of the ground state oxidized dye and reduced acceptor. The

neutral ground state squarylium dye is then regenerated by back-electron transfer from

the acceptor. The factor that most influences the formation of the charge transfer

complex and hence, the transfer of an electron, is the electronic coupling between the

excited squarylium dye and the acceptor. This coupling itself is primarily determined by

the distance between the donor and acceptor species, though in a strict sense, their

respective orientations would also be a factor. If significant electronic overlap exists

then the quantum yield of electron transfer will be high, whereas, if there is little overlap

then the intramolecular deactivation pathways will dominate the excited state

deactivation process.

The first electron acceptor to be tried is *p*NA because it has been known for some

time that nitro containing aromatic compounds are good electron acceptors [22, 23].
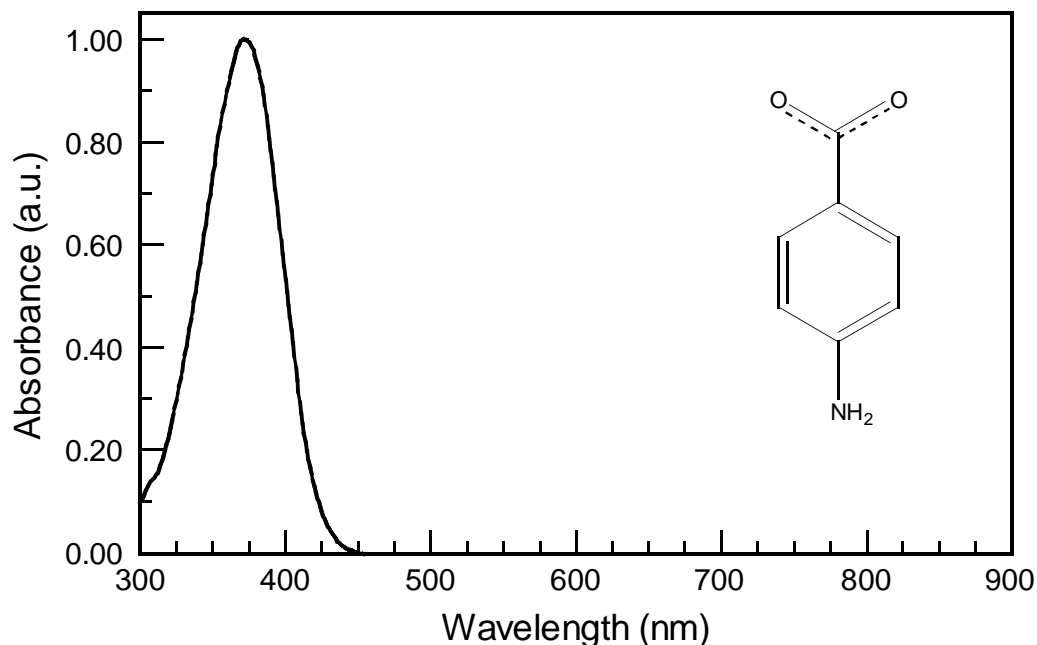
Figure 4-6. The absorption and chemical structure of the electron acceptor *p*-nitroaniline.

Also, the sub-picosecond ground state recovery this molecule possesses is beneficial to

the overall optical response of the system [24]. In Figure 4-6, the absorption spectrum,

as well as the chemical structure of this molecule are given. As can be seen, *p*NA has no

appreciable absorption in the spectral region where the squarylium dyes absorb or

fluoresce, so any quenching of the fluorescence that takes place must be due to electron

transfer. The quenching ability of *p*NA was evaluated by adding it to a precursor sol

containing either SQ-Cy1 (0.6 mg/ml) or SQ-Cy2 (0.7 mg/ml) at a 1 : 1 or 1 : 10, dye to

*p*NA mole ratio. These ratios were chosen because they allowed a convenient way in

which to evaluate the quenching efficiency and electron transfer rate as a function of

quencher concentration. The results obtained are outlined in Table 4-2.

Table 4-2: The electron transfer parameters for SQ-Cy1 and SQ-Cy2 composite films containing *p*-nitroaniline (*p*NA) as an electron acceptor.

Dye	mole ratio dye : *p*NA	Mean Lifetime (ps)	Lifetime Decrease	Quenching Efficiency[a]	Transfer Rate (M^{-1}sec^{-1})[b]
SQ-Cy1	n/a	1286	n/a	n/a	n/a
	1 : 10	839	35 %	8 %	-8.9 x 10^8
	1 : 1	1015	21 %	32 %	5.6 x 10^{10}
SQ-Cy2	n/a	1572	n/a	n/a	n/a
	1 : 10	609	61 %	62 %	1.3 x 10^{10}
	1 : 1	1152	38 %	36 %	5.7 x 10^{10}

[a] The efficiencies were calculated using Eq. (2.4). [b] Electron transfer rates were calculated using Eq. 2.5.

For SQ-Cy1 containing films, the addition of *p*NA at a 1 : 10 mole ratio leads to an 8 % decrease in the fluorescence intensity, or to put it another way, the quenching efficiency is 8 %: the mean lifetime is decreased by 35 %. At a 1 :1 mole ratio, the fluorescence intensity is now decreased by 32 % and the mean lifetime by 21 %. The results for SQ-Cy2 are somewhat different. At a 1 : 10 mole ratio the quenching efficiency is 62 %, while the mean lifetime is decreased by 61 %. For films containing a 1 : 1 mole ratio, the quenching efficiency and decrease in mean lifetime are 37 % and 27 %, respectively. For all films the electron transfer rate remains below 10^{11} sec^{-1} and is actually negative for SQ-Cy1 films containing the highest concentration of *p*NA.

The results above are quite telling. For one, the fact that a *p*NA mole ratio of 1 : 1 shows a higher quenching efficiency than the 1 : 10 ratio for films containing SQ-Cy1 is indicative of the presence of a competitive process that causes an increase in the fluorescence intensity. A clue to the nature of this process can be ascertained by looking at the fluorescence quantum yield of the SQ-Cy1 film containing no *p*NA. The quantum yield of only 25 % suggest that there is significant intramolecular quenching taking place

which infers that a large percentage of SQ-Cy1 molecules exists as aggregates within the film. Addition of *p*NA at such a high concentration, in all likelihood would help to break up these aggregates and increase the relative separation between the individual dye molecules. As a result, intramolecular quenching decreases leading to an increase in the fluorescence intensity. The presence of the *p*NA molecules, however, would tend to decrease fluorescence intensity through electron transfer, and from the small decrease in the fluorescence, it is the dominating process. Since the sulfate groups of SQ-Cy2 increase its solubility and hence inhibit the formation of aggregates, this effect is not seen. This also accounts for why the observed quenching efficiency of *p*NA, is about twice as much for this dye. Moreover, at a 1 : 1 mole ratio the quenching efficiency of *p*NA is closely matched for SQ-Cy1 and SQ-Cy2, indicating that at this concentration there is negligible solubilization effects. Another interesting note is that even at the mole ratio of 1 : 10, the quenching efficiency of *p*NA for either dye never went above 65 % and the reduction in fluorescence lifetimes does not come close to the instrument limited value of 30 ps. Taken together, these facts suggests that *p*NA is not an efficient enough quencher to effectively decrease the excited state lifetimes of the squarylium dyes down into the desired temporal region of a few picoseconds or less.

To overcome the limitations of *p*NA, MV is employed as an electron acceptor. The results using this quencher are shown in Table 4-3. As with *p*NA, this is another well known and often studied quencher. A few femtosecond transient absorption studies have already shown that the forward electron transfer rate from an excited dye molecule to this molecule occurs in the femtosecond time domain [25,26]. More importantly though, is that the back electron transfer was demonstrated to take place on a time scale only

Table 4-3: The electron transfer parameters for SQ-Cy1 and SQ-Cy2 composite films containing methyl viologen (MV) as an electron acceptor.

Dye	mole ratio dye : MV	Mean Lifetime (ps)	Lifetime Decrease	Quenching Efficiency[a]	Transfer Rate $(M^{-1}sec^{-1})$[b]
SQ-Cy1	n/a	1286	n/a	n/a	n/a
	1 : 10	793	38 %	36 %	3.8×10^9
	1 : 1	929	28 %	27 %	4.0×10^{10}
SQ-Cy2	n/a	1572	n/a	n/a	n/a
	1 : 10	93	94 %	97 %	2.6×10^{11}
	1 : 1	1152	87 %	92 %	9.6×10^{11}

[a] The efficiencies were calculated using Eq. (2.4). [b] Electron transfer rates were calculated using Eq. (2.5).

slightly longer than the forward electron transfer. In Figure 4-7, the absorption spectrum, as well as the chemical structure for MV are presented and once again, no spectral overlap occurs between its absorption and that of the squarylium dyes. Unlike *p*NA, however, MV is a di-cation so electrostatic interactions should be a factor, especially in the case of SQ-Cy2 which is a di-anion. Like the *p*NA study, mole ratios of 1 : 10 and 1 : 1 were used and the concentration of the squarylium dyes remained the same.

Addition of MV at a 1 : 10 mole ratio to composite films containing SQ-Cy1 causes a 36 % decrease in the fluorescence intensity while the mean lifetime is reduced by a similar amount (38 %). When the mole ratio is reduce to 1 : 1, the fluorescence intensity is reduced by 27 %, and once again, the reduction in mean lifetime (28 %) closely matched that of the reduction in fluorescence intensity. The calculated rate constant for the 1 : 10 and 1 : 1 mole ratio are 3.8×10^9 and 4.1×10^{10} M^{-1} sec^{-1}, respectively. The results for films containing SQ-Cy2 are considerable different. At a 1 : 10 mole ratio, the fluorescence intensity is reduced by an astonishing 97 %. The reduction in the mean
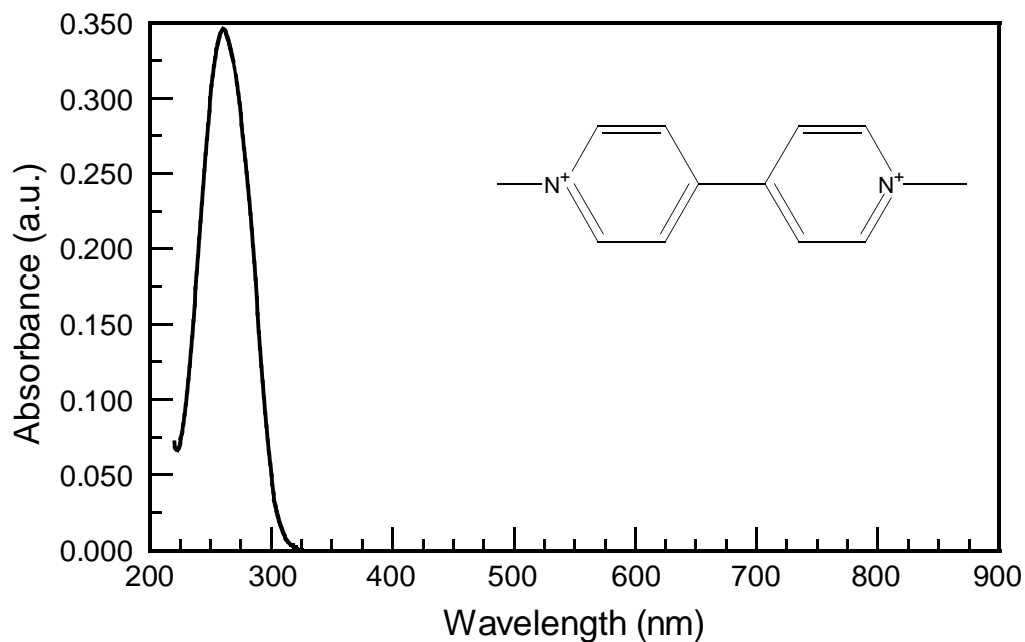
Figure 4-7. The absorption and chemical structure of the electron acceptor methyl viologen.

lifetime at this same mole ratio is a slightly less at 94 %. In terms of mean lifetime

values, this corresponds to the lifetime being reduced down to 93 ps from 1572 ps.

Surprisingly, for the 1 : 1 mole ratio, the reduction in fluorescence intensity is still rather

significant at 91 %. The reduction in mean lifetime followes a similar trend, showing a

reduction of 87 % to 210 ps. The calculated electron transfer rates for both mole ratios

are greater than 10^{11} $M^{-1}sec^{-1}$.

The decrease in fluorescence intensities observed for SQ-Cy1 containing films are

close to the value seen using pNA at the 1 : 1 mole ratio, but not at the 1 : 10 mole ratio.

The values obtained using MV is consistent with the fact that the more quencher

molecules that are present in the system, the greater the decrease in fluorescence

intensity. These results tend to add further support to the above assertion that pNA, at

the 1 : 10 mole ratio, helps to reduce the aggregation of SQ-Cy1 molecules within the

film while at the same time acting to deactivate the dye's excited state. For either electron acceptor, however, their ability to reduce the excited state lifetime of SQ-Cy1 is no where near what is needed to allow the films to be used as the photonic layer. It would appear that neither quencher possesses sufficient electronic coupling with SQ-Cy1.

The effect of electrostatic interactions can clearly be seen for films containing SQ-Cy2 and MV. Since the fluorescence quantum yield for the SQ-Cy2 films containing no MV is 50 %, the results for the film containing a 1 : 10 mole ratio would suggest that practically all excited dye molecules, either underwent electron transfer to a nearby MV molecule or is deactivated by the intramolecular quenching process discussed above. Moreover, is that even when the concentration of MV molecules is reduced by a factor of ten, its quenching efficiency is reduced by only five percent. Likewise, the electron transfer rates differ only slightly and their magnitudes are consistent with there being substantial electronic coupling. These results are indicative of the formation of a tightly bound ground state complex between the di-anion, SQ-Cy2, and the di-cation, MV. Figure 4-8 shows a cartoon representation of a likely orientation these two molecules might acquire within such a complex. Due to the negative charges localized on the sulfate groups of SQ-Cy2, a MV molecule would most likely be situated at this location thereby allowing for maximum charge interaction. Moreover, such tightly bound complexes have previously been reported to form between MV and other anionic dyes with similar electron transfer efficiencies being observed [25-27].

The calculated electron transfer rates are of interest in one other respect. On initial glance, the results appear to be counter intuitive because as the MV concentration is
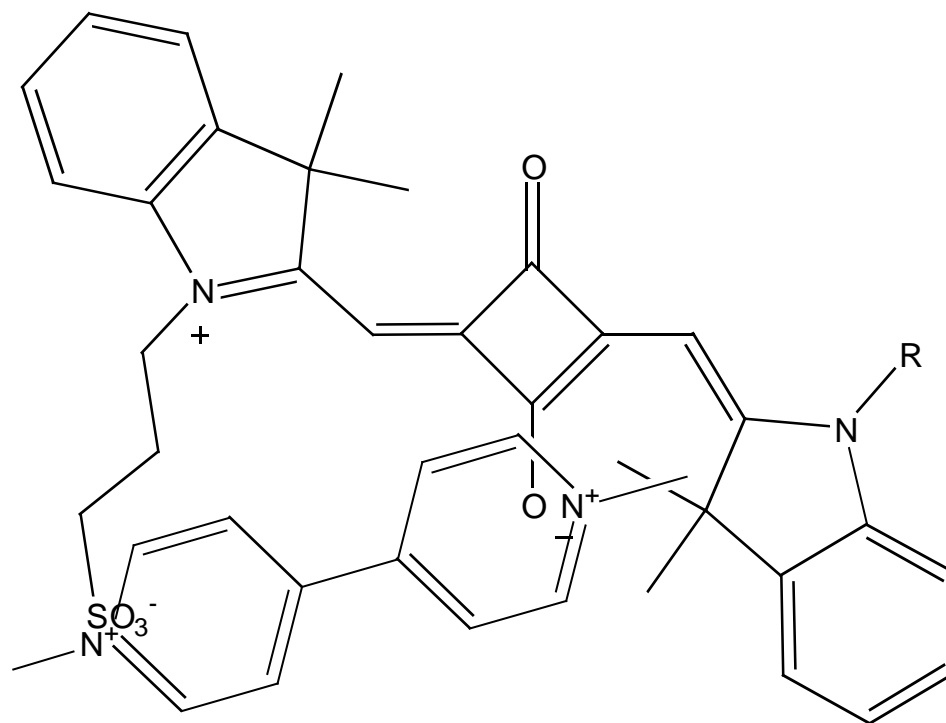
Figure 4-8. A representation of the likely electrostatic interaction between the anionic SQ-Cy2 and cationic MV molecules.

increased the electron transfer rate actually decreases. This is also the case when pNA is used as an electron acceptor. These results plainly show that increasing the electron acceptors concentration to a 1 : 10 mole ratio is of no real benefit as far as transfer rates are concerned. On the face of it, this does not make sense, but what needs to be kept in mind is that within the film no diffusion can take place so the normal predictions made by the Stern-Volmer equation (Eq. 2.5) do not hold. It is certainly the case that as the quencher concentration is increased, the average distance between the dye and the electron acceptors will be reduced. However, this does not take into account any preferential orientations that may exist between the dye and the acceptor for electron transfer to take place. So even if several electron acceptors are within the classical Perrin

quenching sphere, only a few may have the prerequisite orientation that would lead to a

rapid electron transfer i.e. one that requires little or no activation energy to proceed.

Though the electron transfer efficiencies and transfer rates of SQ-Cy2 films

containing MV, are in the range necessary for them to be employed as the photonic layer,

the back electron transfer process still needs to be ascertained before such a judgment can

be made. Ultimately though, it is this back electron transfer that determines the ground

state recovery rate of the neutral dye molecule. To determine the recovery kinetics a

femtosecond transient absorption study is conducted on the SQ-Cy2 films containing MV

at the 1 : 10 mole ratio. The ground state recovery profile for the 20 ps time window

following excitation by a 630 nm, 100 fs pulse, for SQ-Cy2 films with and without MV,

can be seen in Figure 4-9. When no MV is present, no ground state recovery can be seen

in this time window. In contrast, when MV is present, rapid ground state recovery is

evident immediately following excitation, but the recovery process slows significantly

after about 3 ps and appears to be leveling of after about 10 ps. Attempts to fit this

profile to a multi-exponential model proved fruitless and is most likely due to the

complex nature of this back electron transfer process. Such a complex recovery process

may have several origins. The simplest of which is that unlike the forward electron

transfer process, the back electron transfer has an activation barrier that needs to be

overcome. The presence of such activation barriers has previously been used to explain

the slower back electron transfer rate observed for dye sensitized semiconductor

nanoparticles [21]. Electron hopping from the initial MV molecule to other nearby MV

molecules may also explain the slow ground state recovery process. If the initial photo

electron underwent such intramolecular hopping then the time it takes to return to the
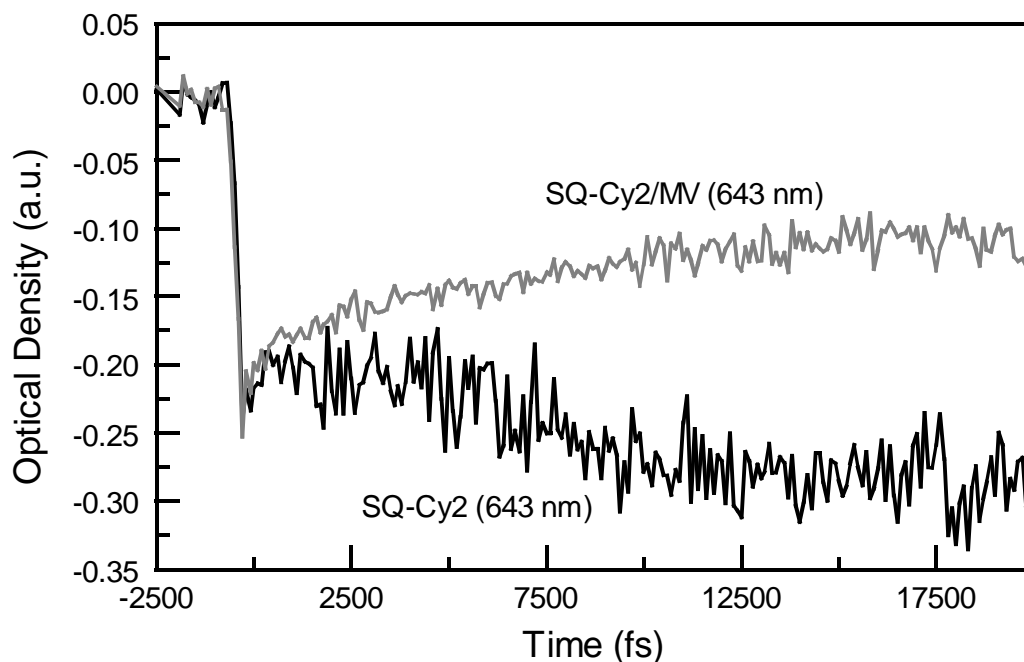
Figure 4-9. Transient absorption spectra of SQ-Cy2 films with and without MV. When MV is present the transient bleach signal indicate a ground state process, whereas, in the pristine films no ground state recovery is evident in this time window.

oxidized SQ-Cy2 molecule would certainly be increased, leading to a much slower

recombination process. A clue to one other possible cause for the slow recovery kinetics

might be found in the leveling of ground state recovery after 10 ps. Since, as suggested

above, an intramolecular energy transfer process between individual squarylium dye

molecules is also responsible for the excited state deactivation of a percentage of the

excited dye molecules then the ground state recovery through this process might be

substantially longer than that of the electron transfer process. This can, in principle, lead

to the observed leveling off after 10 ps, but further studies would have to be conducted to

ascertain the exact nature of this slow back electron transfer process.

No matter the cause of the slow ground state recovery, the fact is that the overall kinetics exhibited by the SQ-Cy2 films containing MV does not lend themselves well towards the targeted application of ultrafast optical switching.

4.5 Excited State Deactivation By Coulombic Exchange

Though the use of electron acceptors to deactivate the photoexcited squarylium dyes proved successful, the slow recovery of the neutral ground state dye through the back electron transfer process makes this approach less than ideal. Another approach taken to expeditiously deactivate the excited squarylium dyes is to use an energy acceptor which operates through a Coulombic, rather than an electron exchange mechanism. As discussed in chapter 1, deactivation through this mechanism requires no transfer of electrons so the recovery of the dye's ground state occurs simultaneously with the transfer of excited state energy to the acceptor. For the cyanine-type squarylium dyes used here, the energy acceptor chosen is the laser dye, rhodamine 800 (LD 800). Being a laser dye, this molecule has good photostability, but more importantly, its absorption band has substantial spectral overlap with the fluorescence bands of the squarylium dyes. In Figure 4-10, the normalized fluorescence spectra for SQ-Cy1 and SQ-Cy2, along with the absorption spectrum of LD800 are plotted. The area under the fluorescence curves which overlaps with the absorption curve defines the spectral overlap. The chemical structure of LD800 is also provided in this figure.

As a result of the long-range nature the Coulombic energy exchange mechanism, the squarylium dye : LD800 mole ratios that are used can be much less than when the electron acceptors, pNA and MV are used. For SQ-Cy1 films, the mole ratios of 1 : 1 and 3 : 1 are used, whereas, mole ratios of 0.5 : 1 and 2 : 1 are used for SQ-Cy2 films.
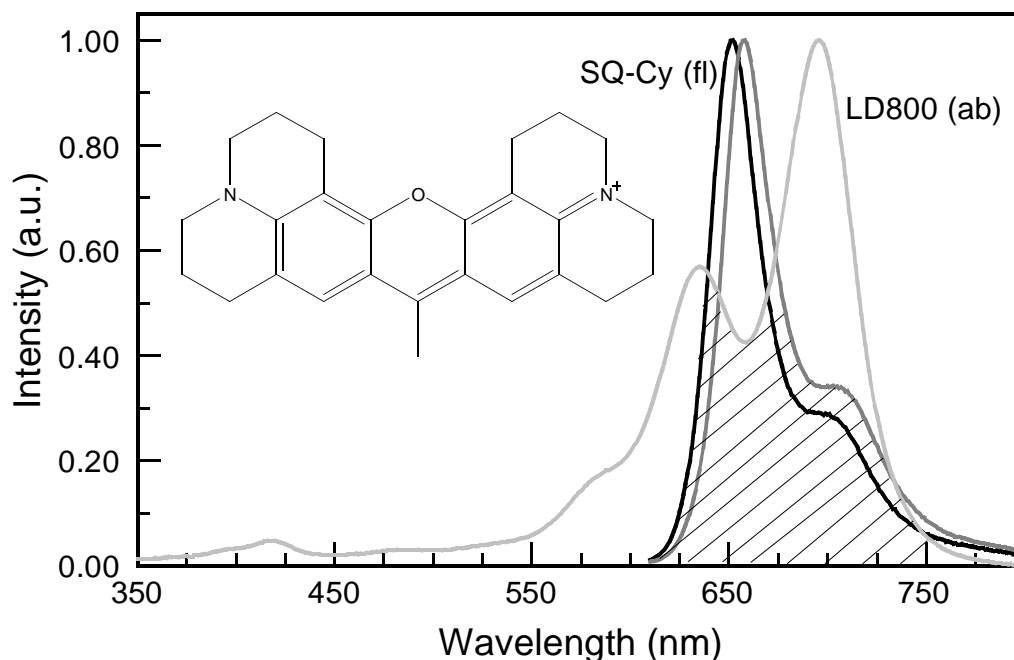
Figure 4-10. Spectral overlap between the absorption (ab) of LD800 and the fluorescence (fl) of the cyanine-type squarylium dyes. The chemical structure of LD800 is also shown.

The corresponding LD800 concentrations, in mg of LD800 per ml of sol, to achieve these ratios are 1 mg/ml and 0.24 mg/ml, respectively. The concentration of the squarylium dyes is the same as used in the above studies involving the electron acceptors. One should note, that for both dye containing films mole ratios in which the squarylium dyes outnumbered the LD800 molecules are employed. Use of such ratios allows the ability of a single LD800 molecule to undergo energy transfer with multiple, nearby squarylium dye molecules to be ascertained.

The obtained energy transfer parameters for SQ-Cy1 and SQ-Cy2 films containing various quantities of LD800 are outlined in Table 4-4. For SQ-Cy1 films, the energy transfer efficiencies is 97.7 % at a 1 : 1 mole ratio. At that same mole ratio, the average distance between the SQ-Cy1 and LD800 molecules is found to be ~ 24 Å. When a mole

Table 4-4: The energy transfer parameters for SQ-Cy1 and SQ-Cy2 composite films containing rhodamine 800 (LD800) as an acceptor.

Dye	mole ratio dye : LD800	Transfer Efficiency[a]	R_0 ($\pm$ 4 Å)[a]	r ($\pm$ 4 Å)[a]	Transfer Rate ($\times 10^{12}$ M^{-1}sec^{-1})[c]
SQ-Cy1	n/a	n/a	46	n/a	n/a
	1 : 1	97.7 %	n/a	25	4.2
	3 : 1	85.4 %	n/a	34	2.5
SQ-Cy2	n/a	n/a	52	n/a	n/a
	0.5 : 1	99.8 %	n/a	18	42.5
	2 : 1	97.8 %	n/a	27	15.1

[a] The efficiencies were calculated using Eq. (2.4). [b] The Förster distance, R_0, obtained using Eq. (2.7). [b] The average distance, r, between the squarylium dyes and LD800 calculated from Eq (2.8). [c] Energy transfer rates were calculated using Eq. (2.6).

ratio of 3 : 1 is used, the transfer efficiencies decrease to 85.4 %, while the average distance increase to ~ 34 Å. Regardless of the mole ratio, the transfer rate remains in the 10^{12} M^{-1}sec^{-1} range. The results for SQ-Cy2 varied somewhat, but in a desirable manner. For one, the transfer efficiencies and rates are higher and likewise, the average donor/acceptor distances are shorter. When a mole ratio of 0.5 : 1 is used, the transfer efficiencies is an astonishing 99.8 % while the rate is in the 10^{13} M^{-1}sec^{-1} range. Decreasing the LD800 content (2 : 1 mole ratio) only results in a minor change in the transfer efficiency: it decreases to 97.8 %. The rate still remains in the 10^{13} M^{-1}sec^{-1} range. The average donor/acceptor distances for these mole ratios are ~ 18 Å and ~ 27 Å, respectively.

From the above results, it can clearly be seen that excited state deactivation of the squarylium dyes through the Coulombic mechanism, results in much higher energy transfer rates and efficiencies than when electron acceptors are used. Whereas, addition of the electron acceptors to SQ-Cy1 containing films resulted in the energy transfer, and hence rapid excited state deactivation, at most 36 % of the time, use of LD800 at a much

lower mole ratio, results in energy transfer over 97 % of the time. Moreover, the energy transfer rate at this mole ratio is two orders of magnitude greater. So not only is practically all the excited SQ-Cy1 molecules undergoing deactivation, they are doing so on a femtosecond time scale. Even when three times more SQ-Cy1 than LD800 molecules are present in the film, the energy transfer efficiency is still above 85%, while the transfer rate decreased only slightly. This suggests that a single LD800 molecule is accepting energy from multiple squarylium dye molecules. Whether such energy transfer occurs in a serial fashion in which a LD800 molecule accepted energy from only one squarylium dye molecule at a time, or in a parallel fashion where multiple squarylium dye molecules donates energy simultaneously to a single LD800 molecule, remains to be seen.

For SQ-Cy2 films, the energy transfer efficiencies and rates are higher than for the SQ-Cy1 films and is undoubtedly due to the electrostatic interaction between the anionic SQ-Cy2 and the cationic LD800. The involvement of electrostatic interaction between SQ-Cy2 and LD800 is supported by the average distances obtained since the calculated distances are always shorter for the SQ-Cy2/LD800 than for the SQ-Cy1/LD800 complexes at similar mole ratios. Also, contrary to the large differences in energy transfer efficiencies seen for SQ-Cy1 films, depending on whether electron acceptors or LD800 was used, the efficiencies seen for SQ-Cy2 is similar when either type of acceptor is employed. This shows that as long as there is sufficient electronic coupling between the donor and acceptor, energy transfer efficiency is independent of the energy transfer mechanism involved. What differs significantly between the two mechanisms is the energy transfer rate. The rates when LD800 is employed are at least two orders of

magnitude bigger and more importantly, are in the same range as the diffusion limit of 10^{13} sec^{-1}. This means that the excited SQ-Cy2 molecules are returning to the ground state within 100 fs.

The measured lifetimes for the squarylium dye films containing LD800 are also of interest. As expected, the fluorescence decay of the squarylium dyes in films containing the highest concentration of LD800 exhibits instrument limited decay profiles (30 ps). Likewise, lowering the LD800 concentration leads to an increase in the lifetimes, but only to a few hundred picoseconds; still much less than when no LD800 is present in the films. What was unexpected, are the results for the LD800's fluorescence lifetimes at the two concentrations used. At a concentration of 1 mg/ml and with no squarylium dyes present, the mean lifetime of the LD800 molecules is 561 ps, while at a concentration of 0.24 mg/ml its lifetime increases to 1705 ps. This disparity in lifetimes, as a result of variation in concentration, is indicative of an intramolecular quenching process similar to that for the squarylium dyes. When LD800 at a concentration of 1 mg/ml is added to films containing SQ-Cy1 and SQ-Cy2, its lifetime decreases to 411 ps and 276 ps, respectively. At the lower concentration (0.24 mg/ml), the LD800 lifetime is now 1486 ps for films containing SQ-Cy1 and 638 ps for films containing SQ-Cy2. The fluorescence decay profiles corresponding to these lifetimes are presented in Figure 4-11. Two things are evident in these results. First, both squarylium dyes reduce the fluorescence lifetime of LD800 and secondly, the effect is more pronounced in SQ-Cy2 containing films. The latter observation provides a clue as to the nature of the quenching process involved in reducing the lifetime of LD800. Since the average distances between the LD800 and SQ-Cy2 molecules are shorter, greater electronic coupling can take place
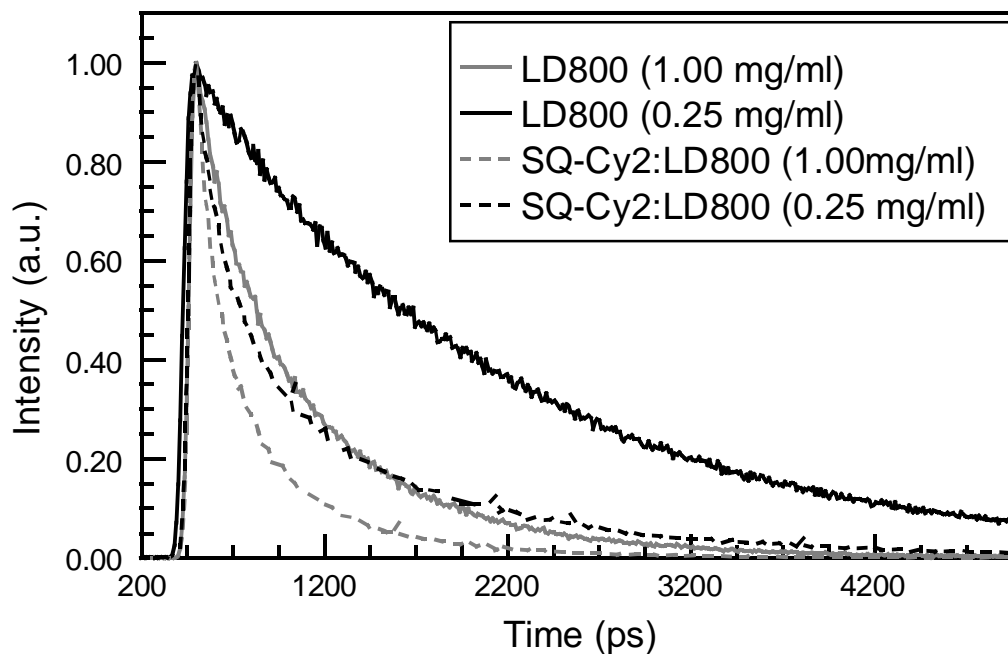
Figure 4-11. The fluorescence decay profiles for LD800 at different concentrations and in the presence of SQ-Cy2. In films containing SQ-Cy2, the decay is much more rapid, indicating a quenching process between the squarylium dye and LD800.

between the two, thereby increasing the likelihood than electron transfer can take place. As such, electron transfer appears to be the most likely quenching mechanism which can account for the reduction of LD800's lifetime. Whether the squarylium dyes or LD800 serve as the electron donor is unclear, however, previous studies have shown than an excited LD800 molecule plays the role of an electron acceptor [28]. Also, since the above study involving the electron acceptors, *p*NA and MV, show that the squarylium dyes serve as electron donors, they likely retain this role when intercalated into films containing LD800.

In order to evaluate the ultrafast dynamics of the energy transfer process between LD800 and the squarylium dyes, a femtosecond transient absorption study is once again undertaken. Since the SQ-Cy2 films containing LD800 at a mole ratio of 0.5 : 1 has the
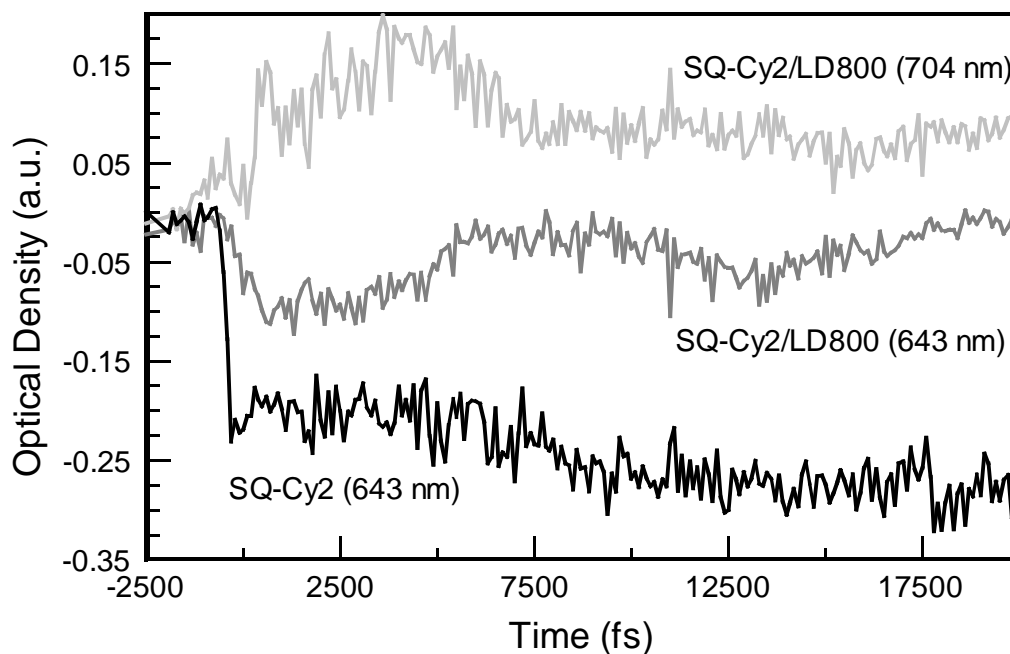
Figure 4-12. Transient absorption spectra of SQ-Cy2 films with and without LD800. When LD800 is present the transient bleach signal is weak, whereas, in the pristine films no ground state recovery is evident in this time window.

highest energy transfer efficiency and rate, it serves as the model system. The transient

absorption time profiles for this film monitored at 643 nm (SQ-Cy2 absorption

maximum) and 704 nm (LD800 absorption maximum) are shown in Figure 4-12. The

profile for the SQ-Cy2 film at 643 nm containing no LD800 is also provided for

comparison. The most noticeable difference when the SQ-Cy2 profiles at 643 nm are

compared is how much less the magnitude of the transient bleach signal is for the films

containing LD800. This is a clear indication that energy transfer is occurring on a time

scale much faster than the ability of the pump-probe system (~ 200 fs time resolution) to

resolve. This is in line with the measured energy transfer rate which indicates that

energy transfer, and hence ground state recovery, occurs in less than 100 fs. The

relatively weak bleach signal and recovery that are observed in the first 5 ps coincides

well with the rise and fall in the transient gain signal at 704 nm and is probably due to the forward and backward electron transfer process that is believed to take place between SQ-Cy2 and LD800. The fact that the gain signal at 704 nm did not decay back to zero following the recovery of the 634 nm bleach signal, indicates that LD800 molecules remained in the excited state following the electron transfer process and this is in accordance with the fluorescence lifetime data.

Unlike the squarylium dye films containing the electron acceptors, *p*NA and MV, the above ultrafast transient absorption kinetics and fluorescent lifetime data clearly show that films containing LD800 are suited for use as the photonic layer. Furthermore, the sub 100 fs ground state recovery these films exhibit would make them capable of switching operations in the terahertz region.

5. Xanthene Dyes

5.1 Introduction

First reported in the literature in the 19th century, anionic xanthene dyes are among the most widely studied and employed class of organic dyes [1-12]. As such, the photophysical properties and excited state dynamics of these dyes, in various environments and under a range of experimental conditions are well known. This fact makes this class of dyes excellent candidates for intercalation into the composite films. For one, they have proven photostability in sol-gel derived silica matrices, and also, interpretation of the observed optical properties is greatly simplified due to the enormous volume of work in existence. The general structure of these dyes is shown in Figure 5-1 and as can be seen, is composed of a benzene and a xanthene moiety which mostly contributes to the optical properties. The fundamental anionic xanthene dyes, fluorescein (FR), eosin, erythrosin, and rose bengal (RB) differ from each other only in aromatic ring
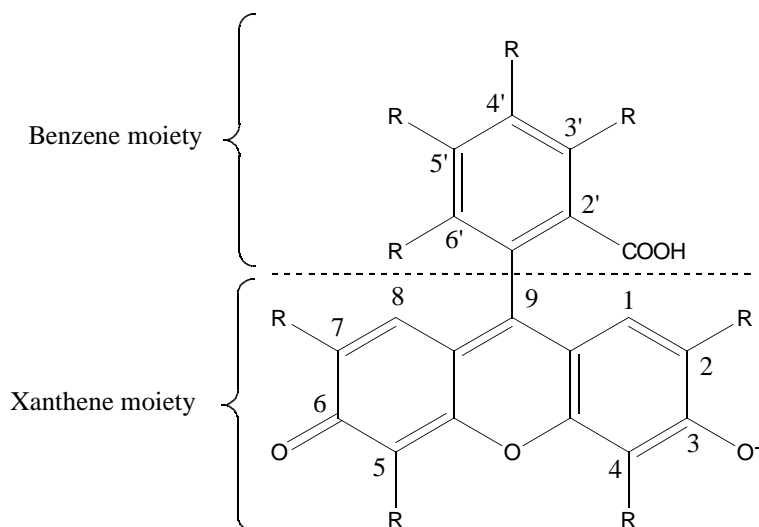
Figure 5-1. The general chemical structure of anionic xanthene dyes. The fundamental xanthene dyes are differentiated from each other by different substituents for R.

substitutions. In fluorescein, positions 1 - 8 and 3' - 6' are substituted with hydrogens, while in eosin, positions 2, 4, 5, and 7 are substituted with bromines. Erythrosin is similar to eosin with the only difference being that iodine is used in place of bromine. Rose bengal is differentiated from erythrosin by having chlorine substitutions at positions 3' - 6'.

Since the photophysical properties of these fundamental xanthene dyes are almost entirely determined by the degree and nature of substituent atoms, they exhibit distinctive photophysical properties. With an all hydrogen substitution, as with FR, the absorption band is shifted to higher energy and the quantum yield of fluorescence approaches unity under certain conditions. When heavy atom substituents are used, as with RB, the absorption band is shifted to the red, while the quantum yield of fluorescence is drastically reduced. The reduction in quantum yield is attributed to the classic heavy atom effect in which excited state, singlet to the triplet intersystem crossing (ISC) efficiency is increased when heavy atoms, such as iodine and chlorine, are present [2]. Furthermore, because of the ability of the oxygen at position 3 to undergo protonation/deprotonation reactions, these dyes all have acid/base indicator properties. Upon protonation, the absorption band in the visible along with the corresponding fluorescence, disappears because electron delocalization over the xanthene moiety is broken.

5.2 Rose Bengal

Though RB possesses the key photophysical properties (good photostability, high absorption coefficient) that makes it well suited towards the use in the photonic layer, another of its intrinsic property may prove to be a major hindrance in such an

application. As a result of the iodine and chlorine substitutions throughout the xanthene and benzene moieties, the ISC yield from the S_1 to the T_1 state is quite high (98 % in solution) [13], so essentially every photoexcited rose bengal molecule will cross over to the long lived (~3 μs) triplet state. Such a long excited state would inherently be detrimental to the ultrafast operation of an all-optical switching device. Also, formation of these long lived triplet states are often the root cause of the irreversible photo-degradation known to take place with most organic dyes [14]. This problem can be averted, however, by use of a suitable energy acceptor capable of undergoing both single and triplet state energy transfer with RB. Employment of such an acceptor is necessary because upon photoexcitation, rapid energy transfer from the S_1 state of RB to the acceptor can take place before ISC can occur. However, if a small fraction of the RB molecules do undergo ISC, then nearby acceptors could still deactivate them through a triplet energy transfer process. In this way, the excited state lifetimes of both the S_1 and T_1 excited states of RB can be reduced to a value which makes it practical for use as the active medium in the photonic layer in an all-optical switching device.

Prior to identifying suitable candidates that can serve as energy acceptors, it is important to ascertain the photophysical properties of RB incorporated into the composite films. The normalized absorption and fluorescence spectra for films containing RB at a concentration (reported in mg of RB to ml of sol) of 1.6 mg/ml and 5 mg/ml are presented in Figure 5-2. The absorption spectra of films containing the two concentrations of RB are similar with the only noticeable differences being a variation in the intensity of the shoulder at ~ 524 nm and a slight broadening in the spectrum for the film containing the higher concentration of RB. The maximum for both absorption
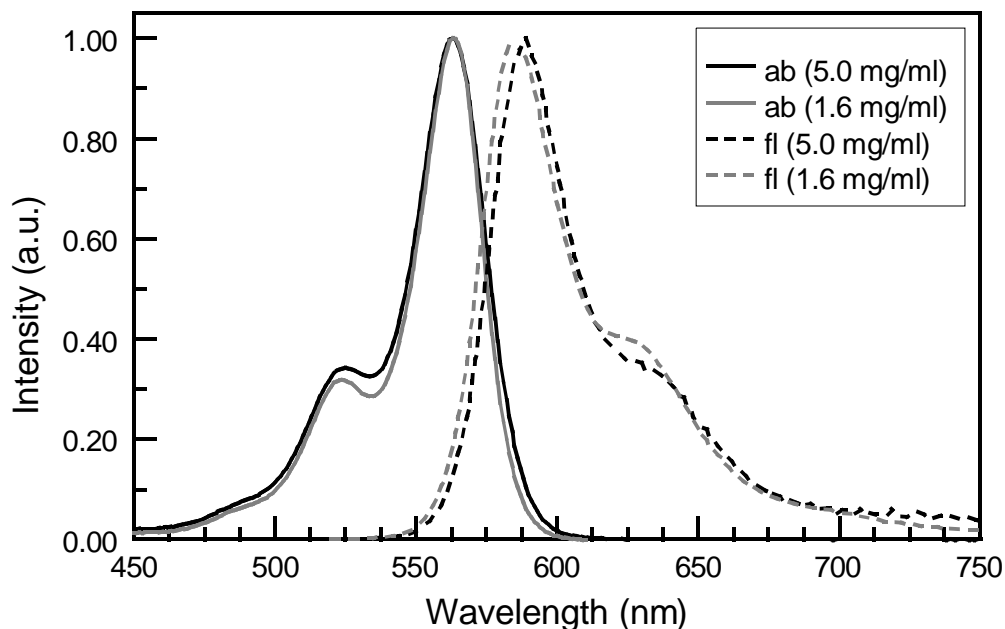
Figure 5-2. The normalized absorption (ab) and fluorescence (fl) spectra of rose bengal (RB) intercalated into the composite film at various concentrations. λ_{ex} 525 nm.

spectra occurs at 563 nm and is red-shifted by some 20 nm, relative to the RB spectrum

in water. This red-shift is indicative of the inclusion of the RB within the Pluronic P123

mesostructures: red-shifts of similar magnitudes have been observed when RB was

occluded within TX-100 and CTAB micelles [15]. The red-shift is attributed to

molecular interactions between RB and the surfactant molecules. Difference in the films

absorption spectra is, in all likelihood, due to the formation of dimers or h-type

aggregates that RB is known to form at higher concentrations [1,2,4]. Further evidence

for the formation of such aggregates can been seen in the fluorescence spectra of these

films.

Similar to the absorption spectra, the fluorescence spectra of the RB films are also

red-shifted compared to the spectrum in water, but now, not only is there a difference in

the shoulders at ~ 630 nm, the maximum for the two RB films does not overlap either.

At the concentrations of 1.6 mg/ml and 5 mg/ml, the fluorescence maximum occurs at

585 nm and 589 nm, respectively. These differences are in line with what would be

expected from the formation of dimers or h-type aggregates. Moreover, the measured

fluorescence quantum yields also lends further support for this assertion. In films

containing the lower concentration of RB, the quantum yield is 19 %, while for films

containing the higher concentration, it decreases to 4 %. Such diminution in the quantum

yields is indicative of a self quenching process between individual RB molecules, most

likely an electron transfer from the benzene moiety of one RB molecule to the xanthene

moiety of an other which is in the excited state [10]. It should be noted, that the quantum

yields presented here are higher than those reported for RB entrapped within micelles by

Gao et al. [15]. This disparity in quantum yields is a clear indication that the excited

state of RB is being stabilized by the formation of a charge transfer (CT) complex [16]

with Pluronic P123 molecules to a greater extent than it did with the previously used

surfactants. The excitation spectra (monitored at 610 nm), which can be seen in Figure

5-3, also shows evidence for the formation of dimers or h-type aggregates in the 5 mg/ml

RB film. At a concentration of 1.6 mg/ml, the excitation spectrum mirrors that of the

absorption spectrum except it is broadened due to the formation of the CT complex. The

excitation spectrum for films containing 5 mg/ml RB, on the other hand, deviates

substantially from the absorption spectrum. Whereas, the absorption spectrum has only

two peaks, the excitation spectrum has three distinct peaks occurring at 524 nm, 547 nm

and 573 nm. The peak at 524 nm clearly corresponds to the shoulder in the absorption

spectrum, but the other two have no corresponding peaks in the absorption spectrum.

These peaks most likely results from dynamic disordering within the dimers or h-type
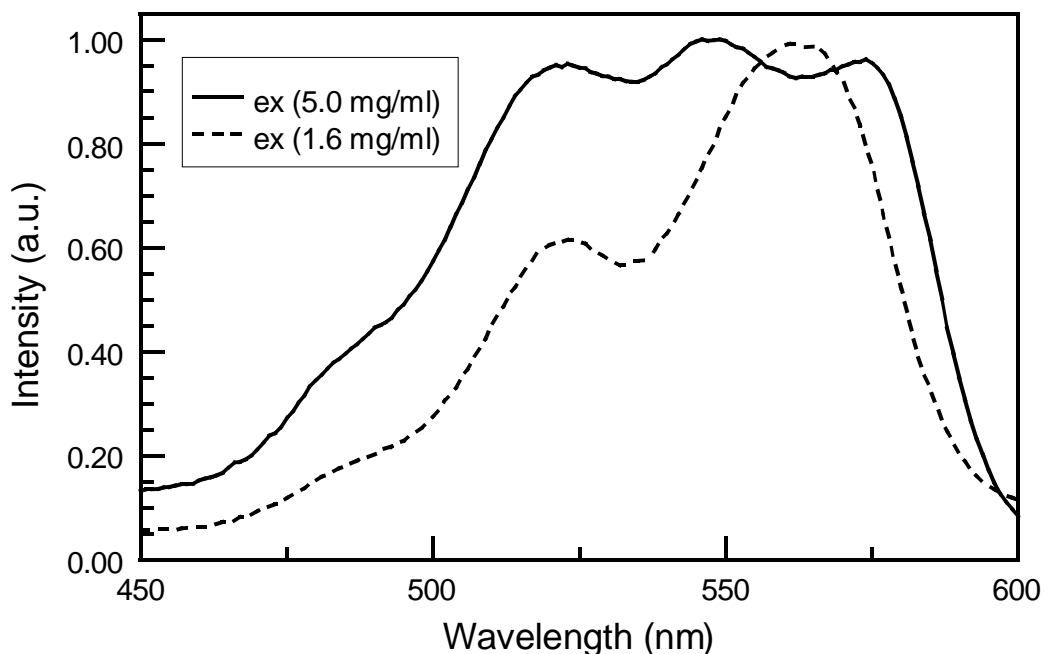
Figure 5-3. The normalized excitation (ex) spectra monitored at 610 nm for RB containing films.

aggregates [17]. Simply put, when multiple RB molecules in the same dimer or aggregate structure are simultaneously excited, the quantum yield of fluorescence decreases due to increased vibrations throughout the aggregate. Such vibrations acts as an additional nonradiative pathway for excited state deactivation.

5.3 Rose Bengal Excited State Deactivation

From the absorption and fluorescence properties exhibited by the RB molecules intercalated within the composite films, it is determined that a suitable energy acceptor is the same cyanine-type squarylium dyes discussed in the previous chapter. From Figure 5-4 it can been seen that the fluorescence band of RB has sufficient spectral overlap with the absorption bands of the squarylium dyes to allow for efficient Coulombic energy exchange. Also, previous work has shown that squarylium dyes are capable of accepting
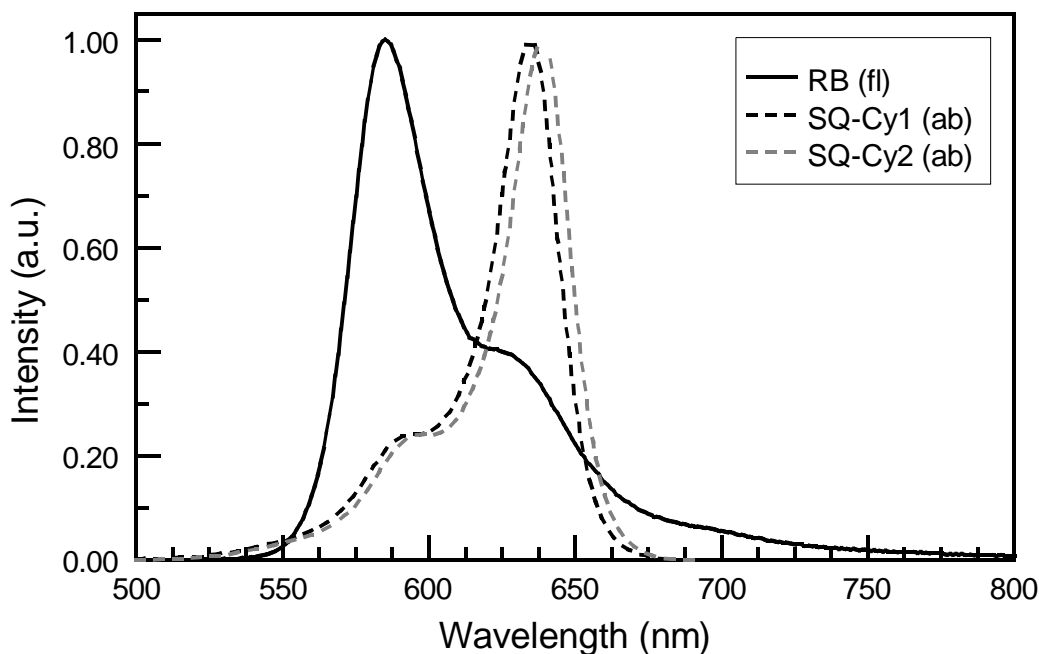
Figure 5-4. Spectral overlap between the absorption (ab) of the cyanine-type squarylium dyes, and the fluorescence (fl) of RB.

energy from a donor molecule in the triplet state [18]. The energy transfer takes place from the T_1 state of the donor to the low-lying T_1 state of the squarylium dye. The RB : squarylium dye mole ratios used for this study, varies from 2 : 1 to as high as 12 : 1. This relatively wide range is chosen in order to probe the spacial relationship of the donor and acceptor species within the Pluronic P123 mesostructures. Also, the higher ratios allows for the ability of a single squarylium dye to accept energy from multiple RB molecules to be determined.

In order to probe the interactions between the monomeric or aggregated RB and the squarylium dyes, detailed fluorescence lifetime studies are done. The key results from these studies are presented in Table 5-1. For films containing 5 mg/ml RB and no squarylium dyes, the fluorescence decay can be fitted well using a two component

Table 5-1: Lifetimes of rose bengal (RB) films containing the squarylium dyes, SQ-Cy1 and SQ-Cy2 at various mole ratios. In these films, the squarylium dyes serve as the energy acceptors. An excitation wavelength of 510 nm was used.

RB : SQ mole ratio	[a]Conc. RB (mg/ml)	[b]Dyes	τ_1 (ps)	τ_2 (ps)	τ_3 (ps)
n/a	5	RB	323 (69 %)	123 (31 %)	
n/a	1.6	RB	878 (100 %)		
2 : 1	5	<u>RB</u> : SQ-Cy1	44 (95 %)	242 (5 %)	
2 : 1	5	RB : <u>SQ-Cy1</u>	397 (76 %)	[c]32 (14 %)	899 (10 %)
3 : 1	5	<u>RB</u> : SQ-Cy2	30 (100 %)		
3 : 1	5	RB : <u>SQ-Cy2</u>	533 (66 %)	237 (20 %)	[c]30 (14 %)
1 : 1	1.6	<u>RB</u> : SQ-Cy1	134 (64 %)	127 (36 %)	
1 : 1	1.6	RB : <u>SQ-Cy1</u>	1687 (78 %)	[c]256 (22 %)	
3 : 1	1.6	<u>RB</u> : SQ-Cy1	668 (88 %)	153 (12 %)	
3 : 1	1.6	RB : <u>SQ-Cy1</u>	2706 (45 %)	2196 (45 %)	[c]173 (10 %)
6 : 1	1.6	<u>RB</u> : SQ-Cy1	662 (85 %)	46 (15 %)	
6 : 1	1.6	RB : <u>SQ-Cy1</u>	2613 (83 %)	[c]1732 (11 %)	[c]167 (6 %)
2 : 1	1.6	<u>RB</u> : SQ-Cy2	92 (78 %)	275 (22 %)	
2 : 1	1.6	RB : <u>SQ-Cy2</u>	1248 (84 %)	[c]150 (16 %)	
6 : 1	1.6	<u>RB</u> : SQ-Cy2	526 (52 %)	210 (48 %)	
6 : 1	1.6	RB : <u>SQ-Cy2</u>	2530 (54 %)	[c]457 (26 %)	3154 (20 %)
12 : 1	1.6	<u>RB</u> : SQ-Cy2	629 (58 %)	262 (42 %)	
12 : 1	1.6	RB : <u>SQ-Cy2</u>	3045 (61 %)	2092 (22 %)	[c]635 (17 %)

[a] Concentration of RB in mg per 1 ml of sol. [b] An underline indicates the dye's fluorescence for which the lifetime is presented. [c] Indicates that this component is a rise component.

exponential model, with the major component having a time constant of 323 ps (69 %), while the minor component had a time constant of 123 ps (31 %). When the RB concentration is reduced to 1.6 mg/ml, the fluorescence decay is mono-exponential with a time constant of 878 ps. This difference in lifetime is further support for the assertion that at a concentration of 5 mg/ml individual RB molecules self-assemble into either dimers or h-type aggregates. As expected, when either squarylium dye is added to the 5 mg/ml RB film, the fluorescence lifetime decreases, but the percent decrease is more pronounced when SQ-Cy2 is employed rather than when SQ-Cy1 is used. Even though less SQ-Cy2 is used, the fluorescence lifetime of RB is reduced down to the instrument

limited value of 30 ps. The greater ability of SQ-Cy2 to reduce the excited state lifetime is most likely due to its greater solubility, which allows more acceptor molecules to be in closer proximity to the RB dimer or aggregate structures. From the discussion in the previous chapter, it was shown that since SQ-Cy1 preferentially formed aggregates at the concentration used, less SQ-Cy1 molecules would be available to undergo energy transfer with RB. This would have the effect of reducing the energy transfer efficiency of SQ-Cy1 relative to SQ-Cy2, and would lead to the observed results.

When the concentration of RB is reduced to 1.6 mg/ml a similar trend is observed, except now neither squarylium dye is able to reduce the fluorescence lifetime of RB down to the instrumented limited value, even though the mole ratios are more closely matched. This suggests that the squarylium dyes are more effective at deactivating the excited state of the RB dimers or aggregates than the isolated RB molecules. A simple explanation for this is that when RB forms dimers or h-type aggregates, its negative charge is passivated to some extent, thereby allowing a closer approach by the squarylium dyes and leading to higher energy transfer efficiencies. When RB isolated within the matrix, no such charge passivation occurs so the electrostatic repulsive force is greater and the squarylium dyes, on average, remain further away from the RB molecules. From this data, it is clear that efficient deactivation of the isolated RB molecules requires that there to be a greater number of squarylium dyes than RB present in the film. One should note that these lifetime measurements only provide information for the deactivation rate of the S_1 state of RB and not the T_1 state. If triplet states are being formed prior to energy transfer taking place, then the overall excited state lifetime of RB will be much longer than is suggested by the measured lifetimes.

The fluorescence decay of the squarylium dyes following the energy transfer from RB are also of interest. Irrespective of the RB concentration in the film, the fluorescence decay of the squarylium dyes always exhibits a minor rise component. Since the number of RB molecules outnumbered the squarylium dyes in every case, it can be concluded that these rise components are due to energy transfer from multiple RB, to a single squarylium dye molecule. In the case of the 1.6 mg/ml RB films containing SQ-Cy1, the lifetime value of this rise component increases from 256 ps to 1732 ps as the RB: SQ-Cy1 mole ratio is increased from a 1 : 1 to 6 : 1. Comparable results are also seen for films containing SQ-Cy2. At a RB : SQ-Cy2 mole ratio of 2 : 1, the lifetime of the rise component is 150 ps, while at mole ratio of 12 : 1 the rise component's lifetime is increases to 635 ps. The smaller lifetime values for the rise components infer that the rate of energy transfer in these films is higher compared to the SQ-Cy1 containing films. Regardless of which squarylium dye results in the greatest energy transfer rate and efficiency, one thing is clear from the data. The confining nature of the Pluronic P123 mesostructures allows multiple RB molecules to under energy transfer with a single squarylium dye molecule, making the energy transfer process more efficient than it would otherwise be.

The overall dynamics and donor/acceptor interactions of the energy transfer process is further elucidated when the energy transfer parameters are calculated. The results of these calculations are presented in Table 5-2. When SQ-Cy1 is used as an energy acceptor, the transfer efficiency (82.5 %) is the highest for the 5 mg/ml RB film, which as mentioned above, contains either RB dimer or h-type aggregates. For the 1.6 mg/ml RB film, the transfer efficiency decreases from 75.0 % to 35.0 % when the mole ratio is

Table 5-2: The energy transfer parameters for RB composite films containing SQ-Cy1 or SQ-Cy2 as energy acceptors.

SQ Dye	[a]Conc. RB (mg/ml)	mole ratio RB : SQ	Transfer Efficiency[b]	R_0 (± 4 Å)[c]	r (± 4 Å)[d]	Transfer Rate (x10^{11} M^{-1}sec^{-1})[e]
SQ-Cy1	n/a	n/a	n/a	62	n/a	n/a
	5	2 : 1	82.5 %		48	6.0
	1.6	1 : 1	75.0 %		52	5.5
	1.6	3 : 1	31.0 %		71	2.4
	1.6	6 : 1	35.0 %		69	6.2
SQ-Cy2	n/a	n/a	n/a	66	n/a	n/a
	5	3 : 1	99.2 %		30	7.8
	1.6	2 : 1	85.0 %		50	50.0
	1.6	6 : 1	57.3 %		63	61.5
	1.6	12 : 1	46.0 %		68	48.0

[a] Concentration of RB in mg per 1 ml of sol. [b] The efficiencies were calculated using Eq. (2.4). [c] The Förster distance, R_0, obtained using Eq. (2.7). [d] The average distance, r, between the RB and squarylium dyes calculated from Eq (2.8). [e] Energy transfer rates were calculated using Eq. (2.6).

varied from 1 : 1 to 6 : 1. Surprisingly, the 3 : 1 mole ratio gives the lowest transfer efficiency (31 %) and is probably due to self aggregation of SQ-Cy1 at the concentration used in this film. The transfer rates for all films remains in the 10^{11} M^{-1} sec^{-1} range, too low to be practical for use as the photonic layer: the transfer rate must be at least 10^{11} M^{-1} sec^{-1}. The average distance, r, between a RB and SQ-Cy1 molecule is also a point of interest. Since an r of ~70 Å is maintained when the mole ratio is increased from 3 :1 to 6 :1, this indicates that the boundaries of the Pluronic P123 mesostructures dictates an upper limit for donor/acceptor separation. If this is not the case, then decreasing the SQ-Cy1 content in the films should result in a concurrent increase in r, not a leveling off of it.

As expected, the calculated energy transfer parameters for RB films containing SQ-Cy2, is similar to what is observed when SQ-Cy1 is used, but with a few differences.

For one, the transfer efficiency now exceeds 99 % for the 5 mg/ml RB film even though less SQ-Cy2 than SQ-Cy1 is used. The reason for this becomes apparent when the average distance, r, of the SQ-Cy2 containing film is examined. With an r value of ~ 30 Å, SQ-Cy2 is getting much closer to the RB dimer or h-type aggregates, and consequently resulting in a higher energy transfer efficiency. However, the transfer rate measured for this film is not the highest among the SQ-Cy2 containing films; as a matter of fact, it is the lowest with a value of 7.8 x 10^{11} M^{-1} sec^{-1}. The transfer rates for the 1.6 mg/ml RB films are all in the 10^{12} M^{-1} sec^{-1}, this is an order of magnitude higher than the 5 mg/ml RB films. It would seem that the energy transfer process from the RB dimer or h-type aggregates, occurs at a slower rate than the transfer from an isolated RB molecule. The reason for this remains unclear at this time, but it could be that in the RB dimer or h-type aggregates, electron exchange (a slower process at the given r) plays a role in the energy transfer process, along with typical Coulombic exchange mechanism. As with the RB films containing SQ-Cy1, r, appears to level off at ~ 70 Å even though the concentration of SQ-Cy2 is half as much. This fact seems to once again confirm the fact that the Pluronic P123 mesostructures serve to limit the separation between the RB and squarylium molecules.

Though a significant amount of information is obtained from the time-resolved fluorescence and energy transfer studies, they provide no real information about the role of RB's ISC has on the overall energy transfer process and excited state dynamics. In order to obtain such information, a femtosecond transient absorption study is carried out. The samples used in this study contains 1.4 mg/ml RB and SQ-Cy2 at a 1 : 1 mole ratio or no SQ-Cy2. A 100 fs, 555 nm pump pulse is used for all samples. In Figure 5-5, the
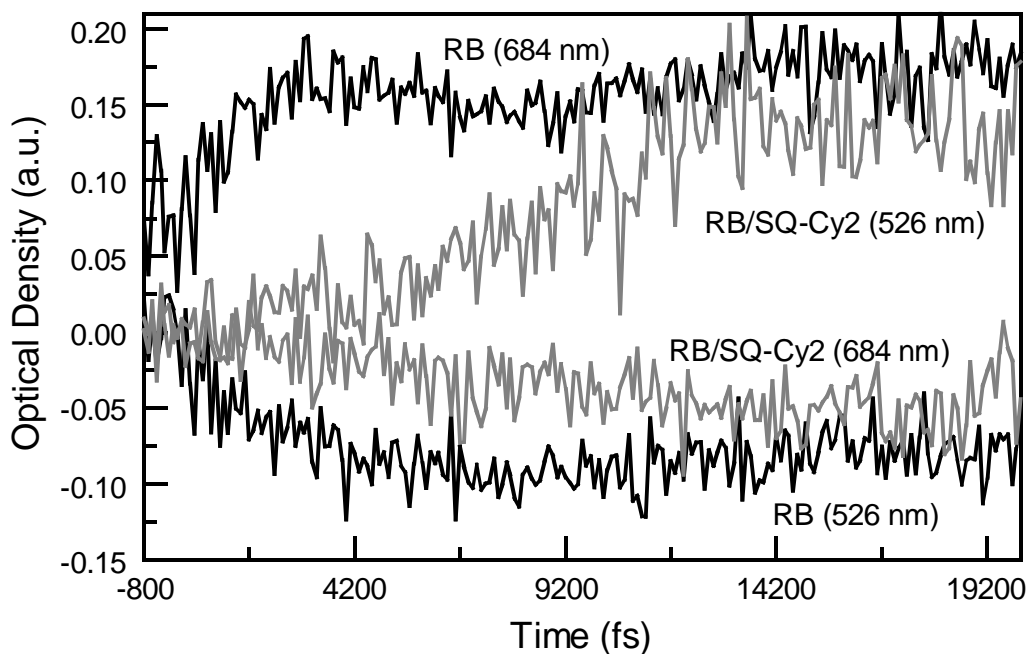
Figure 5-5. Transient absorption spectra of RB films with and without SQ-Cy2. When SQ-Cy2 is present, the transient signals monitored at 684 nm and 526 nm are very different, indicating the presence of an ultrafast energy transfer process.

transient profiles monitored at 526 nm and 684 nm, and for the 20 ps time window

following excitation are shown. For the RB film containing no SQ-Cy2 there is a

transient bleach signal at 526 nm which takes about 7 ps to level off and a transient gain

signal at 684 nm which levels off in about the same time. The signal at 526 nm is clearly

due to the depletion of ground state RB molecules, whereas the one at 684 nm is most

likely attributable to the S_1 to S_4 transition of RB [13]. The relatively slow initial

progression of these signals before leveling off is indicative of the S_1 to T_1 ISC process.

When SQ-Cy2 is added to the film, the bleach signal at 526 nm no longer appears,

instead it is replaced by a gain signal that slowly levels off after ~ 14 ps. Likewise, the

transient gain signal at 684 nm disappears. This means that the energy transfer from the

S_1 state of the RB takes place on a time scale less than the 200 fs resolution of the pump-

probe system. From the energy transfer data, it is found that this process occurs in roughly 100 fs. The origin of the gain signal at 526 nm is not evident at the moment, but visual inspection of the film following data acquisition, shows clear signs of irreversible photodegradation: a ring outlined the area the pump pulse was focused as the sample rotated. As such, this signal is most likely due to the photodegraded products of SQ-Cy2, since the pure RB film shows no signs of photodegradation under identical experimental conditions. Coincidentally, the existence of these products serve as proof that triplet energy transfer is taking place because films containing only SQ-Cy2 show no signs of degradation even when the pump pulse intensity is increased approximately five fold. Unfortunately, the existence of these photodegraded products also indicate that the switching ability of these films would rapidly degrade under operational conditions.

5.4 Fluorescein

Though the rapid deactivation of both the singlet and triplet excited states of RB using squarylium dyes shows that ultrafast optical switching is attainable in composite films containing these dyes, unfortunately the unforeseen photodegradation of the squarylium dyes would make such films unsuitable for the intended application. Several possible solutions exists to eliminate or significantly reduce the photodegradation process taking place. The simplest of which is the use of an energy acceptor that is less susceptible to photodegradation. However, finding or synthesizing such a molecule, whose spectral properties allows for efficient energy transfer to take place with RB and could be intercalated into the composite films at high enough concentrations, would probable be a long and tedious task in this author's opinion. Another approach is to employ a photoprotective additive with a low lying triplet state such has β-carotene [19].

Such additives are shown to improve the photostability of organic dyes in solid matrices [20], but their effectiveness is short lived for the following reason. Since no diffusion of the additives can occur in the host matrix, then once the additive itself photodegrades (which it will eventually do) the organic dye it is meant to protect will be left unprotected and photodegradation of this dye will most likely follow. Furthermore, the radical species from the photodegradation of the additive could react with the organic dyes, causing them to permanently lose their optical properties. Taken these factors into consideration, another, more practical solution, is to replace RB with one of the other xanthene dyes which do not undergo ISC as readily. The dye chosen is FR, which, as a result of the all-hydrogen substitution on the xanthene and benzene moieties, has a very low ISC yield.

Within the composite film, FR at a concentration of 0.8 mg/ml has an absorption and fluorescence spectra that closely match that in a 0.1 N NaOH solution [10]. As can be seen in Figure 5-6, the absorption and fluorescence maxima are at 494 nm and 515 nm, respectively. In solution these maxima occurs at 492 nm and 511 nm. This relatively small difference in the film and solution spectra, indicates that there is little electronic interaction between FR and the Pluronic P123 molecules that compromise the mesostructures, in the ground or excited state. The fluorescence quantum yield in the film is close to unity (99 %), whereas, in the basic solution a value of 76 % was reported [12]. Such an increase in the quantum yield is consistent with what is observed when FR is intercalated into CTAB micelles [12]. The measured lifetime in the film is 3870 ps and is shorter than the measured value in solution or within the CTAB micelles.
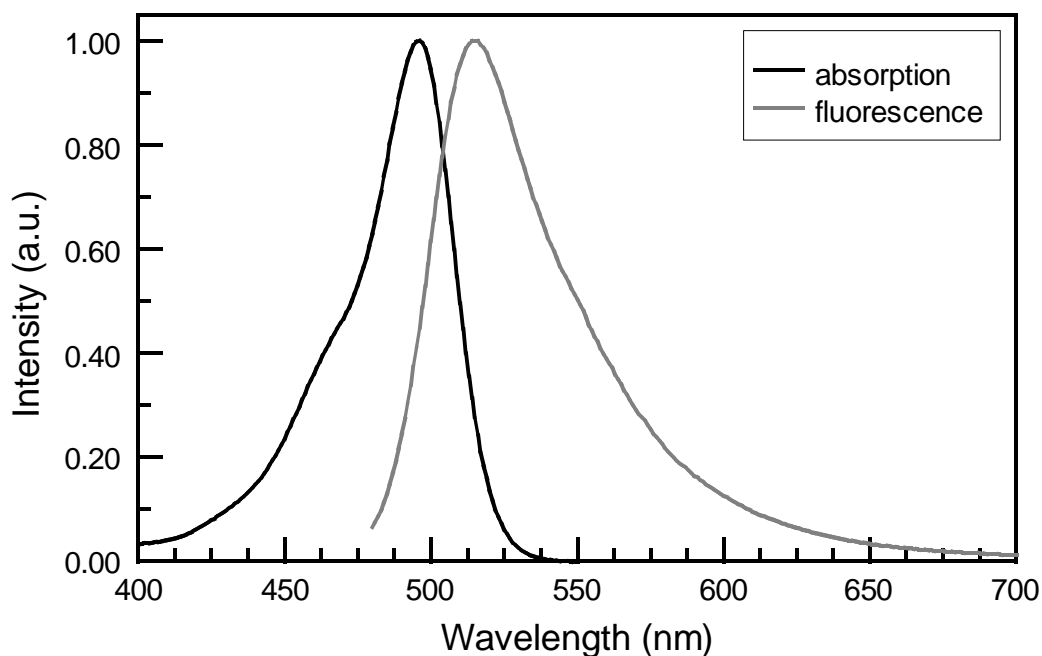
Figure 5-6. The normalized absorption and fluorescence spectra of fluorescein (FR) intercalated into the composite film. λ_{ex} 470 nm.

Indubitably, with such a high quantum yield and long lived excited state, very little, if any, ISC is taking place.

From comparison of the fluorescence spectrum of FR and the absorption spectra of the squarylium dyes, it is apparent that there is less spectral overlap than with the RB/squarylium dye system. As a result, it is expected that the squarylium dyes will be less effective at reducing the excited state lifetime of FR and that is exactly what is observed. In Table 5-3, the lifetimes of the FR films containing various mole ratios of SQ-Cy1 and SQ-Cy2 are presented. It is found that neither squarylium dye reduced FR's lifetime below 100 ps at the mole ratios used. Increasing the concentration of the squarylium dyes by a factor of two or three probably would have resulted in further reduction in the lifetime, but the film quality would have been adversely affected. Also,

Table 5-3: Lifetimes of fluorescein (FR) films containing the squarylium dyes, SQ-Cy1 and SQ-Cy2 at various mole ratios. In these films, the squarylium dyes serve as the energy acceptors. The excitation wavelength was 490 nm.

FR : SQ mole ratio	[a]Conc. FR (mg/ml)	[b]Dyes	τ_1 (ps)	τ_2 (ps)	τ_3 (ps)
n/a	0.8	FR	3870 (100 %)		
1 : 1	0.8	FR : SQ-Cy1	178 (58 %)	538 (42 %)	
1 : 1	0.8	FR : SQ-Cy1	766 (63 %)	[c]233 (37 %)	3151 (0.3 %)
2 : 1	0.8	FR : SQ-Cy1	322 (52 %)	1114 (48 %)	
2 : 1	0.8	FR : SQ-Cy1	1470 (65 %)	[c]484 (35 %)	
2 : 1	0.8	FR : SQ-Cy2	143 (66 %)	493 (34 %)	
2 : 1	0.8	FR : SQ-Cy2	674 (37 %)	[c]275 (33 %)	1070 (30 %)
4 : 1	0.8	FR : SQ-Cy2	285 (62 %)	825 (38 %)	
4 : 1	0.8	FR : SQ-Cy2	1825 (65 %)	[c]484 (35 %)	

[a] Concentration of FR in mg per 1 ml of sol. [b] An underline indicates the dye's fluorescence for which the lifetime is presented. [c] Indicates that this component is a rise component.

rise components compromised a greater percentage of the overall fluorescence decay than is seen with the RB systems and is suggestive of a slower energy transfer process. The calculated energy transfer parameters, which are outlined in Table 5-4, are more informative. When SQ-Cy1 is used as an acceptor, the maximum transfer efficiency is 91.5 %, with a corresponding transfer rate of 2.7 x 10^{11} M^{-1} sec^{-1}. Use of SQ-Cy2 does not result in much of an improvement in either the energy transfer rate or efficiency. The maximum efficiency is 93.2 %, while the corresponding rate is 6.5 x 10^{11} M^{-1} sec^{-1} for FR films containing SQ-Cy2. This translated into excited state deactivation of the FR molecules occurring within 1.5 ps. The obtained *r* are, on average, smaller than is found for the non-aggregated RB systems and might account for the higher energy transfer efficiencies for these systems. Unfortunately, higher transfer efficiencies does not result in higher transfer rates. This one fact effectively makes these FR films poorly suited for use as the photonic layer.

Table 5-4: The energy transfer parameters for FR composite films containing SQ-Cy1 or SQ-Cy2 as energy acceptors.

SQ Dye	[a]Conc. FR (mg/ml)	mole ratio FR : SQ	Transfer Efficiency[b]	R_0 (± 4 Å)[c]	r (± 4 Å)[d]	Transfer Rate (x10^{11} M^{-1}sec^{-1})[e]
SQ-Cy1	n/a	n/a	n/a	61	n/a	n/a
	0.8	1 : 1	91.5 %		41	2.7
	0.8	2 : 1	82.0 %		47	2.3
SQ-Cy2	n/a	n/a	n/a	65	n/a	n/a
	0.8	2 : 1	93.2 %		42	6.5
	0.8	4 : 1	87.3 %		47	6.5

[a] Concentration of FR in mg per 1 ml of sol. [b] The efficiencies were calculated using Eq. (2.4). [c] The Förster distance, R_0, obtained using Eq. (2.7). [d] The average distance, r, between the FR and squarylium dyes calculated from Eq (2.8). [e] Energy transfer rates were calculated using Eq. (2.6).

Ultimately, the ability of FR films to be used as the photonic layer is going to depend on finding an energy acceptor whose absorption band possesses a greater spectral overlap with the fluorescence band of FR. This will not only increase the efficiency of the energy transfer process, but more importantly, will allow the transfer rate to approach the diffusion limited value. The acceptor chosen is the triphenylmethane dye, crystal violet (CRV) [21,22]. Aside from the significant spectral overlap between the absorption band of this dye and the fluorescence band of FR, its cationic nature also means that electrostatic interaction would decrease the average separation between the two dyes. This decrease in r will undoubtedly aid in increasing the energy transfer efficiency and rate. The spectral overlap, along with the structure of CRV are shown in Figure 5-7. For FR/CRV films, mole ratios of 1 : 1, 1 : 3, and 6 : 1 are used. Also, the FR concentration is now 1.5 mg/ml.

In Table 5-5, the fluorescence lifetimes of films containing FR and CRV at various mole ratios are presented. The pristine FR film exhibits a two component fluorescence
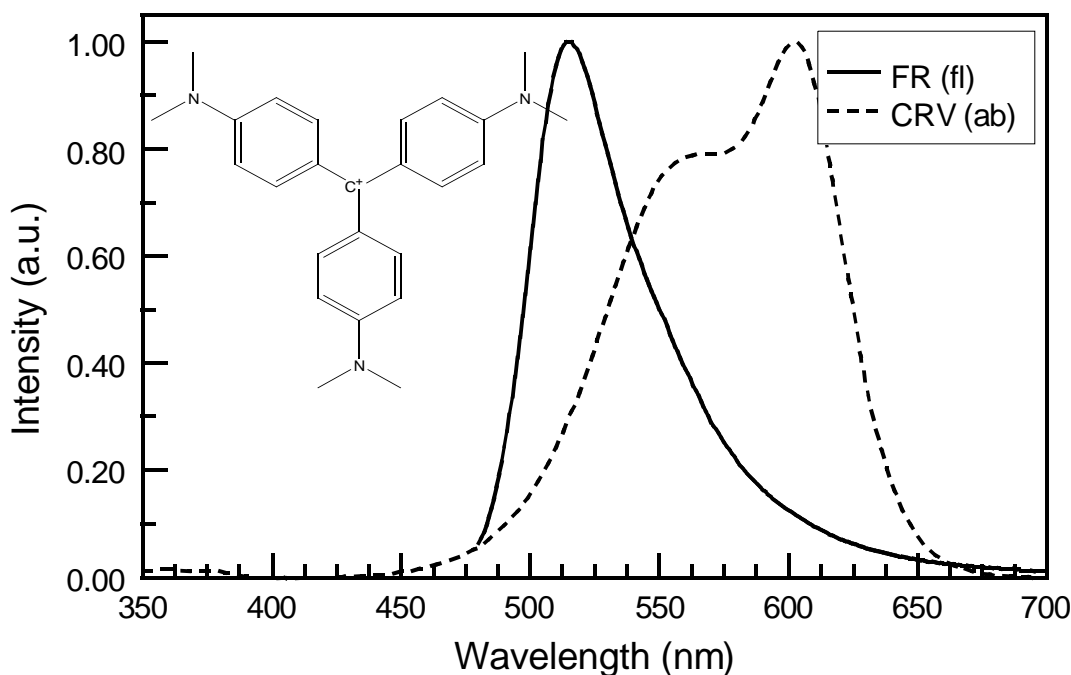
Figure 5-7. Spectral overlap between the absorption (ab) of crystal violet (CRV) and the fluorescence (fl) of fluorescein (FR).

decay profile, whose time constants are 1160 ps (60 %) and 2260 (40 %). The

corresponding fluorescence quantum yield for this film is 30 %. Taken together, these

results are consistent with the presence of an intramolecular quenching mechanism

between individual FR molecules, as is the case with the higher concentration (5 mg/ml)

Table 5-5: Lifetimes of fluorescein (FR) films containing the energy acceptor crystal violet (CRV) at various mole ratios. The excitation wavelength was 490 nm.

FR : CRV mole ratio	[a]Conc. FR (mg/ml)	[b]Dyes	τ_1 (ps)	τ_2 (ps)
n/a	1.5	FR	1160 (60 %)	2260 (40 %)
1 : 1	1.5	<u>FR</u> : CRV	30 (100 %)	
1 : 1	1.5	FR : <u>CRV</u>	139 (77 %)	512 (23 %)
3 : 1	1.5	<u>FR</u> : CRV	71 (81 %)	233 (19 %)
3 : 1	1.5	FR : <u>CRV</u>	231 (73 %)	657 (27 %)
6 : 1	1.5	<u>FR</u> : CRV	145 (67 %)	514 (33 %)
6 : 1	1.5	FR : <u>CRV</u>	455 (67 %)	1033 (33 %)

[a] Concentration of FR in mg per 1 ml of sol. [b] An underline indicates the dye's fluorescence for which the lifetime is presented.

RB film. When CRV is present at a 1 : 1 mole ratio, the measured FR lifetime decreases

to the instrumented limited value of 30 ps. Decreasing CRV content to achieve the mole

ratios of the 3 : 1 and 6 : 1, leads to increases in the FR mean lifetimes, but the values are

still much less than is found when no CRV is added. These significant reductions in

fluorescence lifetimes are indicative of an ultrafast, highly efficient, energy transfer

process between FR and CRV. The fluorescence decay, monitored at the wavelengths

which corresponds to the CRV fluorescence, are also of interest. Unlike the decay

profiles of the squarylium dyes, which possess rise components, those of CRV do not.

There is an increase in the major component's lifetime value from 139 ps to 455 ps on

increasing the FR : CRV mole ratio from 1 : 1 to 6 : 1, but no rise component can be

detected. Lack of such rise components lends further support to the argument that it is an

ultrafast energy transfer process that occurs between FR and CRV.

The calculated energy transfer parameters provides an even clearer picture showing

just how fast the energy transfer process is, and likewise, the applicability of these films

to be used as the photonic layer. These parameters are outlined in Table 5-6. At a 1 : 1

mole ratio, the energy transfer efficiency and rate are found to be 99.6 % and 13.2×10^{12}

Table 5-6: The energy transfer parameters for FR composite films containing CRV as
an energy acceptor.

[a]Conc. FR (mg/ml)	mole ratio FR : CRV	Transfer Efficiency[b]	R_0 (± 4 Å)[c]	r (± 4 Å)[d]	Transfer Rate ($\times 10^{12}$ M^{-1}sec^{-1})[e]
n/a	n/a	n/a	61	n/a	n/a
1.5	1 : 1	99.6 %		24	13.2
1.5	3 : 1	96.7 %		35	3.3
1.5	6 : 1	88.8 %		43	1.8

[a] Concentration of FR in mg per 1 ml of sol. [b] The efficiencies were calculated using Eq.
(2.4). [c] The Förster distance, R_0, obtained using Eq. (2.7). [d] The average distance, r,
between the FR and CRV calculated from Eq (2.8). [e] Energy transfer rates were
calculated using Eq. (2.6).

M^{-1} sec^{-1}, respectively. To put it simply, practically all of the FR molecules that are excited, return to the ground state in less than a 100 fs. Moreover, even when a mole ratio of 6 : 1 is used, the efficiency remains above 88 % while the rate is still in the 10^{12} M^{-1} sec^{-1} range. That still means that excited state deactivation of most of the excited FR molecules is occurring within 1 ps. These results and the lack of any rise component in the fluorescence decay profile of CRV, strongly suggests the ability of a single CRV molecule to simultaneously except energy from multiple, nearby, FR molecules. Such a process is akin to a two-photon absorption. This is of no surprise since CRV has been shown to readily undergo two-photon absorption [21]. The effectiveness of the electrostatic attraction between FR and CRV to minimize r, is also observed. For example, at the 1 : 1 mole ratio, an r value of 24 Å is obtained. This is much less than the r values seen using the squarylium dyes at similar mole ratios and could only be due to electrostatic interaction since there is not a substantial size difference between these two molecules.

6. Rhodamine 6G

6.1 Introduction

Rhodamines are a class of cationic xanthene dyes which are characterized by their strong absorption in the visible region, high fluorescence quantum yields, substantial nonlinear properties, and good thermal and optical stability. Among these dyes, probably the most widely studied and employed is rhodamine 6G (R6G). The structure of this dye is shown in Figure 6-1. With a fluorescence quantum yield near unity (0.94 in ethanol), as well as good optical and thermal stability, R6G has been extensively employed as the lasing medium in both liquid and solid optically pumped dye lasers [1-6]. In fact, R6G is often considered the yard stick to which other organic laser dyes are measured against [1]. The sensitivity of R6G's fluorescence to the surrounding environment, has also led to its use as a biological label for cell fluorescence microscopy, and as the active component in thin film and fiber optic chemical sensors [7-10]. Owing to its high absorption coefficient in the visible and good photostability, R6G has also been used as a sensitizer for nanoparticle based solar cells [11,12]. Furthermore, the
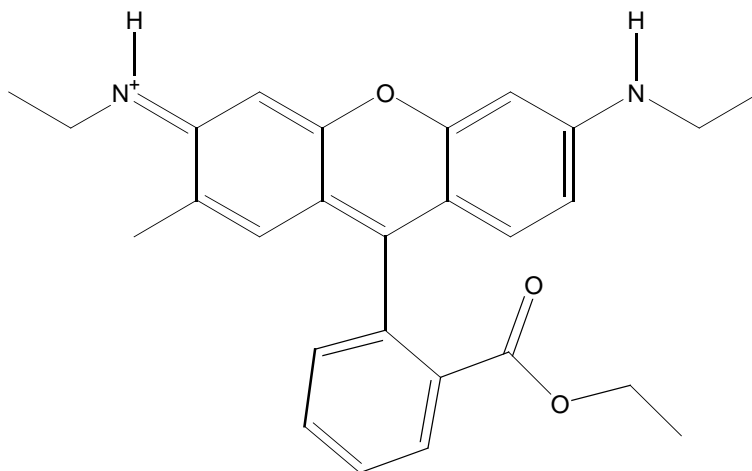
Figure 6-1. The chemical structure of the laser dye rhodamine 6G (R6G).

nonlinear properties R6G exhibits, in particular two-photon absorption, have been exploited to show the feasibility of true 3D displays [13]. Indeed, due to its unique photophysical properties, the applications of R6G have been quite diverse. This being the case, it is only natural that composite films containing this dye be explored for potential use as the photonic layer. However, as with the other organic dyes discussed thus far, R6G's relatively long-lived excited state needs to be significantly reduced to allow for optical switching operations in the terahertz region. In order to accomplish this, both techniques of induced aggregation, and formation of donor/acceptor energy transfer complexes are employed.

6.2 Aggregation

Since the majority of applications in which R6G is used exploit its strong absorption and fluorescence in the visible region, steps are often taken to minimize the self-assembly aggregation process between individual dye molecules. Not only does the formation of aggregates significantly reduce the quantum yield of fluorescence, it also leads to intensity decrease and to a lesser extent, broadening of the absorption band. Fortunately, for the intended application as the active medium in the photonic layer, the negative effects on these optical properties as a result of aggregation, would not be detrimental to the performance of the optical switching device. What is important is whether or not aggregation led to rapid excited state deactivation, as it does with cyanine dyes, TTBC and DODC explored in chapter 3.

The aggregation behavior of R6G intercalated into thin films, for most part, has been ignored in the literature, but recent studies by Arboloa et al. have added some illumination on the nature of these aggregates [14]. By absorbing R6G into Laponite
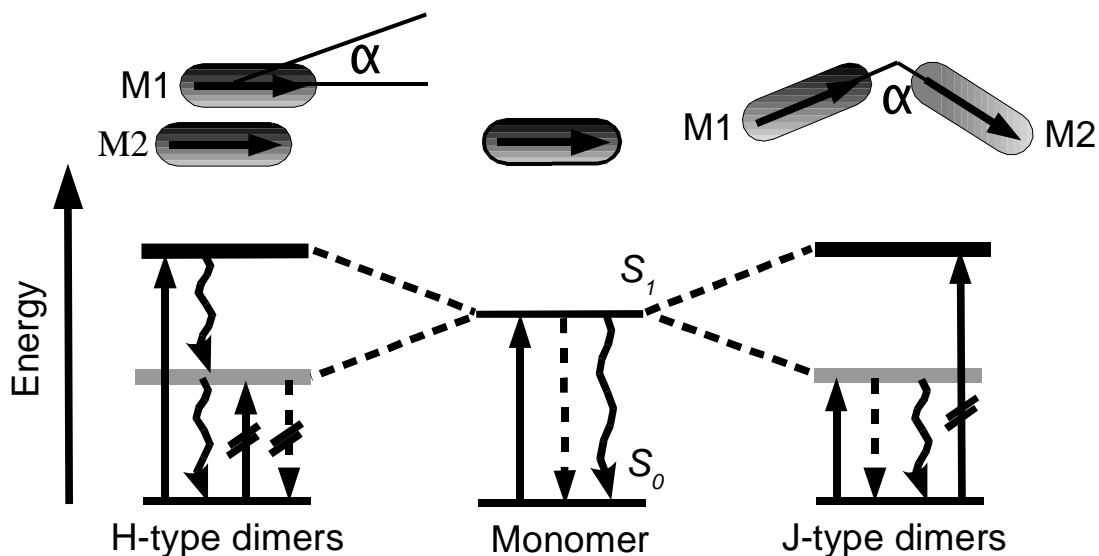
Figure 6-2. The exciton splitting of the electronic excited states for H- and J-type dimer aggregates formed by R6G intercalated into the composite film. M1 and M2 are the transition dipole moments, and α is the interaction angle between the monomer units. The degree to which transitions with two slashes are allowed is dependent on α.

clay films at various concentrations, they show that as the concentration is increased, various H- and J-type dimer aggregates would form and coexist within the film. In Figure 6-2, the proposed exciton splitting of the electron excited states, along with the corresponding geometric orientation of these dimer aggregates can be seen. In the typical H-aggregate the monomer units are stacked in such a way that only transitions from the ground state to the upper exciton state is allowed, while deactivation occurs through a non-radiative internal conversion process. On the other hand, in H-type dimer aggregates, transitions from the ground state to both the lower and upper exciton states are allowed and radiative transitions from the lower exciton state to the ground state is no longer prohibited. The degree to which transitions to the lower exciton state is allowed is governed by the angle between the monomer units, α. When α is zero, the dimer takes on the electronic properties of the typical H-aggregate, but when it deviates from zero,

then transitions which are forbidden, become allowed. Likewise, J-type dimer aggregates also exhibit electronic transitions which are dependent on α, but in this case, it is the upper exciton state that becomes allowed as α deviates from zero. Also, it should be noted that the energy levels of the exciton states of both the H- and J-type dimer aggregates are closer to the monomer's than in the typical H- and J-aggregates because of the shorter coherence length involved in these dimer aggregates.

The affect on the absorption spectrum of R6G intercalated within the composite film when its concentration is increased is shown in Figure 6-3. The spectrum in ethanol is also provided for comparison. At a concentration of 0.8 mg/ml, the film spectrum is almost identical to that in solution, with the only difference being a 4 nm shift to the red in the film. Such a shift is most likely due to a weak ground state interaction between the R6G molecules and Pluronic P123 molecules of the host mesostructure. Similar red-shifts have been observed when other xanthene dyes are incorporated into micelles consisting of the nonionic surfactant, TX-100 [15]. When the concentration is doubled to 1.6 mg/ml, the intensity of the shoulder at ~ 500 nm increases slightly and is indicative of the formation of the H-type aggregates discussed above. Upon further increase in the concentration to 7 mg/ml, the shoulder at ~ 500 nm becomes much more well defined and the peak maximum also undergoes an additional shift to the red. The absorption spectrum for this sample is also broadened relative to the 0.8 mg/ml sample. Taken together, these changes most likely signify the formation of a greater number of H-type dimer aggregates along with the formation of J-type aggregates. It is these J-type aggregates which causes the spectrum to shift to the red and become spectrally broadened.
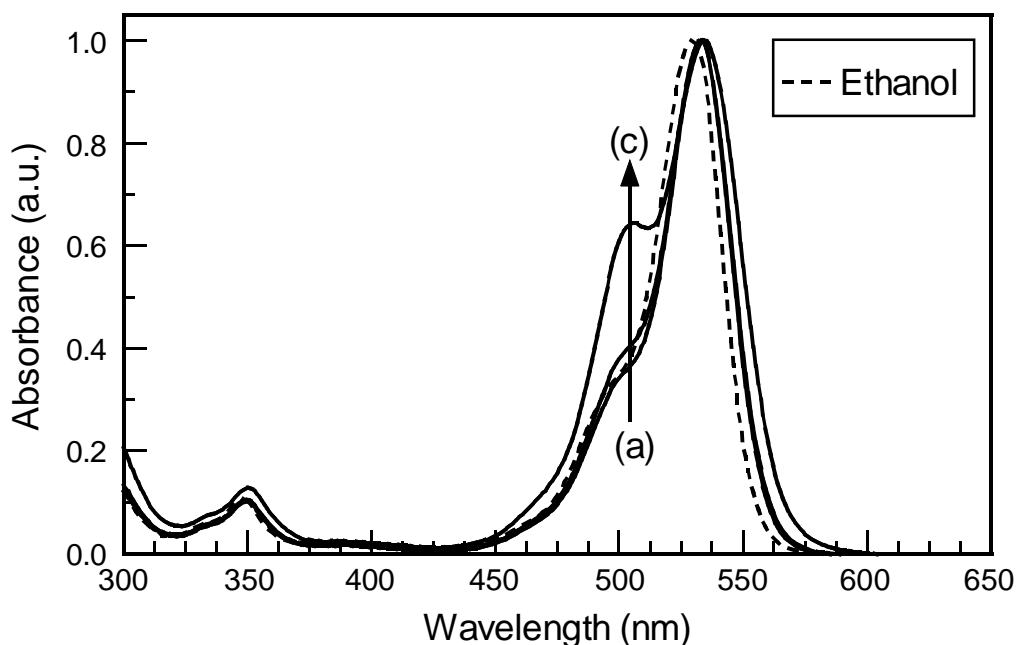
Figure 6-3. The normalized absorption spectra of R6G in ethanol, and intercalated within the composite film at various concentrations. (a) 0.8 mg/mlm (b) 1.6 mg/ml, (c) 7.0 mg/ml.

Whereas, only minor variations are observed in the absorption spectra for the R6G film and solution samples, as far as peak location and shape are concerned, significant differences are seen in their fluorescence spectra. It should be noted, that such differences can have be the result of an inner filter effect, but since the front-face configuration is employed to collect the fluorescence signal, contributions to the signal from this effect, in all likelihood, is minimized [8]. The normalized fluorescence spectra for the solution and film samples are plotted in Figure 6-4. For films containing a 0.8 mg/ml R6G concentration, the fluorescence spectrum is now broadened compared to the solution spectrum. Since such broadening is not observed in the absorption spectrum for this film, it is most likely attributable to the formation of an excited state complex between the R6G and the Pluronic P123 molecules [16]. When the concentration is
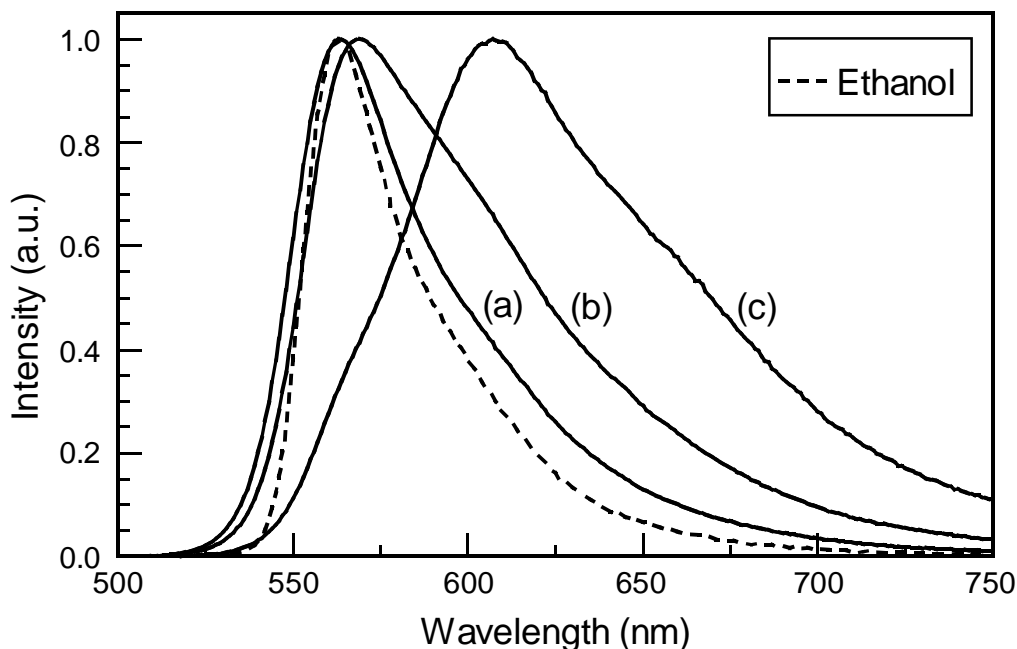
Figure 6-4. The normalized fluorescence spectra of R6G in ethanol, and intercalated within the composite film at various concentrations. (a) 0.8 mg/mlm (b) 1.6 mg/ml, (c) 7.0 mg/ml.

increased to 1.8 mg/ml, not only does the spectrum further broaden, but also, the

maximum is now shifted 6 nm to the red. The broadening, in conjunction with the

spectral shift is certainly due to the presence of H-type dimer aggregates, as suggested by

the shoulder in the absorption spectrum for this film. Furthermore, the appearance of a

shoulder at ~ 600 nm, can be attributed to the fluorescence of these H-type aggregates

exclusively. At a concentration of 7 mg/ml, the fluorescence spectrum is now very

different from that of the solution or even the lower concentration film samples. The

maximum now occurs at 610 nm, compared to 564 nm for the 0.8 mg/ml film and

solution sample. Moreover, significant broadening of the spectrum takes place. These

changes are clearly the result of a high percentage of H- and J-type aggregates, with

various interaction angles, α, coexisting within the film. The existence of these

aggregates can also account for the disappearance of the monomer's fluorescence band at 564 nm. Since the H- and J-type aggregates possess exciton states whose energy levels lie below the monomer S_1 state, they would serve to efficiently quench its fluorescence through an energy transfer process.

The presence of H- and J-type aggregates, as indicated by the spectral changes in the absorption and fluorescence spectra, still do not attest to the applicability of these films to be used as the photonic layer. In order to answer this question, time-resolved fluorescence studies are conducted on the films. Such studies also help to illuminate the nature of the aggregates. The results from these studies, as well as the calculated quantum yields are outlined in Table 6-1. In ethanol, the lifetime of R6G is reported to be 3850 ps, with a fluorescence quantum yield of 0.94 [14]. At a concentration of 0.5 mg/ml, the decay profile can be fitted using a two component exponential model with lifetime values of 3960 ps (92 %) and 255 ps (8 %). The slight increase in lifetime of the dominant component further supports the above assertion that the excited state is somewhat stabilized through interactions with the Pluronic P123 molecules of the mesostructure. The origin of the minor component can not be ascertained at this point, but could be due to the excited state CT complex between R6G and surrounding Pluronic P123 molecules. Increasing the concentration to 0.8 mg/ml still resulted in a two component decay profile being seen, but now the major component's lifetime is decreased to 3490 ps (90 %), while the minor component's increases to 989 ps (10 %). Doubling the concentration to 1.6 mg/ml leads to a further decrease in the major component's lifetime, but now a third, much longer lived component, possessing a lifetime value of 4743 ps (17 %) appears. This long-lived component is ascribed to

Table 6-1: Lifetimes and quantum yields of R6G in solution and intercalated within the composite film, at various concentrations. An excitation wavelength of 470 nm was used.

[a]Conc. R6G	Environment	τ_1 (ps)	τ_2 (ps)	τ_3 (ps)	[b]Quantum yield
—	ethanol	[c]3850 (100 %)			[c]0.94
0.5 mg/ml	film	3960 (92 %)	255 (8 %)		—
0.8 mg/ml	film	3490 (90 %)	989 (10 %)		0.71
1.6 mg/ml	film	1023 (72 %)	4743 (17 %)	181 (11 %)	0.30
7 mg/ml	film	44 (68 %)	3036 (19 %)	182 (15 %)	0.06

[a] Concentration of R6G in mg per 1 ml of sol for film samples. [b] The quantum yield of fluorescence obtained using Eq. (2.1), and a refractive index of 1.476 for the composite film. [c] Data from reference [12].

radiative H-type dimer aggregates [14]. Since the diminution in the major component's lifetime and overall contribution to the decay profile, is also accompanied by a substantial reduction in the quantum yield of fluorescence, this component is assigned to the monomer's fluorescence. This decrease in lifetime and quantum yield, on increasing concentration, indubitably results from quenching by the H-type dimer aggregates, and to a lesser extent, from nearby R6G monomers in the ground state.

For films containing a 7 mg/ml concentration of R6G, the fluorescence decay profile is dominated by a near instrument limited component with a lifetime value of 44 ps (68 %). As with the 1.6 mg/ml film, there is also two minor components with lifetimes of 3036 ps (19 %) and 182 ps (15 %). This decay profile, along with those for the 0.8 mg/ml and 1.6 mg/ml films, are shown in Figure 6-5. As with the 1.6 mg/ml film, the long-lived component can be attributed to the fluorescence from the H-type aggregates and/or J-Type aggregates. The much shorter component, however, can not be so readily assigned. The simplest explanation for this component is that it is due to the fluorescence of the R6G monomer whose lifetime is significantly reduced because of quenching by H- and J-type aggregates. However, this explanation does not make sense
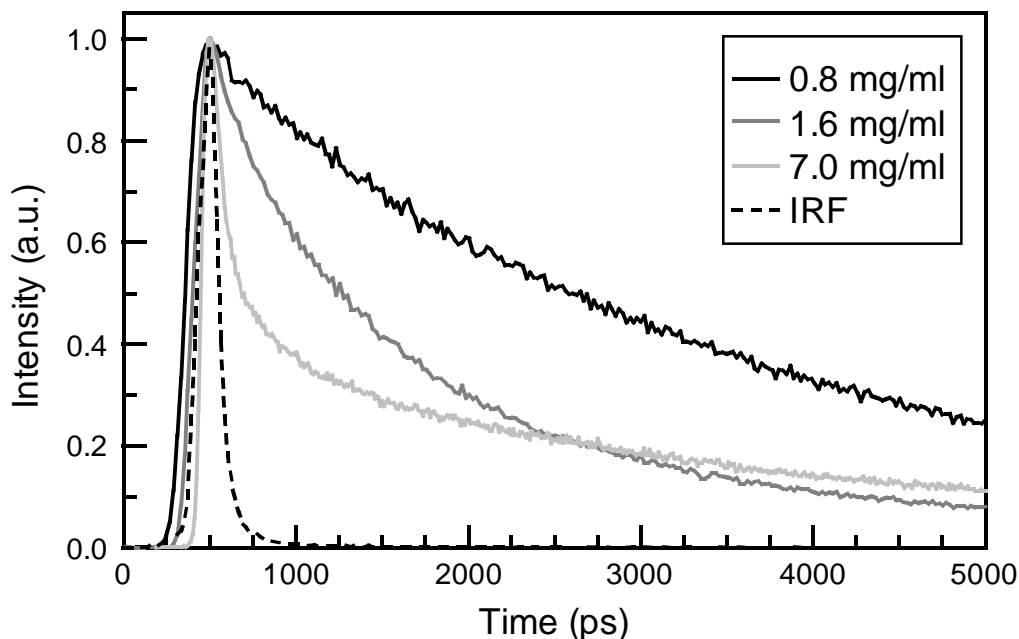
Figure 6-5. The normalized fluorescence decay profiles for various concentrations of R6G intercalated into the composite film.

because from the steady-state fluorescence spectrum, it can be seen that the monomer

contributes little to the overall fluorescence signal. Only the shoulder at ~ 564 nm can be

attributed to the monomer's fluorescence with a high level of certainty. Also, if the

above explanation is correct, then the fast component would be a minor component and

not the most dominant one. Another, more plausible explanation for this decay

component, is that it is due to the exciton-exciton annihilation process discussed in

chapter 3. If this is the case, then the maximum of this component should be blue shifted

relative to the decay from the other components as time progressed. This is exactly what

is observed. In Figure 6-6, it can be seen that for the first 400 ps following excitation,

the maximum occurs at ~ 580 nm, but as time progressed, it rapidly shifts to ~ 610 nm.
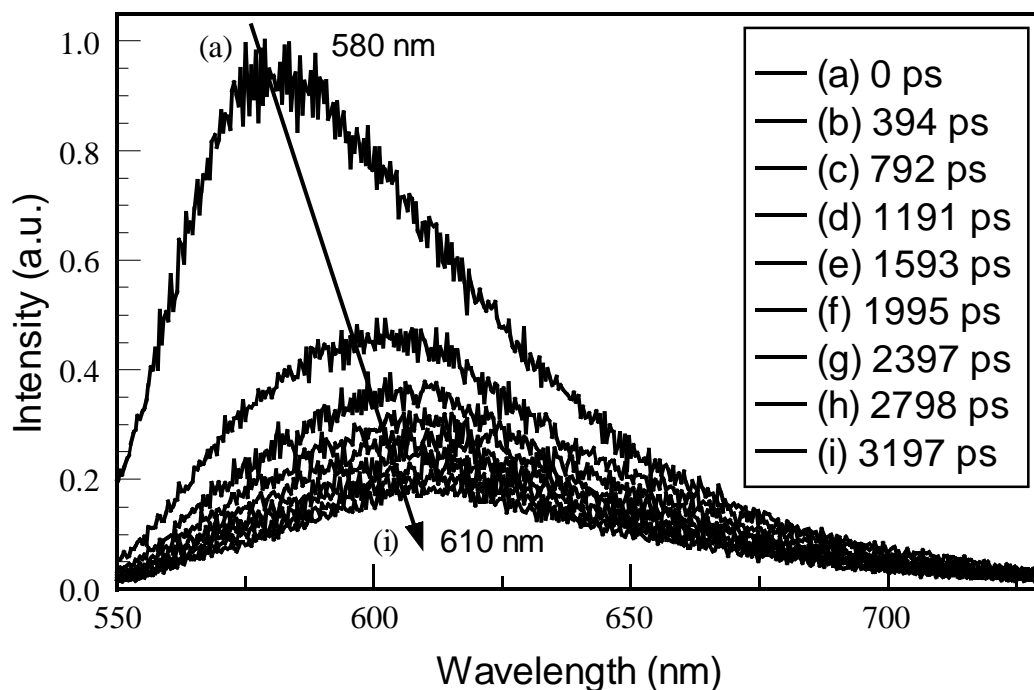
Figure 6-6. Time-resolved fluorescence spectra for the 7.0 mg/ml R6G composite film. Spectra were recorded from 0 to 3200 ps after excitation at every 400 ps or so.

Such a drastic shift in the fluorescence maximum, as time progressed, can only be due to the aforementioned exciton-exciton annihilation process.

No matter the origin of this rapidly decaying component, one thing is clear, its presence signifies that ultrafast deactivation of the majority of the excited R6G molecules is taking place. This inherently makes these films suitable for employment as the photonic layer.

6.3 Excited State Deactivation

Although the formation of H- and J-type dimer aggregates, at relatively high concentrations, proves effective at substantially reducing the excited state lifetime of R6G, there are a few pitfalls using this approach. One of those, and probably the most

troubling, is the fact that a long-lived species still remains after the initial rapid, near instrument limited decay of the majority of excited R6G molecules. Albeit, the overall percentage of excited state molecules which undergo this slow decay process is below 20 %, but their presence would tend to impact negatively on the photostability of the film. As mentioned in earlier chapters, the photostability of organic dyes is largely dependent on whether or not reactive triplet states are formed [17]. So since the long-lived species in R6G films has an excited state lifetime that is longer than the monomer's, there is an increased likelihood that intersystem crossing (ISC) can take place and thereby introduce photochemically reactive species in the film. It is not clear whether simply increasing the R6G concentration would eliminate the aggregate species which possess this long-lived excited state. Doing so, however, would have most likely impacted negatively on the films properties. For example, increasing the concentration can lead to the films becoming to optical dense, and more problematically, can cause substantial defects in the casted film past a certain concentration. In order to minimize, or even circumvent these problems, an energy acceptor is instead employed to bring about rapid deactivation of both the monomeric and aggregated R6G species in the film.

As an energy acceptor, the anionic dye bromophenol blue, BPB is used. This dye has already been shown capable of forming a tightly bound energy transfer complex with R6G, as well as other cationic dyes [18,19]. The acid/base indicator properties [20,21] of BPB also makes it a good candidate for the following reason. When BPB is protonated very little spectral overlap between its absorption band and the fluorescence band of R6G takes place. However, in the depronated form, significant spectral overlap with R6G's fluorescence exists. Moreover, since deprotonation of BPB can be accomplished by
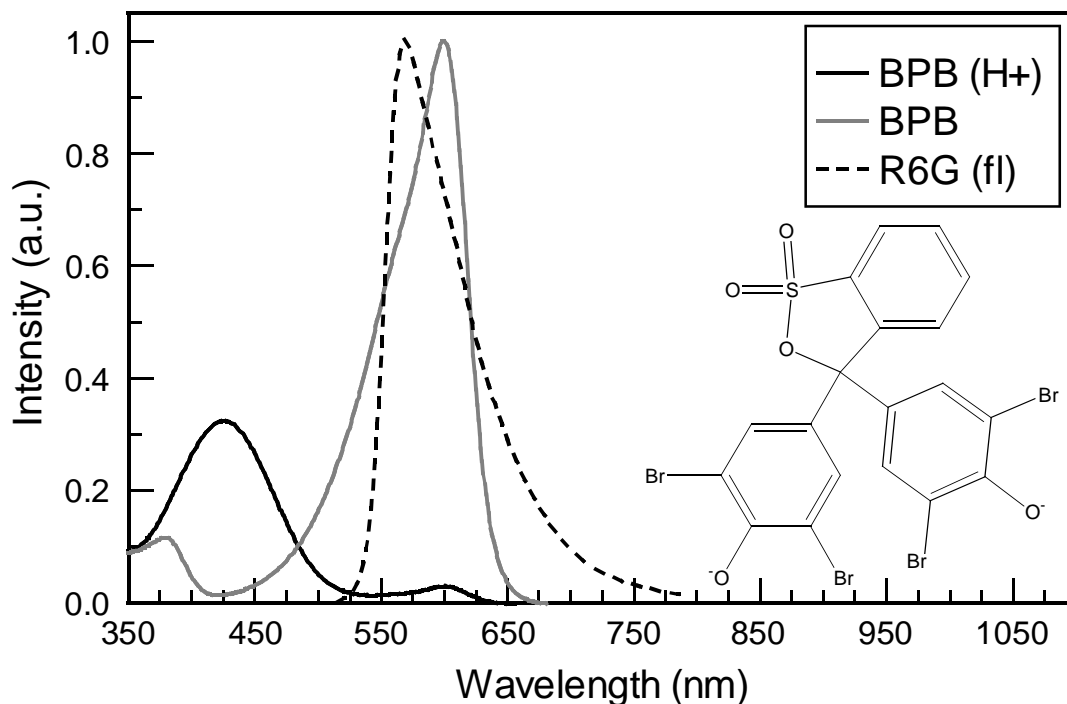
Figure 6-7. Spectral overlap between the absorption of the protonated and deprotonated form of BPB and the fluorescence (fl) of R6G. The chemical structure of BPB is also presented.

simply exposing the casted films to ammonia vapor, the ability to selectively tune the spectral overlap becomes a possibility. This ability is exploited to study the role of electron transfer, if any, in the energy transfer process between R6G and BPB. The absorption spectra for the protonated and deprotonated form of BPB are shown in Figure 6-7 along with its chemical structure. Also, the normalized fluorescence spectrum for R6G is provided to allow the spectral overlap to be examined.

The effectiveness of BPB, as an energy acceptor, is first ascertained by conducting time-resolved fluorescence studies on R6G films containing BPB at various mole ratios. The results of these studies are outlined in Table 6-2. When the R6G : BPB mole ratio is varied from 0.5 : 1 to 2 : 1, the measured radiative lifetime for R6G is found to be the

Table 6-2: Lifetimes of R6G composite films containing BPB at various mole ratios. The excitation wavelength was 470 nm.

R6G : BPB mole ratio	[a]Conc. R6G (mg/ml)	τ_1 (ps)	τ_2 (ps)
0.5 : 1	0.8	30 (100 %)	
[b]1 : 1	1.4	159 (60 %)	610 (40 %)
1 : 1	1.4	30 (100 %)	
2 : 1	1.6	30 (100 %)	
3 : 1	1.6	90 (89 %)	470 (11 %)
6 : 1	1.6	118 (88%)	620 (12 %)

[a] Concentration of R6G in mg per 1 ml of sol. [b] No NH_4OH added to sol.

instrument limited value of 30 ps. This is a definitive indication that BPB is rapidly deactivating the excited state of R6G by an efficient Coulombic, and possible electron exchange, energy transfer process. Moreover, even the protonated form of BPB can effectively reduce the lifetime of R6G, but as expected, it is nowhere near as effective as the deprotonated form at doing so. For films containing a 1 : 1 mole ratio of the protonated form of BPB, the decay profile of R6G can be fitted using a two component model with time constants of 159 ps (60 %) and 610 ps (40 %). The pristine R6G film at this concentration has a complex three component decay profile that is synonymous with the presence of H-type dimer aggregates. The time constants for this decay profile are 1538 ps (51 %), 4220 ps (44 %), and 2012 ps (6 %). Since there is little spectral overlap between the R6G and the deprotonated form of BPB, the reduction in lifetime is mostly likely due to a combination of electron and Coulombic energy exchange mechanisms. The normalized fluorescence spectra for these films are also shown in Figure 6-8, and as can be seen, when the BPB in the film is deprotonated, the previously weak fluorescence from the R6G completely disappears. The relatively low intensity band at ~ 640 nm is that of the deprotonated BPB and not R6G. Further increasing the mole ratio to 3 : 1 and 6 : 1, leads to a gradual increase in the major component's
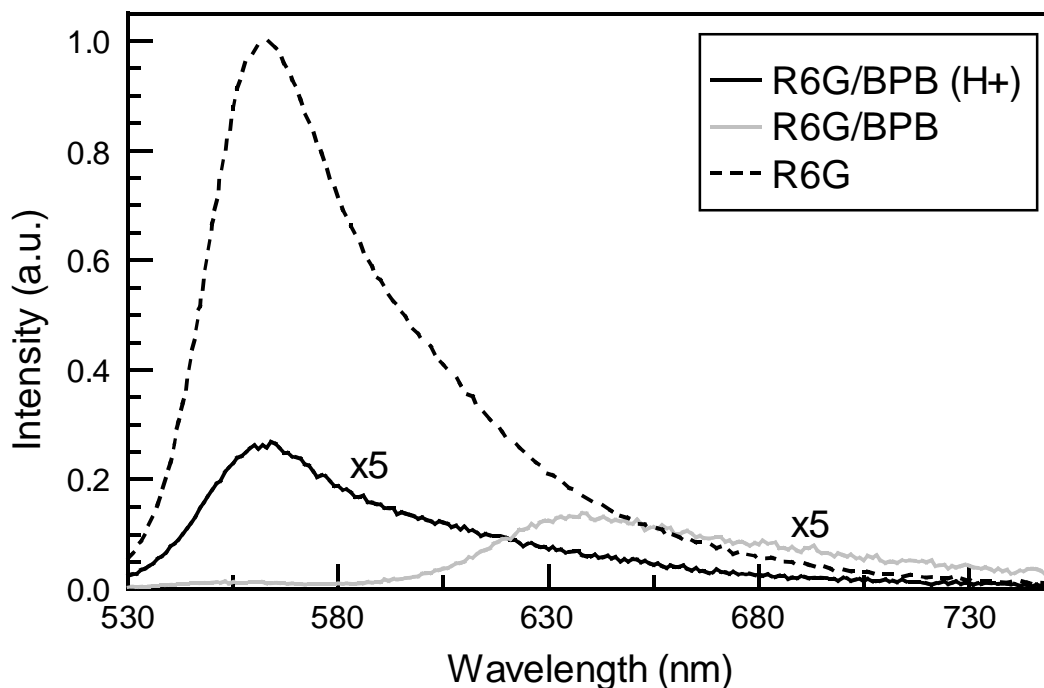
Figure 6-8. The normalized fluorescence spectra for the 1.6 mg/ml R6G film containing BPB in the protonated and deprotonated form.

lifetime, but it does not come close to the lifetime value when no BPB is added to the film. Such low lifetime values relative to the R6G film containing no BPB, even when 6 times more R6G molecules are present in the film than BPB, indicates that a single BPB molecule is undergoing energy transfer with multiple R6G molecules. The phenomenal quenching ability of BPB is certainly aided by its electrostatic interaction with R6G, which causes the two molecules to be in closer proximity than they would otherwise be.

The results from the time-resolved fluorescence study are again echoed when the energy transfer parameters are evaluated. Those parameters are presented in Table 6-3. At a mole ratio of 0.5 : 1, the energy transfer efficiency is 99.5 %, with a corresponding rate of $4.6 \times 10^{12} \ M^{-1} sec^{-1}$. Increasing the mole ratio to 1 : 1 results in a slight increase in the transfer efficiency to 99.8 %, but now the corresponding rate is about three times as

much. At first glance, these results appear to be counterintuitive because the transfer

efficiency and rate actually decrease with increasing BPB content. This disparity,

however, can be ascribed to the difference in the R6G concentration in the two films. In

the 0.5 : 1 mole ratio film, the R6G molecules exists predominantly as monomers,

whereas in the 1 : 1 mole ratio, they exists as a combination of monomers and H-type

dimer aggregates. Energy transfer to BPB clearly takes place more readily with the R6G

aggregates than it does with the monomers. The reason for this remains unclear at the

moment, but might have to do with the fact that the aggregates can act as energy

conduits, allowing the energy from an excited monomer to more readily hop to a nearby

BPB molecule. At a mole ratio of 2 : 1, the transfer efficiency and rate change little from

the 1 : 1 mole ratio. Even at a mole ratio of 6 : 1, the efficiency still remains above 93

%, and the rate is still in the 10^{12} M^{-1} sec^{-1} range. Such high transfer efficiencies and

rates, even when the donor outnumbered the acceptor six fold, is no doubt due to a

combination of aggregate formation, electrostatic interaction, and good spectral overlap.

All these factors results in the deactivation of the excited state of R6G molecules within

100 fs, a rate more than sufficient to allow these films to be employed as the photonic

layer.

As mentioned above, electron transfer may also play a role in the energy transfer

process between R6G and BPB. Further evidence for this can be more clearly seen when

the energy transfer parameters for the 1 : 1 mole ratio film containing either the

protonated, or deprotonated form of BPB, are compared. When the deprotonated form of

BPB is present, the transfer efficiency drops to 99.5 %, from 99.8 %, but the energy

transfer rate drops by almost a factor of ten. These results are in line with what would be

Table 6-3: The energy transfer parameters for R6G composite films containing BPB as an energy acceptor.

^{a}Conc. R6G (mg/ml)	mol ratio R6G : BPB	Transfer Efficiency^b	R_0 (± 4 Å)^c	r (± 4 Å)^d	Transfer Rate (x10^{12} M^{-1}sec^{-1})^e
n/a	n/a	n/a	62	n/a	n/a
0.8	0.5 : 1	99.5 %		26	4.6
^{f}1.4	1 : 1	95.0 %		21	0.58
1.4	1 : 1	99.8 %		23	15.3
1.6	2 : 1	99.5 %		26	19.1
1.6	3 : 1	97.5 %		34	2.4
1.6	6 : 1	93.6 %		40	1.8

^{a} Concentration of R6G in mg per 1 ml of sol. ^{b} The efficiencies were calculated using Eq. (2.4). ^{c} The Förster distance, R_0, obtained using Eq. (2.7). ^{d} The average distance, r, between the R6G and BPB calculated from Eq (2.8). ^{e} Energy transfer rates were calculated using Eq. (2.6). ^{f} Contains the protonated form of BPB.

expected on moving from a predominantly electron exchange, to a predominantly Coulombic exchange mechanism. Since transfer efficiency is relatively independent of transfer mechanism, there should be little variation in its value between the two films, and this is the case. The transfer rate, on the other hand, should be more sensitive to the energy exchange mechanism since energy transfer by electron exchange is more sensitive to the average donor/acceptor spacing, r. The rate of energy transfer by the Coulombic exchange mechanism has a $r^{1/6}$ dependency, whereas that dependence is exponential for the electron exchange mechanism [22]. Simply put, for a given donor/acceptor spacing greater than 10 Å or so, the rate of energy transfer by the Coulombic exchange mechanism will always be greater than that for the electron exchange mechanism.

From the time-resolved fluorescence and energy transfer studies it is clear that rapid excited state deactivation of the R6G molecules is taking place. However, these studies provide no real information about the ultrafast dynamics of the overall energy transfer

process. In order to obtain such information, a femtosecond transient absorption study is carried out. The samples used for this study contains 1.6 mg/ml R6G and BPB at a 1 : 1 mole ratio, or no BPB. A 100 fs, 530 nm pump pulse is used for all samples. In Figure 6-9, the transient profiles monitored at 588 nm for these samples and for the 10 ps time window following excitation are presented. For the R6G film containing no BPB, there is a strong transient signal at 588 nm whose profile is indicative of an energy transfer process. Initially, there is an almost instantaneous rise in this signal following excitation, but it soon maximized after about 1 ps then starts to decrease. At about 2 ps, the signal starts to rise again until about 9 ps, at which point it startes to undergo a second decrease. This repetitive rise and fall behavior in the transient gain profile is most likely due to an energy transfer process from the monomeric R6G molecules to the H-type dimer
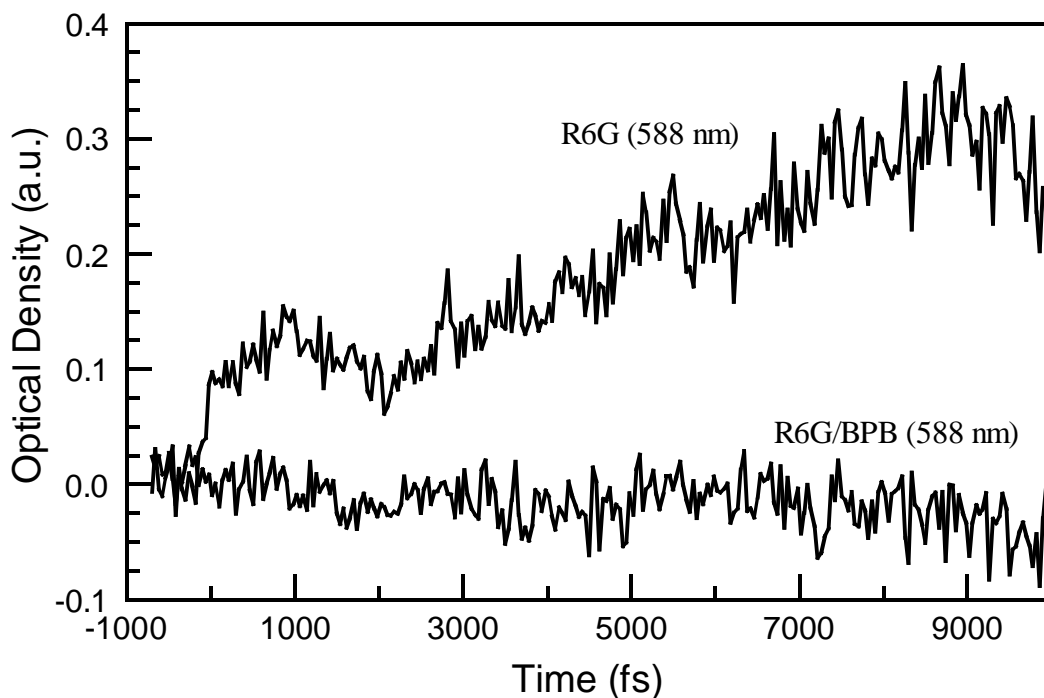
Figure 6-9. Transient absorption spectra of R6G films with and without BPB. When BPB is present, there was no transient gain signal at 588 nm, indicating the presence of an ultrafast energy transfer process.

aggregates, which have been shown in the above discussion to form at the concentration used in the film. Keeping with this explanation, the transient gain signal within the first 2 ps can be assigned to the monomeric R6G molecules which then undergo energy transfer to the H-type aggregates, leading to the gradually rising signal for the next 7 ps. Whatever the processes which cause such a complex transient gain signal to occur, upon addition of BPB to the film, this signal disappears completely. In fact, no transient signals due to R6G can be observed for films containing BPB. This is expected from the obtained energy transfer rates. With an energy transfer rate in the 10^{13} M^{-1} sec^{-1} range, virtually all the excited R6G molecules are undergoing deactivation within 100 fs. This rate is faster than the 200 fs resolution of the pump-probe system and reconfirms the suitability of these films for use as the photonic layer.

7. Summary

Optical time-division multiplexing (OTDM) is one of the few technologies which shows great potential for delivering the high bandwidth multimedia digital content to the next generation computers and network connected devices. The fundamental operational principle of OTDM is the ability to transmit data as a series of closely spaced light pulses. The closer the temporal spacing between these pulses, the higher the data throughput. However, in order for data throughput to exceed the Tb/s (terabits/second) mark, significant strides need to be made in the development of the operational components of the OTDM system, namely the ultrafast all-optical demultiplexing switch. One such switching device is the time-to-space converter which is a passive device that makes use of a femtosecond gating pulse and a photonic layer possessing ultrafast nonlinear optical responses in order to perform the demultiplexing process on the stream of data pulses.

In this work, the use of sol-gel derived inorganic/organic composite films, doped with organic dyes, were explored for use as the photonic layer in these all-optical time-to-space converters. The dyes by themselves, did not possess the necessary ultrafast optical response (i.e. rapid deactivation of the excited state following optical excitation) necessary for optimum operation of a switching device, so methods which brought about this response were employed. For dyes which form H- and J-type aggregates, preparative methods that induced aggregation was used, whereas for the other dyes, energy acceptors were employed to bring about ultrafast deactivation of the dye's excited state. Both methods proved successful at increasing the optical response of the

intercalated dyes to a point that would make these composite films applicable for use as the photonic layer.

The sol-gel derived composite films employed, consisted of a silica framework, and self-assembled organic mesostructures formed by the nonionic surfactant Pluronic P123. These films showed remarkable physical and optical properties. The excellent processability of the precursor sol made it possible to fabricate high quality films, of varying thicknesses, using either drop-casting, dip- or spin-coating. Spin- and dip-coated films had thicknesses measuring a few hundred nanometers, while drop-casted films exhibited an average thickness of 6 ± 0.5 μm. Regardless of the film fabrication method employed, the RMS surface roughness was never more than a few nanometers. Such low surface roughness resulted in the films having an average optical transmission greater than 92 % throughout the visible region. The ability of the occluded Pluronic P123 mesostructures to solubilize low molecular weight organic molecules made these films ideal host matrices for organic dyes and molecular assemblies, possessing substantial nonlinear susceptibilities.

Incorporation of the cyanine dyes, TDBC and DODC, above a certain concentration into these composite films, resulted in the formation of J- and H- type aggregates, respectively. From the steady-state and time-resolved studies, it was concluded that the photophysical properties of these molecular assemblies are much different than those formed in solution. In solution, one type (as defined by the coherence length) of aggregate dominates, whereas, the broad absorption and fluorescence bands in the film, indicated that aggregates with various coherence lengths coexisted. Moreover, the time-resolved fluorescence spectra showed that the excited state of aggregates was rapidly

deactivated through either stimulated emission or exciton-exciton annihilation. These exciton dynamic processes resulted in the films having ultrafast nonlinear optical responses, making them suitable for use as the photonic layer in the all-optical switch. There was, however, one drawback associated with these films. The clustering of the coherent aggregates to form micron size macroaggregates which protruded the surface, caused the films to have increased light scattering. Such scattering would inherently lead to signal losses in an operational switching device so attempts must be made to minimize their formation and/or size.

Upon intercalation into the composite films, the cyanine-type squarylium dyes (specifically, SQ-Cy1 and SQ-Cy2) exhibit different photophysical properties when compared to the same properties in homogeneous solution. From steady-state and time-resolved spectroscopic studies it was observed that the constricting and hydrophobic environment within the Pluronic P123 mesostructures results in red shifts of both the absorption and fluorescence maxima, but to varying degrees. The spectral shifts, intensity differences, and fluorescence dynamics have been explained through a combination of optical spectral measurements, as well as quantum chemical, time-dependent DFT calculations. It was deduced that conformational variability within the mesostructures and intramolecular interactions between the individual squarylium dye molecules explain the bulk of spectroscopic and time-resolved measurements.

In order to make these squarylium dye containing films suitable for use as the photonic layer, various quencher molecules were used to bring about rapid excited state deactivation of the dyes. Use of the well known electron acceptor *p*-nitroaniline resulted in poor quenching efficiencies in films containing either squarylium dye, and was most

likely due to insufficient electronic coupling between pNA and the dyes. By contrast, SQ-Cy2 (a di-anion) films containing the di-cation electron acceptor, methyl viologen, showed quenching efficiencies close to 100 % and electron transfer rates a few orders of magnitude below the diffusion limited value of 10^{13} sec^{-1}. However, femtosecond transient absorption studies indicated that ground state recovery of the oxidized SQ-Cy2 dye, through back electron transfer, occurred on a time-scale that would prevent these films from being used as the photonic layer. To circumvent the back electron transfer problem, another quencher, rhodamine 800 (LD800), which operated through the Coulombic exchange mechanism was used. In films containing either squarylium dye, the energy transfer efficiencies approached 100 %, while the rates were at least 10^{12} M^{-1} sec^{-1} for films containing SQ-Cy1 and even was as high as 10^{13} M^{-1} sec^{-1} for SQ-Cy2 films. These results indicated that ground state recovery of the squarylium dyes took place on a femtosecond time-scale. These results were a testament to the long-range nature of the Coulombic mechanism. The ultrafast energy transfer, and hence ground state recovery, for the squarylium dyes was also confirmed by femtosecond transient absorption studies. The energy transfer occurred at a rate that was beyond the 200 fs resolution of the pump-probe system and from the calculated rates, occurred in less than 100 fs. Time-resolved fluorescence data, in conjunction with the transient absorption data also indicated the presence of a slower electron transfer process between the squarylium dyes and LD800, which took place after the initial energy transfer process. Because this electron transfer process appeared to only take place with a small percentage of the excited squarylium dye molecules, it did not affect the overall ultrafast

optical response of the films. As such, these films would be well suited for use as the photonic layer in the all-optical switching device discussed here.

The anionic xanthene dyes, rose bengal (RB) and fluorescein (FR), exhibited properties which made them well suited for use in the photonic layer in the all-optical switching device. Along with retention of their well defined and intense absorption bands, both dyes also retained their long-lived singlet and in the case of RB, triplet excited states. In order to rapidly deactivate these long-lived excited states, the squarylium dyes, SQ-Cy1 and SQ-Cy2, as well as the triphenylmethane dye, crystal violet (CRV), were employed as energy acceptors. In view of the high ISC yield from the S_1 to the T_1 state of RB, the squarylium dyes were used as energy acceptors for this dye system because of their ability to accept energy from both these states. It was found that the efficiency and rate of the energy transfer process between RB and the squarylium dyes, strongly depended on whether RB existed as isolated molecules or as molecular aggregates within the film. The most desirable results, as far as transfer efficiency was concerned, was obtained for the films containing RB as molecular aggregates and SQ-Cy2 as an acceptor. The highest transfer rates, however, were obtained for films containing RB as isolated molecules using SQ-Cy2 as the energy acceptor. A femtosecond transient absorption study confirmed that energy transfer to the squarylium dyes was occurring from both the S_1 and T_1 states of RB, and more importantly, at a rate faster than the 200 fs resolution of the pump-probe system. Unfortunately, it was also evident from the data that triplet energy transfer to the squarylium dyes caused them to undergo irreversible photodegradation.

Since such degradation would render these RB films useless under the operational conditions of the all-optical switch, FR, with its very low ISC yield was used in place of RB. Use of the squarylium dyes as the energy acceptors in the FR films resulted in energy transfer efficiencies and rates which were too low to allow these films to be used in the intended application. Since this was due to the poor spectral overlap between FR and the squarylium dyes another energy acceptor, CRV, was used instead. The results using CRV were quite impressive to say the least, and was no doubt due to the good spectral overlap and the electrostatic interaction it had with FR. At a mole ratio of 1 : 1, the transfer efficiency was almost 100 %, while energy transfer was taken place in less than 100 fs. These energy transfer characteristics would effectively allow such films to perform optical switching in the terahertz time domain.

The ultrafast excited state dynamics of composite films containing the well known and often studied laser dye, rhodamine 6G (R6G) was also examined for their potential use as the photonic layer in an all-optical switching device. When R6G was added to the composite film at a concentration of 0.5 mg/ml, it displayed fluorescence dynamics that was similar to that in solution. However, when the concentration was increased, both the absorption and fluorescence spectra indicated the formation of H- and/or J-type dimer aggregates. Formation of these aggregates significantly altered spectral properties and the excited state dynamics of R6G. At the highest concentration used, 7 mg/ml, time-resolved fluorescence studies revealed a complex three component decay in which the dominant component had a near instrument limited time constant of 44 ps (68 %). This ultrafast component was assigned to the exciton dynamics of the H-type dimer aggregates and suggested that such films could be used as the photonic layer.

Furthermore, the cationic dye bromophenol blue (BPB) was employed as an energy acceptor in order to rapidly deactivate a greater percentage of the excited R6G molecules. Steady-state absorption and fluorescence studies revealed that as a result of the good spectral overlap and electrostatic attraction between these two molecules, close to 100 % of the excited R6G molecules underwent energy transfer as the primary means of excited state deactivation. Moreover, time-resolved fluorescence and transient absorption studies showed that energy transfer occurred in less than 100 fs, a value close to the diffusion limited value. Once again, the presence of such ultrafast dynamics in these films made them good candidates for use as the photonic layer.

Given the proven ultrafast optical response of the dye doped composite films presented here, future work on these films should focus on improving the overall photostability of the intercalated dyes. Until such steps are taken, the application of such films will be limited to research and development use and not real-world deployment. Improvement of the intercalated dyes photostability could be accomplished by several methods. The simplest of which, is the addition of organic additives which would prevent or limit the formation of the reactive triplet states of the dyes. The protective action of such additives, however, would be short lived because they would eventually undergo degradation themselves. Synthesis of dyes with greater photostability than those used here is also another solution to this problem, but in this author's opinion, the synthesis of such dyes will be no trivial undertaken. A more practical and cost effective method towards solving the dye photostability problem, would be not to use dyes at all. Rather, inorganic quantum dots should be employed as the active chromophore. As a result of their inorganic nature, these quantum dots have been shown to possess vastly

superior photostability than any known organic dye. Furthermore, their optical properties can be readily tuned by controlling their size. As such, composite films containing these quantum dots may very well prove to be the ideal photonic layer for the ultrafast, all-optical switching devices of the future.

Bibliography

Chapter 1.

[1] Kamiya, T.; Saito, F; Wada, O.; Yajima, H., Eds., *Femtosecond Technology*, Berlin: Springer-Verlag, 1999.

[2] Gupta. M.C., Ed., *Handbook of Photonics*, Florida: CRC Press LLC, 1997.

[3] Kuhn, K. J., *Laser Engineering*, New Jersey: Prentice-Hall, Inc., 1998.

[4] Furuki, M.; Tian, M.; Sato, Y.; Pu, L.S. *Appl. Phys. Lett.* **2000**, *77*, 472.

[5] Rullière, C., Ed., *Femtosecond Laser Pulses*, Berlin: Springer-Verlag, 1998.

[6] Suah, F. B. M.; Ahmad, M.; Taib, M. N. *Sens. Actuators B* **2003** *90*, 182.

[7] Senarath-Yapa, M. D.; Saavedra, S. S. *Anal. Chim. Acta* **2001**, *432*, 89.

[8] Stathatos, E.; Lianos, P.; Krontiras, C. *J. Phys. Chem.* B **2001**, *105*, 3486.

[9] Hori, T.; Tagaya, H.; Nagaoka, T.; Kadokawa, J.; Chiba, K. *Appl. Surf. Sci.* **1997**, *121-122*, 530.

[10] Chaumel, F.; Jiang, H.; Kakkar, A. *Chem. Mater.* **2001**, *13*, 3389.

[11] Collinson, M. M. *Trends Anal. Chem.* **2002**, *21*, 30.

[12] Hana, X. M.; Lina, J.; Xing, R. B.; Fub, J.; Wang, S. B. *Mater. Lett.* **2002**, *4170*, 1.

[13] Jeronimo, P. C. A.; Araujo, A. N.; Montenegro, C. B. S. M.; Satinsky, D.; Solich, P. *Anal. Chim. Acta* **2004**, *504*, 235.

[14] Wang, E.; Chow, K. -F.; Kwan, V.; Chin, T.; Wong, C.; Bocarsly, A. *Anal. Chim. Acta* **2003**, *495*, 45.

[15] MacCraith, B. D.; McDonagh, C. M.; G. O'Keeffe, G.; McEvoy, A. K.; Butler, T.; Sheridan, F. R. *Sens. Actuators B* **1995**, *29*, 51.

[16] Yang, Y.; Wang, M.; Qian, G.; Wang, Z.; Xianping Fan, X. *Opt. Mater.* **2004**, *24*, 621.

[17] Weiss, A.M.; Yariv, E.; Reisfeld, R. *Opt. Mater.* **2003**, *24*, 31.

[18] Nhung, T. H.; Canva, M.; Chaput, F.; Goudket, H.; Roger, G.; Brun. A.; Manh, D. D.; Hung, N. D.; Boilot, J. -P. *Opt. Commun.* **2004**, *232*, 343.

[19] Schottner, G. *Chem. Mater.* **2001**, *13*, 3422.

[20] Canva, M.; Roger, G.; Cassagne, F.; Levy, Y.; Brun, A.; Chaput, F.; Boilot, J. -P.; Rapaport, A.; Heerdt, C.; Bass, M. *Opt. Mater.* **2002**, *18*, 391.

[21] Turro, N. J., *Modern Molecular Photochemistry*, California: University Science Books, 1991.

[22] Collinson, M. M.; Wang, H.; Makote, R.; Khramov, A. *J. Electroanal. Chem.* **2002**, *519*, 65.

[23] Huang,Y.; Chou, K. *Ceram. Int.* **2003**, *29*, 485.

[24] Zhao, W.; Hou, Y.J.; Wang, X. S.; Zhang, B. W.; Cao, Y.; Yang, R.; Wang, W. B.; Xiao, X. R. *Sol. Energy Mater. Sol. Cells* **1999**, *58*, 173.

[25] Flanagan, J.H. Jr.; Khan, S.H.; Menchen, S.; Soper, S.A.; Hammer, R.P. *Bioconjugate Chem.* **1997**, *8*, 751.

[26] Oguz, U.; Akkaya, E. U. *J. Org. Chem.* **1998**, *63*, 6059.

[27] Zhou, H.; Watanabe, T. *Mater. Lett.* **2002**, *57*, 589.

[28] Zhou, H.; Watanabe, T. *Mater. Sci. Eng.* B **2002**, *00*, 1.

[29] Schelle, C.; Mennig, M.; Krug, H.; Jonschker, G.; Schmidt, H. *J. Non-Cryst. Solids* **1997**, *218*, 163.

[30] Mishra, A.; Behera, R. K.; Behera, P. K.; Mishra, B. K.; Behera, G. E. *Chem. Rev.* **2000**, *100*, 1973.

[31] van Burgel, M.; Wiersma, D. A.; Duppen K. *J. Chem. Phys.* **1995**, *102*, 20.

[32] Kasha, M. *Rev. Modern Phys.* **1959**, *31*, 162.

[33] Kasha, M. *Radiat. Res.* **1963**, *20*, 55.

Chapter 2.

[1] Huang,Y.; Chou, K. *Ceram. Int.* **2003**, *29*, 485.

[2] Misawa, K.; Ono, H.; Minoshima, K.; Kobayashi, T. *J. Lumin.* **1994**, *60&61*, 812.

[3] Zhao, W.; Hou, Y. J.; Wang, X. S.; Zhang, B. W.; Cao, Y.; Yang, R.; Wang, W. B.; Xiao, X. R. *Sol. Energy Mater. Sol. Cells* **1999**, *58*, 173.

[4] Flanagan, J. H. Jr.; Khan, S. H.; Menchen, S.; Soper, S. A.; Hammer, R. P.

Bioconjugate Chem. **1997**, *8*, 751.

[5]   Oguz, U.; Akkaya, E. U. *J. Org. Chem.* **1998**, *63*, 6059.

[6]   Bartolotti, L. J.; Flurchick, K. M. In Reviews in Computational Chemistry, Vol. 7; Lipkowitz, K. B.; Boyd, D. B., Eds.; VCH Publishers Inc.: New York, 1996; Chapter 4.

[7]   Becke, A. D. *Phys. Rev. A* **1988**, 38, 3098.

[8]   Lee, C.; Yang, W.; Parr, R. G. *Phys. Rev. B* **1993**, 37, 785.

[9]   Gordon, M. S. *Chem. Phys. Lett.* **1980**, 76, 163.

[10] Rullière, C., Ed., *Femtosecond Laser Pulses*, Berlin: Springer-Verlag, 1998.

[11] Maciejewski, A.; Naskrecki, R.; Lorenc, M.; Ziolek, M.; Karolczak, J.; Kubicki, J.; Matysiak, M.; Szymanski, M. *J. Mol. Struct.* **2000**, *555*, 1.

[12] Demtröder, W., *Laser Spectroscopy*, 2nd ed.; Basic Concepts and Instrumentation; Berlin: Springer-Verlag, 1998.

[13] Lakowicz, J. R., *Principles of Fluorescence Spectroscopy*, 2nd ed.; New York: Kluwer Academic, 1999.

[14] Magde, D.; Brannon, J. H.; Cremers, T. L.; Olmsted, J. *J. Phys. Chem.* **1979**, *83*, 696.

[15] The IntruView Program, http://casilab10.sci.ccny.cuny.edu/~nathan

Chapter 3.

[1]   Liua, M.; Kirab, A. *Thin Solid Films* **2000**, *359*, 104.

[2]   Vacha, M.; Saeki, M.; Hashizume, K.; Tani, T. *Chem. Phys.* **2002**, *285*, 149.

[3]   Tani, T.; Saeki, M.; Yamaguchi, Y.; Hayashi, T.; Oda, M. *J. Lumin.* **2004**, *107*, 339.

[4]   Tani, T.; Saeki, M.; Yamaguchi, Y.; Hayashi, T.; Oda, M.; Vacha, M. *J. Lumin.* **2003**, *102-104*, 27.

[5]   Dey, S. K.; Manik, N. B.; Bhattacharya, S.; Basu, A. N. *Synth. Met.* **2001**, *118*, 19.

[6]   Forrest, S. R.; Burrows, P. E.; Bulovic, V.; Kozlov, V.; Shen, Z.; Thompson, M. E. *Mater. Lett*. **1998**, *34*, 103.

[7]   Scheblykin, I. G.; Lepnev, L. S.;Vitukhnovsky, A. G.; Van der Auweraer, M. *J.*

Lumin. **2001**, *94-95*, 461.

[8] Yang, S.; Meng, F.; Tian, H.; Chen, K. *Eur. Polym. J.* **2002**, *38*, 911.

[9] Talhavini, M.; Atvars, T. D. Z. *J, Photochem. Photobiol., A* **1999**, *120*, 141.

[10] Moura, J. C. V. P.; Oliveira-Campos, A. M. F.; Griffiths, J. *Dyes Pigm*. **1997**, *33*, 173.

[11] Yang, Y.; Qian, G.; Su, D.; Wang, M. *Chem. Phys. Lett.* **2005**, *402*, 389.

[12] Griffiths, J.; Park, S. *Tetrahedron Lett.* **2002**, *43*, 7669.

[13] Huang,Y.; Chou, K. *Ceram. Int.* **2003**, *29*, 485.

[14] De Rossi, U.; Daehne, S.; Reisfeld, R. *Chem. Phys. Lett.* **1996**, *251*, 259.

[15] Schottner, G. *Chem. Mater.* **2001**, *13*, 3422.

[16] Yang, Y.; Wang, M.; Qian, G.; Wang, Z.; Xianping Fan, X. *Opt. Mater.* **2004**, *24*, 621.

[17] Canva, M.; Roger, G.; Cassagne, F.; Levy, Y.; Brun, A.; Chaput, F.; Boilot, J. -P.; Rapaport, A.; Heerdt, C.; Bass, M. *Opt. Mater.* **2002**, *18*, 391.

[18] Yang, X.; Dai, Z.; Miura, A.; Tamai, N. *Chem. Phys. Lett.* **2001**, *334*, 257.

[19] Gao, F. *Dyes Pigm.* **2002**, *52*, 223.

[20] Xu, Y.; Zhang, B.; Fan, W. H.; Wu, D.; Sun, Y.H. *Thin Solid Films* **2003**, *440*, 180.

[21] Hammarberg, E.; Roos, A. *Thin Solid Films* **2003**, *442*, 222.

[22] Schelle, C.; Mennig, M.; Krug, H.; Jonschker, G.; Schmidt, H. *J. Non-Cryst. Solids* **1997**, *218*, 163.

[23] Alexandridis, P.; Hatton, T.A. *Colloids Surf., A* **1995**, *96*, 1.

[24] Bearzotti, A.; Bertolo, J. M.; Innocenzi, P.; Falcaro, P.; Travers, E. *J. Eur. Ceram. Soc.* **2004**, *24*, 1969.

[25] Besson, S.; Ricolleau, C.; Gacoin, T.; Jacquiod, C.; Boilot, J. -P. *Microporous Mesoporous Mater.* **2003**, *60*, 43.

[26] Alberius, P. C. A.; Frindell, K. L.; Hayward, R. C.; Kramer, E. J.; Stucky, G. D.; Chmelka, B. F. *Chem. Mater.* **2002**, 14, 3284.

[27] Mishra, A.; Behera, R. K.; Behera, P. K.; Mishra, B. K.; Behera, G. E. *Chem. Rev*.

2000, *100*, 1973.

[28] Lampoura, S. S.; Spitz, C.; Dahne, S.; Knoester, J.; Duppen, K. *J. Phys. Chem. B* **2002**, *106*, 3103.

[29] Gaizauskasa, E.; Fellerb, K. -H. *Opt. Commun.* **2003**, *216*, 217.

[30] Kano, H.; Saito, T.; Kobayashi, T. *J. Phys. Chem. A* **2002**, *106*, 3445.

[31] Hamanaka, Y.; Kurasawa, H.; ,Nakamura, A.; Uchiyama, Y.; Marumoto, K.; Kuroda, S. *Chem. Phys. Lett.* **2002**, *363*, 233.

[32] Furuki, M.; Tian, M.; Sato, Y.; Pu, L. S. *Appl. Phys. Lett.* **2000**, *77*, 472.

[33] Minoshima, K.; Taiji, M.; Misawa, K.; Kobayashi, T. *Chem. Phys. Lett.* **1994**, *218*, 67.

[34] Nelson, D. F.; Cuthbert, J. D.; Dean, P. J.; Thomas, D. G. *Phys. Rev. Lett.* **1966**, *17*, 1262.

[35] Özçelik, S.; Akins, D. L. *J. Phys. Chem. B* **1999**, *103*, 8926.

[36] Kobayashi, T.; Misawa, K. *J. Lumn.* **1997**, *72-74*, 38.

[37] Gaizauskas, E.; Feller, K. -H. *J. Lumn*. **2003**, *102-103*, 13.

[38] Xu, W.; Akins, D. L. *J. Phys. Chem. B* **2002**, *106*, 1991.

[39] Xu, W.; Guo, H.; Akins, D. L. *J. Phys. Chem. B* **2001**, *105*, 7686.

[40] Zhang, T.; Chen, C.; Wang, S.; Yang, H. *Chem. Phys. Lett.* **1998**, *298*, 236.

[41] Özçelik, S.; Akins, D. L. *J. Phys. Chem. B* **1997**, *101*, 3021.

[42] Nasr, C.; Hotchandani, S. *Chem. Mater.* **2000**, *12*, 1529.

Chapter 4.

[1] Zhao, W; Hou, Y. J.; Wang, X. S; Zhang, B. W.; Cao, Y.; Yang, R.; Wang, W. B.; Xiao, X. R. *Sol. Energy Mater. Sol. Cells* **1999**, 58, 173.

[2] Hwang, S. H.; Kim, N. K.; Koh, K. N.; Kim, S. H. *Dyes Pigm.* **1998**, 39, 359.

[3] Ohyama, T.; Maruo, Y. Y.; Tanaka, T.; Hayashi, T. *Sens. Actuators, B* **1999**, 59, 16.

[4] Furuki, M.; Tian, M.; Sato, Y.; Pu, L. S. *Appl. Phys. Lett.* **2000**, 77, 472.

[5] Scott, G.W.; Tran, K. *J. Phys. Chem.* **1994**, *98*, 11563.

[6] Bigelow, R. W.; Freund, H.-J. *Chem. Phys.* **1986**, 107, 159.

[7] Paterson, M. J.; Blancafort, L.; Wilsey, S.; Robb, M. A. *J. Phys. Chem. A* **2002**, *106*, 11431.

[8] Tong, L.; Bi-Xian, P. *Dyes Pigm.* **1999**, *43*, 73.

[9] Dirk, C. W.; Herndon, W. C.; Cervantes-Lee, F.; Selnau, H.; Martinez, S.; Kalamegham, P.; Tan, A.; Campos, G.; Velez, M.; Zyss, J.; Ledoux, I.; Cheng, L.-T. *J. Am. Chem. Soc.* **1995**, *117*, 2214.

[10] Ock, K.; Jang, G.; Roh, Y.; Kim, S.; Kim, J.; Koh, K. *Microchem. J.* **2001**, *70*, 301.

[11] Ertekin, K.; Yenigul, B.; Akkaya, E. U. *J. Fluores.* **2002**, *12*, 263.

[12] Santos, P. F.; Reis, L. V.; Almeida, P.; Oliveira, A. S.; Vieira Ferreira, L. F. J. *Photochem. Photobiol. A* **2003**, *160*, 159.

[13] Kamat, P. V.; Das, S.; Thomas, K. G.; George, M. V. *J. Phys. Chem.* **1992**, *96*, 195.

[14] Bonnett, R.; Martinez, G. *Tetrahedron* **2001**, *57*, 9513.

[15] Scherera, D.; Dorfler, R.; Feldner, A.; Vogtmann, T.; Schwoerer, M.; Lawrentz, U.; Grahn, W.; Lambert, C. *Chem. Phys.* **2002**, *279*, 179.

[16] Law, K.-Y. J. *Phys. Chem.* **1987**, *91*, 5184.

[17] Gude, C.; Rettig, W. *J. Phys. Chem. A* **2000**, *104*, 8050.

[18] Huber, R.; Moser, J.; Grätzel, M.; Wachtveitl, J. *J. Phys. Chem. B* **2002**, *106*, 6494.

[19] Yang, X.; Dai, Z.; Miura, A.; Tamai, N. *Chem. Phys. Lett.* **2001**, *334*, 257.

[20] Cherepy, N. J.; Smestad, G. P.; Grätzel, M.; Zhang, J. Z. *J. Phys. Chem. B* **1997**, *101*, 9342.

[21] Hilgendorff, M.; Sundström, V. *J. Phys. Chem. B* **1998**, *102*, 10505.

[22] Wolleben, J.; Testa, A. C. *J. Phys. Chem.* **1975**, *79*, 1137.

[23] Seely, G.R. *J. Phys. Chem.* **1969**, *78*, 125.

[24] Kovalenko, S. A.; Schanz, R.; Farztdinov, V. M.; Hennig, H.; Ernsting, N. P. *Chem. Phys. Lett.* **2000**, *323*, 312.

[25] Andersson, M.; Davidsson, J.; Hammarstrom, L.; Korppi-Tommola, J.; Peltola, T. *J.*

Phys. Chem. B **1999**, *103*, 3258.

[26] Prayer, C.; Tran-Thi, T. -H.; Pommeret, S.; d'Oliveira, P.; Meynadier, P. *Chem. Phys. Lett.* **2000**, *323*, 467.

[27] de Borba, E. B.; Amaral, C. L. C.; Politi, M.J.; Villalobos, R.; Baptista, M. S. *Langmuir* **2000**, *16*, 5900.

[28] Pugžlys, A.; den Hartog, H. P.; Baltuska, A.; Pshenichnikov, M. S.; Umapathy, S.; Wiersma, D. A. *J. Phys. Chem. A* **2001**, *105*, 11407.

Chapter 5.

[1] Kapoor, R. C.; Ain, M. K.; Mishra, V. N. *J. Lumin.* **1981**, *22*, 429.

[2] Xu, D.; Neckerst, D. C. *J. Photochem. Photobiol., A* **1987**, 40, 361.

[3] Daraio, M.E.; Román, E.S. *Helv. Chim. Acta* **2001**, *84*, 2601.

[4] Bilski, P.; Holt, R.N.; Chignell, C. F. *J. Photochem. Photobiol.,* A **1997**, *110*, 67.

[5] Talhavini, M.; Atvars, T.D.Z. *J. Photochem. Photobiol., A* **1999**, *120*, 141.

[6] Gillanders, R. N.; Tedford, M. C.; Crilly, P. J.; Bailey, R. T. *J. Photochem. Photobiol., A* **2004**, *163*, 193.

[7] Lam, S. K.; Chan, M. A.; Lo, D. *Sens. Actuators B* **2001**, *73*, 135.

[8] Alvarez-Pez, J. M.; Ballesteros, L.; Talavera, E.; Yguerabide, J. *J. Phys. Chem., A* **2001**, *105*, 6320.

[9] Lam, S. K.; Lo, D. *Chem. Phys. Lett.* **1997**, *281*, 35.

[10] Urano, Y.; Kamiya, M.;Kanda, K.; Ueno, T.; Hirose, K.; Nagano, T. *J. Am. Chem. Soc.* **2005**, *127*, 4888.

[11] Browne, C. A.; Tarrant, D. H.; Olteanu, M. S.; Mullens, J. W.; Chronister, E. L. *Anal. Chem.* **1996**, *68*, 2289.

[12] Song, A.; Zhang, J.; Zhang, M.; Shen, T.; Tang, J. *Colloids Surf., A* **2000**, *167*, 253.

[13] Larkin, J. M.; Donaldson, W. R.; Foster, T.H.; Knox, R. S. *Chem. Phys.* **1999**, *244*, 319.

[14] Bonnett, R.; Martinez, G. *Tetrahedron* **2001**, *57*, 9513.

[15] Gao, F. *Dyes Pigm.* **2002**, *52*, 223.

[16] Bhowmik, B.B.; Ganguly, P. *Spectrochim. Acta, Part A* **2004**, *61*, 1997.

[17] van Burgle, M.; Wiersma, D. A.; Duppen, K. J. Chem. Phys. **1995**, *102*, 20.

[18] Kamat, P. V.; Das, S.; Thomas, K. G.; George, M. V *J. Phys. Chem.* **1992**, *96*, 195

[19] Bachilo, S. M. *J. Photochem. Photobiol., A* **1995**, *91*, 111.

[20] Yang, Y.; Qian, G.; Su, D.; Wang, Z.; Wang, M. *Chem. Phys. Lett.* **2005**, *402*, 389.

[21] Rao, Y.; Guo, X.-m.; Tao, Y.-S.; Wang, H.-f. *J. Phys. Chem. A* **2004**, *108*, 7977.

[22] Maruyama, Y.; Magnin, O.; Satozono, H.; Ishikawa, M. *J. Phys. Chem. A* **1999**, *103*, 5629.

Chapter 6.

[1] Pavlopoulos, T. G. *Prog. Quantum Electron.* **2002**, *26*, 193.

[2] Brackmann, U. Lambdachrome Laser Dyes, 3rd ed.; URL http://www.lambdaphysik.com.

[3] Gunter, S.; Wohrle, D.; Duffel, B.; Schoonhey, R. Microporous Mesoporous Mater. **2002**, *51*, 91.

[4] Yang, Y.; Wang, M.; Qian, G.; Wang, Z.; Xianping Fan, X. *Opt. Mater.* **2004**, *24*, 621.

[5] Singh, S.; Kanetkar, V.R.; Sridhar, G.; Muthuswamy, V.; Raja, K. *J. Lumin.* **2003**, *101*, 285.

[6] Rao, A.P.; Rao, A.V. *Mater. Lett.* **2003**, *57*, 3741.

[7] Kulmala, S.; Suomi, J. *Anal. Chim. Acta* **2003**, *500*, 21.

[8] Lakowicz, J. R., *Principles of Fluorescence Spectroscopy*, 2nd ed.; New York: Kluwer Academic, 1999.

[9] Preininger, C.; , Gerhard, M. J. *Anal. Chim. Acta* **1997**, *342*, 207.

[10] MacCraith, B. D.; McDonagh, C. M.; O'Keeffe, G.; McEvoy, A. K.; Butler, T.; Sheridan, F. R. *Sens. Actuators, B* **1995**, *29*, 51.

[11] Jana, A. K. *J. Photochem. Photobiol., A* **2000**, *132*, 1.

[12] Mackay, R. A. ; Lai, W. -C. *Colloids Surf., A* **2005**, *254*, 115.

[13] Canva, M.; Roger, G.; Cassagne, F.; Levy, Y.; Brun, A.; Chaput, F.; Boilot, J. -P.; Rapaport, A.; Heerdt, C.; Bass, M. *Opt. Mater.* **2002**, *18*, 391.

[14] Martínez, V. M.; Arbeloa, F. L.; Prieto; J. B.; Arbeloa, L. I. *J. Phys. Chem. B* **2005**, *109*, 7443.

[15] Song, A.; Zhang, J.; Zhang, M.; Shen, T.; Tang, J. *Colloids Surf., A* **2000**, *167*, 253.

[16] Gao, F. *Dyes Pigm.* **2002**, *52*, 223.

[17] Bonnett, R.; Martinez, G. *Tetrahedron* **2001**, *57*, 9513.

[18] Preininger, C.; , Gerhard, M. J. *Anal. Chim. Acta* **1997**, *342*, 207.

[19] Mohr, G. J.; Draxler, S.; Trznadel, K.; Lehmann, F.; Lippitsch, M. E. *Anal. Chim. Act*a **1998**, *360*, 119.

[20] Samiey, B.; Alizadeh, K.; Moghaddasi, M. A.; Mousavi, M. F.; Alizadeh, N. *Bull. Korean Chem. Soc.* **2004**, *25*, 726.

[21] Suah, F. B. M.; Ahmad, M.; Taib, M. N. *Sens. Actuators, B* **2003**, *90*, 182.

[22] Turro, N. J., *Modern Molecular Photochemistry*, California: University Science Books, 1991.